SEISMIC STRENGTHENING OF MASONRY INFILLED REINFORCED CONCRETE FRAMES WITH PRECAST CONCRETE PANELS

A THESIS SUBMITTED TO
THE GRADUATE SCHOOL OF NATURAL AND APPLIED SCIENCES
OF
MIDDLE EAST TECHNICAL UNIVERSITY

BY
MELİH SÜSOY

IN PARTIAL FULFILLMENT OF THE REQUIREMENTS FOR THE DEGREE OF
MASTER OF SCIENCE
IN
CIVIL ENGINEERING

DECEMBER 2004

Approval of the Graduate School of Natural and Applied Sciences

Prof. Dr. Canan ÖZGEN
Director

I certify that this thesis satisfies all the requirements as a thesis for the degree of Master of Science.

Prof. Dr. Erdal ÇOKCA
Head of Department

This is to certify that we have read this thesis and that in our opinion it is fully adequate, in scope and quality, as a thesis for the degree of Master of Science.

Prof. Dr. Tuğrul TANKUT
Supervisor

Examining Committee Members (first name belongs to the chairperson of the jury and the second name belongs to supervisor)

Prof. Dr. Uğur ERSOY	(METU, CE)	
Prof. Dr. Tuğrul TANKUT	(METU, CE)	
Prof. Dr. Güney ÖZCEBE	(METU, CE)	
Asst. Prof. Dr. Erdem CANBAY	(METU, CE)	
Prof. Dr. Sinan ALTIN	(GAZI U.)	

I hereby declare that all information in this document has been obtained and presented in accordance with academic rules and ethical conduct. I also declare that, as required by these rules and conduct, I have fully cited and referenced all material and results that are not original to this work.

Name, Last Name : Melih, Sisoy

Signature :

ABSTRACT

SEISMIC STRENGTHENING OF MASONRY INFILLED R/C FRAMES WITH PRECAST CONCRETE PANEL INFILLS

SÜSOY, Melih

M.Sc., Department of Civil Engineering

Thesis Supervisor: Prof. Dr. Tuğrul Tankut

December 2004, 140 pages

Over 90% of the land area of Turkey lies over one of the most active seismic zones in the world. Hazardous earthquakes frequently occur and cause heavy damage to the economy of the country as well as human lives.

Unfortunately, the majority of buildings in Turkey do not have enough seismic resistance capacity. The most commonly observed problems are faulty system configuration, insufficient lateral stiffness, improper detailing, poor material quality and mistakes during construction. Strengthening of R/C framed structures by using cast-in-place R/C infills leads to a huge construction work and is time-consuming. On the other hand, using prefabricated panel infills can be preferred as a more feasible, rapid and easy technique during which the structure can remain operational.

The aim of this experimental study is to observe the seismic behavior of R/C frames strengthened by precast concrete panel infills by testing different types of panel and connection designs in eight single-story single-bay reinforced concrete frame specimens.

Keywords: Earthquake, Repair and Strengthening, Lateral Stiffness, Shear Wall, Reinforced Concrete Infill, Prefabricated Panel, Panel Connection.

ÖZ

DOLGULU BETONARME ÇERÇEVELERİN ÖNÜRETİMLİ BETON PANELLERLE DEPREME KARŞI GÜÇLENDİRİLMESİ

SÜSOY, Melih
Yüksek Lisans, İnşaat Mühendisliği Bölümü
Tez Danışmanı: Prof. Dr. Tuğrul Tankut

Aralık 2004, 140 sayfa

Türkiye topraklarının %90'ından fazlası dünyanın en aktif sismik bölgelerinden birinin üzerinde bulunmaktadır. Hasar verici depremler sıklıkla olmakta ve ülke ekonomisi ve insan hayatı için de ağır kayıplara yol açmaktadır.

Maalesef, Türkiye'deki binaların çoğu yeterli deprem dayanımına sahip değildir. En çok gözlenen sorunlar hatalı sistem seçimi, yetersiz yanal rijitlik, yanlış detaylandırma, zayıf malzeme kalitesi ve yapım sürecinde rastlanan hatalardır. betonarme dolgu kullanarak güçlendirme büyük miktarda inşaat işi gerektirmektedir ve oldukça zaman alır. Diğer taraftan, önüretimli panel dolgular kullanmak, yapının boşaltılmasını gerektirmeyen, daha ekonomik, çabuk ve kolay bir teknik olarak tercih edilebilir.

Bu deneysel çalışmanın amacı farklı panel ve bağlantı tipleri deneyerek önüretimli beton panel dolgularla güçlendirilmiş betonarme çerçeveli yapıların sismik davranışlarını sekiz adet tek katlı tek açıklıklı çerçeve eleman üzerinde incelemektir.

Anahtar Kelimeler : Deprem, Onarım ve Güçlendirme, Yatay Rijitlik, Perde Duvar, Betonarme Dolgu Duvar, Önüretimli Panel, Panel Bağlantısı.

Dedicated to my wife Alev

ACKNOWLEDGEMENTS

It was a great opportunity to study under the supervision of Prof. Dr. Tuğrul Tankut and an irreplaceable and honorable experience that will provide a guide in all of my future endeavors. Therefore, I would like to convey my sincere appreciation to him for his professional guidance and constructive criticism.

I owe special thanks to Prof. Dr. Uğur Ersoy and Prof Dr. Güney Özcebe for their helpful suggestions and guidance throughout the project.

I would like to offer sincere thanks to Mr. Mehmet Baran who has provided invaluable contribution to this study. It was a great pleasure to work along with him. Also, working together with Ms. Dilek Okuyucu has been an honor. Mr. Gökhan Özdemir also deserves my special thanks for his assistance during the laboratory works.

I would also like to convey my thanks to the capable staff of METU Structural Mechanics Laboratory. Mr. Burhan Avcı, Mr. Hasan Metin, Mr. Murat Pehlivan and Mr. Hasan Hüseyin Güner have provided exceptional support for accomplishing this study. I also would like to offer special thanks to Mr. Ömer Metin and Mr. Osman Keskin for their endless efforts for completing this project.

I gratefully acknowledge the financial support given by the Scientific and Technical Research Council of Turkey (TUBITAK-IÇTAG I-575) and North Atlantic Treaty Organization (NATO-SFP 977231)

Finally, I am deeply grateful to my wife Alev for her endless support, encouragement and love. I also would like to convey my deepest thanks to my family who gave me enormous support throughout this study.

TABLE OF CONTENTS

CHAPTER 1 INTRODUCTION **1**

1.1 General *1*

1.2 Object and Scope of the Study *3*

CHAPTER 2 LITERATURE SURVEY **4**

2.1 General *4*

2.2 Previous Studies *4*

2.3 Prevıous Studıes within the Current Research Project *10*

CHAPTER 3 TEST SPECIMENS **13**

3.1 General *13*

3.2 Dimensions of the Test Specimens *15*

3.3 Detailing of the Specimens *18*

3.4 Universal Base *22*

3.5 Precast Panels *23*

3.6 Materials *36*

CHAPTER 4 TEST SETUP AND PROCEDURE **42**

4.1 Test Setup *42*

4.2 Loading System *44*

4.3 Instrumentation *47*

4.4 Test Procedure *50*

CHAPTER 5 **TEST RESULTS** **52**

5.1 General *52*

5.2 Specimen CR *52*

5.3 Specimen CIA4 ..... *60*

5.4 Specimen CIB4 ..... *66*

5.5 Specimen CIC4 ..... *72*

5.6 Specimen CID4 ..... *78*

5.7 Specimen LR *85*

5.8 Specimen LIC4 ..... *91*

5.9 Specimen LID4 ..... *97*

CHAPTER 6 **EVALUATION OF TEST RESULTS** **104**

6.1 General *104*

6.2 Response Envelopes *104*

6.3 Strength *107*

6.4 Stiffness *109*

6.5 Energy Dissipation *112*

6.6 Displacement History *115*

6.7 Summary *117*

6.8 Comparison with Two-Story Test Specimens *118*

CHAPTER 7 **CONCLUSIONS 128**

7.1 Summary 128

7.2 Conclusions 129

7.3 Recommendations 130

LIST OF TABLES

Table 3.1 – Test Specimens 14

Table 3.2 – Dimensions of the Formwork Segments 17

Table 3.3 – Properties of Reinforcing Bars in the Frames 22

Table 3.4 – Frame Concrete Mix Proportions (for 1 m^3 of concrete) 36

Table 3.5 – Results of Cylinder Tests for Frame Concrete (MPa) 37

Table 3.6 – Panel Concrete Mix Proportions (for 1 m^3 of concrete) 37

Table 3.7 – Results of Cylinder Tests for Panel Concrete (MPa) 38

Table 3.8 – Properties of Reinforcing Bars 38

Table 3.9 – Results of Compression Tests of Brick Tiles (MPa) [1] 39

Table 3.10 – Mix Proportions for Plaster and Mortar 39

Table 3.11 – Results of Cylinder Tests for Mortar and Plaster (MPa) 40

Table 3.12 – Properties of Sikadur-31 (as given in the catalog) 41

Table 4.1 – Axial Load Levels in the Tests 51

Table 6.1 – Maximum Recorded Lateral Load for Each Specimen 108

Table 6.2 – Strength Increase for Specimens with Continuous and Lap-Spliced Reinforcement 109

Table 6.3 – Initial Stiffness of Test Specimens 110

Table 6.4 – Total Energy Dissipation of Each Test Specimen 113

Table 6.5 – Summary of the Test Results 117

Table 6.6 – Test Results of CR Specimens 120

Table 6.7 – Test Results of CIA4 Specimens 122

Table 6.8 – Test Results of CIB4 Specimens 124

Table 6.9 – Test Results of CIC4 Specimens 126

LIST OF FIGURES

Figure 1.1 – Seismic Rehabilitation Strategy and Measures [2] 2

Figure 3.1 – General View of the Test Specimen 13

Figure 3.2 – Dimensions of the Test Specimens (dimensions in mm) 16

Figure 3.3 – Dimensions of the Hollow Clay Tile Bricks Used for Masonry Infill (dimensions in mm) 16

Figure 3.4 – Geometry of the Formwork 17

Figure 3.5 – Assembled View of the Formwork 18

Figure 3.6 – General View of Reinforcement 19

Figure 3.7 – Details of Reinforcement (dimensions in mm) 19

Figure 3.8 – Reinforcement Details of the Specimens with Continuous Reinforcement (dimensions in mm) 20

Figure 3.9 – Close View of Lap-Spliced Connection 20

Figure 3.10 – Details of Reinforcement (dimensions in mm) 21

Figure 3.11 – Reinforcement Details of the Specimens with Lap-Spliced Reinforcement (dimensions in mm) 21

Figure 3.12 – Dimensions and Details of the Universal Base (dimensions in mm) 23

Figure 3.13 – Details of Type A Panels (dimensions in mm) 25

Figure 3.14 – Type A Panels 26

Figure 3.15 – Panel Connection Details ... 27

Figure 3.16 – Embedment of Dowels before Application of Type A Panels (dimensions in mm) ... 27

Figure 3.17 – Panel Arrangement for Type A Panels ... 28

Figure 3.18 – Application of Type A Panels ... 28

Figure 3.19 – Details of Type B Panels (dimensions in mm) ... 29

Figure 3.20 – Type B Panels ... 30

Figure 3.21 – Embedding of Dowels before Application of Type B Panels (dimensions in mm) ... 31

Figure 3.22 – Panel Arrangement for Type B Panels ... 31

Figure 3.23 – Details of Type C Panels (dimensions in mm) ... 32

Figure 3.24 – Type C Panels ... 32

Figure 3.25 – Arrangement of Type C Panels (dimensions in mm) ... 33

Figure 3.26 – Application of Type C Panels ... 33

Figure 3.27 – Details of Type D Panels (dimensions in mm) ... 34

Figure 3.28 – Type D Panels ... 35

Figure 3.29 – Arrangement of Type D Panels (dimensions in mm) ... 35

Figure 3.30 – Construction and Final View of the Masonry Infill (without plaster) ... 40

Figure 4.1 – Test Setup ... 42

Figure 4.2 – Specimen in the Test Setup........ 43

Figure 4.3 – Ball Bearings 44

Figure 4.4 – Elements of the Vertical Loading System 44

Figure 4.5 – Lateral Loading System........ 45

Figure 4.6 – Lateral Loading System........ 46

Figure 4.7 – Close View of the Pin Connections 46

Figure 4.8 – Steel Plates for Loading in Two Directions........ 47

Figure 4.9 – Instrumentation 48

Figure 4.10 – Dial Gauge Positions 49

Figure 4.11 – LVDTs 49

Figure 5.1 – Directions and Names Used for Describing the Observations 52

Figure 5.2 – Loading Histories of Test Specimens 53

Figure 5.3 – Measurement of South Column Deformation at the Base (units in mm) 54

Figure 5.4 – Lateral Load - Lateral Displacement Curve of Specimen CR 56

Figure 5.5 – Lateral Load - Shear Deformation Curve, Specimen CR 56

Figure 5.6 – Lateral Load-North Column Deformation at the Base, Specimen CR 57

Figure 5.7 – Lateral Load-South Column Deformation at the Base, Specimen CR 57

Figure 5.8 – Separation in the Sixth Cycle, Specimen CR 59

Figure 5.9 – Damage in the South Column in the Ninth Cycle, Specimen CR 59

Figure 5.10 – General View of Specimen CR after the Test (front)........................... 60

Figure 5.11 – General View of Specimen CR after the Test (back) 60

Figure 5.12 – Lateral Load - Top Displacement Curve, Specimen CIA4.................. 62

Figure 5.13 – Lateral Load-North Column Deformation at the Base, Specimen CIA4 63

Figure 5.14 – Lateral Load-South Column Deformation at the Base, Specimen CIA4 63

Figure 5.15 – Lateral Load-Shear Displacement Curve, Specimen CIA4 62

Figure 5.16 – Column Base Crack in the Nineteenth Cycle, Specimen CIA4 64

Figure 5.17 – Diagonal Cracking on the Infill in the Sixteenth Cycle, Specimen CIA4 65

Figure 5.18 – Damage in the South Beam-Column Joint, Specimen CIA4............... 65

Figure 5.19 – Damage on the Infill, Specimen CIA4 65

Figure 5.20 – Specimen CIA4 at the End of the Test 66

Figure 5.21 – Lateral Load - Top Displacement Curve for Specimen CIB4 67

Figure 5.22 – Lateral Load - North Column Deformation at the Base, Specimen CIB4 68

Figure 5.23 – Lateral Load - South Column Deformation at the Base, Specimen CIB4 68

Figure 5.24 – Lateral Load - Shear Displacement Curve, Specimen CIB4 69

Figure 5.25 – Joint Cracks in the Sixth Cycle, Specimen CIB4 70

Figure 5.26 – Cracking on the Infill in the Fourteenth Cycle, Specimen CIB4 71

Figure 5.27 – Damage at the Joints, Specimen CIB4 71

Figure 5.28 – General View of Specimen CIB4 after the Test 71

Figure 5.29 – Lateral Load - Top Displacement Curve, Specimen CIC4 73

Figure 5.30 – Lateral Load-North Column Deformation at the Base, Specimen CIC4 74

Figure 5.31 – Lateral Load-South Column Deformation at the Base, Specimen CIC4 74

Figure 5.32 – Lateral Load-Shear Displacement Curve, Specimen CIC4 75

Figure 5.33 – Joint Cracking in the Eighth Cycle, Specimen CIC4 77

Figure 5.34 – Infill Cracks in the Tenth Cycle, Specimen CIC4 77

Figure 5.35 – Infill Cracks in the Seventeenth Cycle, Specimen CIC4 77

Figure 5.36 – General View of Specimen CIC4 after the Test 78

Figure 5.37 – Damage in the Beam-Column Joints after the Test, Specimen CIC4 78

Figure 5.38 – Lateral Load - Top Displacement Curve, Specimen CID4 80

Figure 5.39 – Lateral Load - Shear Displacement Curve, Specimen CID4 80

Figure 5.40 – Lateral Load-North Column Deformation at the Base, Specimen CID4 81

Figure 5.41 – Lateral Load-South Column Deformation at the Base, Specimen CID4 81

Figure 5.42 – Panel Cracks in the Ninth Cycle, Specimen CID4 83

Figure 5.43 – Cracking on the Infill in the Sixteenth Cycle, Specimen CID4 83

Figure 5.44 – Column Base Damage in the Nineteenth Cycle, Specimen CID4 84

Figure 5.45 – Separation of the Column from the Infill, Specimen CID4 84

Figure 5.46 – Infill Cracking, Specimen CID4 84

Figure 5.47 – General View of Specimen CID4 after the Test 85

Figure 5.48 – Lateral Load vs. Top Displacement Curve, Specimen LR 87

Figure 5.49 – Lateral Load - Shear Displacement Curve, Specimen LR 87

Figure 5.50 – Lateral Load-North Column Deformation at the Base, Specimen LR 88

Figure 5.51 – Lateral Load-South Column Deformation at the Base, Specimen LR 88

Figure 5.52 – Cracking at the Column Base and Lap-Splice Level in the Fourth Cycle, Specimen LR 90

Figure 5.53 – Deformation in the Frame during the Test, Specimen LR 90

Figure 5.54 – General View of Specimen LR after the Test 90

Figure 5.55 – Lateral Load - Top Displacement Curve, Specimen LIC4 92

Figure 5.56 – Lateral Load-North Column Deformation at the Base, Specimen LIC4 93

Figure 5.57 – Lateral Load-South Column Deformation at the Base, Specimen LIC4 93

Figure 5.58 – Lateral Load-Shear Displacement Curve, Specimen LIC4 94

Figure 5.59 – Damage in the Column and Joint Region in the Seventh Cycle, Specimen LIC4 96

Figure 5.60 – Cracks on the Infill in the Tenth Cycle, Specimen LIC4 96

Figure 5.61 – Widening of Cracks According to Loading Direction, Specimen LIC4 96

Figure 5.62 – Column Base Crack (left) and Joint Cracks (right), Specimen LIC4 97

Figure 5.63 – General View of Specimen LIC4 after the Test 97

Figure 5.64 – Lateral Load - Top Displacement Curve, Specimen LID4 98

Figure 5.65 – Lateral Load - Shear Displacement Curve, Specimen LID4 99

Figure 5.66 – Lateral Load - North Column Deformation at the Base, Specimen LID4 99

Figure 5.67 – Lateral Load - South Column Deformation at the Base, Specimen LID4 100

Figure 5.68 – Infill Cracking Pattern, Specimen LID4 101

Figure 5.69 – Damage in the South Beam-Column Joint, Specimen LID4 102

Figure 5.70 – Development of Infill Cracks, Specimen LID4 102

Figure 5.71 – Cracking at the Column Base and Lap-Splice Region, Specimen LID4 102

Figure 5.72 – Damage in the Lap-Splice Region of the Column, Specimen LID4 103

Figure 5.73 – General View of Specimen LID4 after the Test 103

Figure 6.1 – Response Envelopes of Specimens with Continuous Reinforcement 105

Figure 6.2 – Comparison for Response Envelopes of Lap-Spliced Specimens 105

Figure 6.3 – Stiffness Degradation Curves for Specimens with Continuous Reinforcement 111

Figure 6.4 – Stiffness Degradation Curves for All Specimens 111

Figure 6.5 – Cumulative Energy Dissipation for Specimens with Continuous Column Steel 114

Figure 6.6 – Comparison of Cumulative Energy Dissipation Curves for All Specimens 115

Figure 6.7 – Displacement Histories 116

Figure 6.8 – Elastic Frame Deformations Assuming Infinitely Rigid Beams for Comparison of Two-story and One-story Test Frames 118

Figure 6.9 – Lateral Load vs. First Story Displacement of CR Specimens 120

Figure 6.10 – Comparison of Response Envelopes of CR Specimens 120

Figure 6.11 – Lateral Load vs. First Story Displacement of CIA4 Specimens 122

Figure 6.12 – Comparison of Response Envelopes of CIA4 Specimens................. 122

Figure 6.13 – Lateral Load vs. First Story Displacement of CIB4 Specimens 124

Figure 6.14 – Comparison of Response Envelopes of CIB4 Specimens................. 124

Figure 6.15 – Lateral Load vs. First Story Displacement of CIC4 Specimens 126

Figure 6.16 – Comparison of Response Envelopes of CIC4 Specimens................. 126

Figure A.1 – Rectangular shape distortion.. 136

CHAPTER 1

INTRODUCTION

1.1 GENERAL

In the past years, earthquakes caused an enormous loss of human lives and great damage to many structures including residential buildings, industrial facilities and infrastructure systems. Turkey, being located over one of the most active seismic zones on the earth, faces major and devastating earthquakes frequently and struggles with this hazard. The forces of ground motion becomes destructive for inadequately constructed buildings which comprise a major group among the total building stock in Turkey, as witnessed at the aftermath of the recently occurring major earthquakes. The necessity of intervention in order to provide safety to damaged structures and earthquake prone structures which are at risk is evident.

After major earthquakes, comprehensive rehabilitation programs had to be carried out to bring the damaged and undamaged structures to an acceptable level of structural safety. Seismic rehabilitation is to bring up the structural system or some structural members to a specified seismic performance level. Seismic repair is the rehabilitation of a damaged structure to ensure satisfactory performance under a pre-specified seismic action. Seismic strengthening is the rehabilitation of an undamaged existing structure to upgrade its seismic performance to an acceptable level of structural safety [1].

The objectives for a seismic rehabilitation approach are listed by Sugano [2] as the following:

- To recover original structural performance
- To upgrade original structural performance
- To reduce the seismic response

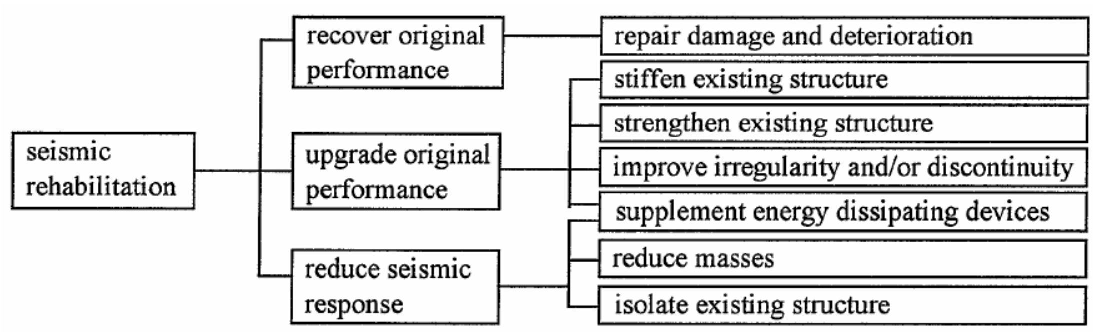

Figure 1.1 – Seismic Rehabilitation Strategy and Measures [2]

Rehabilitation of buildings to improve the seismic behavior is being widely used all over the world. The aim in seismic rehabilitation is to upgrade the strength, ductility and especially the lateral rigidity. Strengthening of individual members (beams and columns) becomes feasible when the number of members to be rehabilitated is limited and the lateral rigidity of the building is adequate, but most of the time the situation is the opposite. So, if the number of the members to be rehabilitated is large and lateral stiffness of the structure is not adequate, system improvement approach would be more convenient.

Adding new shear walls to reinforced concrete frames is a common and reliable method of system improvement. By constructing a cast-in-place reinforced concrete infill wall, in some cases in the place of a partitioning wall, the building gains considerable strength and lateral stiffness increase [3]. Many buildings in Turkey were repaired or strengthened with this method, especially after major earthquakes. However, there are some drawbacks of cast-in-place infill wall strengthening. The application of this method requires heavy construction work, so it is necessary to evacuate the building. The workmanship in this rehabilitation method is difficult and time-consuming. It also necessitates acquiring and transporting large amounts of material.

In Turkey, there exist a great number of buildings which need retrofit against a possible earthquake, but the application of infill wall or any other current method seems to be uneconomical and unpractical.

1.2 OBJECT AND SCOPE OF THE STUDY

The aim of this study is to investigate the behavior of the seismic strengthening method by bonding precast concrete panels on hollow brick masonry infill walls of existing reinforced concrete frames in order to convert the infill into a load carrying system acting as a cast-in-place concrete shear wall. The panels would be readily available and easily transported and assembled to their place. This method of seismic strengthening is expected to be a much more practical and feasible technique, and not disturbing the occupants and function of the building. Also, by decreasing the time and the workmanship, a great number of vulnerable buildings can be retrofitted and prepared against earthquakes. This method would be suitable for the existing building stock and convenient in terms of the materials and workmanship practice used in Turkey and South-Eastern Europe.

In this study, the test frames were one-story, one-bay reinforced concrete frames of one-third scale. The frames have the same properties as the two-story test frames of previous studies, possessing commonly observed weaknesses, such as:

- Poor concrete quality
- Plain bars were used as longitudinal and transverse reinforcement
- Insufficient confinement (insufficient transverse reinforcement, stirrups were hooked 90º, column ends and joint regions were not sufficiently confined)
- Beams are stronger than columns
- Insufficient lap-splice length (20ϕ) for lap-spliced specimens

These model frames were tested after strengthening with high-strength precast concrete panels. Unstrengthened frame tests were also included as reference. The main parameters studied for this study were:

- Panel geometry (full height strip or nearly square)
- Panel to panel connections (shear keys, welding, only epoxy)
- Panel to frame connections (welding, dowels at two or four sides)
- Effect of lap-splice and axial load

CHAPTER 2

LITERATURE SURVEY

2.1 GENERAL

In this chapter, previous significant studies on related seismic strengthening methods are summarized.

2.2 PREVIOUS STUDIES

Ersoy and Uzsoy (1971) made an experimental research with nine tests on one-story, one-bay reinforced concrete frames tested under monotonic loading in order to observe and analyze the effects of strengthening with cast-in-place reinforced concrete infills. The main parameters investigated in the study were aspect ratio, infill thickness, effect of vertical loads, connection between frame and panel, and the ratio of beam stiffness to column stiffness. The frames were strengthened with reinforced concrete infills and tested under a monotonically increasing lateral load. Authors concluded that the presence of an infill increased the lateral load carrying capacity of the frame by approximately 700% and reduced the lateral deflection at failure by 65%. It was concluded that the infill increased the elastic lateral rigidity of the frame by 500% and the bond between the panel and the frame did not affect the lateral capacity and rigidity of infilled frames significantly.

Yuzugullu (1979) performed an experimental research on strengthening with multiple precast panels with ten one-story, one-bay reinforced concrete test frames. Precast panels of 30-mm thickness were assembled as an infill shear wall enclosed by the test frames and the specimens were tested under reversed cyclic loading. Effects of panel size, panel-to-panel and panel-to-frame connection type on the efficiency of strengthening were investigated. Both damaged and undamaged frames were used in the test series.

The results of this experimental study were published in a report as follows:

- Initial stiffness of the frame increased by 1.3 ~ 2.9 times (with respect to the bare frame)
- The load carrying capacity increased by 7 ~ 9 times
- Energy dissipation increased by 1.3 ~ 4.9 times
- Failure mode was not influenced by the reversed loading
- Increasing the panel number from two to four or the existence of panel-column connection did not change the failure mode but had a slight influence on the initial stiffness
- Increasing the number of panels and using continuous connection increased energy dissipation
- Initial stiffness decreased by the ratio of 50% to 60% in case a damaged frame is strengthened

Kahn and Hanson (1979) made infill wall strengthening experiments by testing five one story, one bay reinforced concrete frames. Two of these specimens were tested as references, one being a bare frame and the other having a monolithically cast shear wall. Three specimens were strengthened with three different infill wall schemes. One wall was cast within an existing frame, a second was precast as a single unit and mechanically connected within the frame, and the third was precast in six individual sections that were mechanically connected to the frame and to each other. All specimens were tested under reversed cyclic loading.

According to the test results, the cast-in-place wall showed nearly the same lateral strength as the monolithically cast wall. The infilled wall with six individual precast panels behaved as a series of deep beams, having about one-half the ultimate load capacity of the monolithical specimen.

Monolithically cast structure dissipated twice as much energy as the other infilled walls because this was the only specimen that behaved as a single unit in flexure up to the failure. Multiple panel wall showed about the same cumulative dissipated energy with the cast-in-place wall.

Hayashi, Niwa and Fukuhara (1980) made an experimental research for investigating and comparing the effects of strengthening by cast-in-place reinforced concrete shear walls and column strengthening by mortar reinforced with welded wire fabrics. For strengthening with infill walls, six one-third scale, one-bay, one-story reinforced concrete frames were tested. A reference bare frame and a frame strengthened with monolithically cast shear wall were included in the tests. Other specimens were strengthened with new concrete shear walls with different connection methods including concrete shear keys bonded to frame elements and straight or roughened dowel bars anchored to the beam element or all frame elements. The frames were tested under a constant axial load of 12 tons distributed to the columns and a cyclically applied lateral load from the centerline of the beam.

The test results showed that the strengthened specimens showed 0.5-0.72 times the lateral strength of the monolithic specimen and achieved 3.5-5.0 times the lateral strength of the bare frame. Also, considerable stiffness increase was observed. It was concluded that reinforced concrete infilled wall strengthening technique indicated general adequacy according to test results. Also, within the research, column strengthening with mortar and welded wire fabrics were studied with 4 test specimens, and the results were found to be satisfactory for increasing ductility and shear strength of the columns.

Ohki and Bessho (1980) made tests on five one-half scale, one-story, one-bay reinforced concrete frames in order to model the aseismic strengthening of the one-story Morioka Station building of the Japanese National Railways. The specimens were tested under reversed cyclic lateral load applied at the beam centerline with a constant axial load on each column corresponding to 15% of column axial load capacity. A bare frame was tested as a reference, and another test frame had a monolithically cast shear wall for comparison use. Two specimens were strengthened with 15-cm thick infilled shear walls with different anchorage techniques. Another specimen was applied column strengthening with steel plate encasing.

Main conclusions reached through this experimental project are that infilled shear wall strengthening of existing frames demonstrates ample earthquake resistance of bending type and it increases the maximum strength of the unreinforced frames about 5.6 times, and this corresponds to 74% of the maximum strength of the frames with monolithically cast shear walls. Also, the initial stiffness of the infilled frames was about 64% in comparison with the monolithic specimens. Improved anchorage between infill and the frame members indicated an increased ductility.

Higashi, Endo, Okhubo and Shimuzu (1980) made tests on thirteen one-third scale, single-bay, single-story reinforced concrete frames for comparison of different strengthening methods, such as; reinforced concrete cast in place infill wall, precast concrete infill panels with or without door openings, steel bracing, steel frame and steel truss. Test results for all strengthening schemes showed lateral strengths between that of bare frame and monolithic wall. Among the methods in the experimental research, the highest strength increase was observed for cast-in-place concrete infill and precast concrete panels without opening. Also, an analytical model was also presented in the paper. In this model, the columns and beams were considered to be rigidly connected to the frame and the infill walls or precast concrete panels were idealized as compressive bracing or, compressive bracing plus tensile bracing. Both ends of these bracing members were assumed to be pin-connected with or without springs. The area of the bracing depended on many factors as given in the paper.

Sugano and Fujimura (1980) conducted experimental research including ten one-third scale single-story, single-bay reinforced concrete frames. Various types of infilling and bracing techniques were used for strengthening of the frames in order to observe the characteristic behaviour of each method. Among the ten test specimens, five of them were strengthened by infilling, two specimens were strengthened by bracing, two were monolithically cast shear walls with different thicknesses and one was an unstrengthened frame for reference.

Altın, Ersoy and Tankut (1992) tested fourteen two-story, one-bay reinforced concrete frames one of which was a reference bare frame. The frames were strengthened with infilled shear walls and tested under reversed cyclic lateral loads. The main variables in the experimental investigation were:

- Reinforcement pattern of the infill and connection of the infill to the frame
- Column axial load level
- Concrete strength
- Column capacity

For each of the parameters, there was one reference specimen in which the infill and the frame were cast together (monolithic). All of the infilled frames tested reached their ultimate flexural capacities. The final failure was sliding shear at the foundation level.

The authors suggested the following conclusions according to the results of this experimental research:

- All of the three reinforcement patterns used for infills (grid, diagonal and concentrated reinforcement at the boundaries) were found to be satisfactory. Ratios of base moment capacities of infilled frames to those of bare frames varied from 3 to 7. Ratios of stiffnesses varied from 10 to 40.
- Increasing the column capacity by increasing the ratio of longitudinal bars and axial load on columns increased the capacity of infilled frames.
- The connection of the infill to the existing frame was found to be very important and should be detailed to provide satisfactory behavior.

Phan, Cheok and Todd (1995) analyzed existing experimental research results for seismic strengthening tests in their multi-year research project at the National Institute of Standards and Technology (NIST). The objective of this study was to develop guidelines for seismic strengthening techniques by reviewing the experimental observations of 54 lightly reinforced concrete frame tests.

The analytical results obtained from the parametric study were used in conjunction with experimental observations extracted from these experimental programs, which were systematically reviewed and as a result of this study, the following conclusions were suggested as design guidelines for seismic strengthening with cast-in-place or precast panel infills:

- Infill wall thickness, of both cast-in-place and precast infill walls, should be not less than 2/5 the thickness of the bounding column or the top beam of the frame, whichever is smaller, and should not be greater than the thickness of the top beam.
- Based on experimental observation, the ratio of the total cross sectional area of the connecting anchors to the area of the infill walls at the wall/frame interface (A_c/A_w) should not be less than 0.8% for successful connection between the wall and the existing frame. However, the experiments examined only two ratios, 0.3% and 0.81%. Thus, it is believed that the 0.81% ratio is rather conservative. The parametric study showed a steady increase in both the maximum story drift and shear strength at a ratio of 0.45%, and the increase became less significant for ratios greater than 0.9%. Thus, to be conservative, the number of connecting anchors and their sizes are recommended so that the ratio of A_c/A_w is approximately 0.8% as observed in previous experiments.

Frosch (1996) made an experimental research in order to investigate various parameters affecting infill wall strengthening by assembling precast panels. The main variables analysed in the total of four tests were panel thickness and connection types. Variations in size and embedment depth of anchorages were studied. According to the test results, design provisions and application recommendations were given. The following fourteen tests performed by Frosch aimed at further investigating the following variables:

- Shear key configuration
- Shear key size
- Panel spacing
- Vertical reinforcement
- Grout strength
- Panel thickness

The following conclusions were reported by the author:

- Joint failures occurred in all cases at the top of the horizontal grout interface.
- The shear key configuration (alignment and spacing) had no significant effect on the peak capacity and no effect on the residual capacity
- The shear key size had a modest affect on the peak capacity; the capacity of the specimen with the larger key was 20 percent higher. There was no effect on the residual capacity
- The spacing of adjacent precast panels did not affect the peak or residual capacity
- The relative strength between the grout and panel concrete influenced the joint behavior. The lower strength material controlled the peak capacity and failure surface location. The residual capacity, however, was not affected.
- The peak and residual capacity of the walls increased directly with the wall thickness
- Increasing the vertical reinforcement increased both the peak and residual capacities of the specimen.

2.3 PREVIOUS STUDIES WITHIN THE CURRENT RESEARCH PROJECT

The concept of seismic strengthening by bonding precast concrete panels on brick masonry infill was first introduced by the current research project supervised by Dr. Tankut. Assemblage of precast concrete blocks had been used for seismic strengthening in some previous studies, but making use of the existing masonry infill had not been considered. This technique of applying panel units over the infill and making them behave as a composite system provides an effective, occupant friendly, economical and rapid seismic strengthening method. Experimental studies were initiated with Duvarci in 2003, and currently continued by Baran and Okuyucu, besides this study. Extensive experimental and analytical research is being continued in order to analyze and improve the method.

Duvarci (2003) studied strengthening with precast panels bonded on masonry infills by testing three one-third scale reinforced concrete specimens with one bay and two stories, in addition to two preliminary specimens. The three successful experiments include one reference frame with only masonry infill and two strengthened specimens by using Type A and Type B precast panels. The panels were bonded over the masonry infill of the test frames. Type A panels were rectangular and arranged in three rows and four columns over the infill. Type B panels were thin strip panels extending from bottom to top and placed side by side. Both panel types had shear keys. Epoxy mortar was used for bonding the panels on the infill and also between the panels. Panel-to-panel and panel-to-frame connections were enhanced by welding the corner extensions of the panel steel bars to each other and to dowel embedded in the frame members.

Following conclusions were derived according to the data obtained from these three tests:

- The tests indicated that the performance of the precast concrete panels was very effective. The precast concrete panels improved the system behavior considerably
- The lateral strength increased 2.4 ~ 2.6 times in strengthened specimens
- It was observed that the shape of the panels did not have a significant effect in strengthening.
- Number of dowel connections increased the lateral strength slightly
- Precast concrete panels increased the initial stiffness by 300% relative to the reference specimen
- The increase in energy dissipation was 254% ~ 320%. Precast concrete panels significantly improved energy dissipation characteristics.
- Interstory drift characteristics were acceptable in all specimens. The precast concrete panels controlled the drift considerably. From the test results, it is seen that the loops are stable in the limits of the Turkish Seismic Code.
- Shear keys and the epoxy mortar functioned successfully and the precast concrete panels improved the performance nearly as good as the monolithically cast shear wall.

As a result of this study, the author concluded that using precast concrete panels as a strengthening technique can greatly shorten the construction time, eliminate the need for large formwork during construction, and therefore reduce revenue loss. When the economy is concerned, it can be said that precast concrete panel strengthening technique is less expensive than monolithic shear wall.

Baran (in progress) performed fourteen tests on further investigating the strengthening method by bonding precast panels. The test specimens were identical to the frames used by Duvarci. In this test series, different panel types were used which had no shear keys and designated as Type C and Type D. The following variables were studied in this study:

- Effect of shear keys
- Effect of anchorage
- Effect of lap-splice in reinforcement

Other than the listed parameters, Baran studied the behavior of strengthened specimens for bonding the panels to the exterior sides. The difficulties related with bonding to the exterior side and the anchorage pattern necessary for providing a satisfactory behavior was investigated within the test series.

According to test results of this study, the method was found to be very effective.

Okuyucu (in progress) is conducting an experimental and analytical study of the same method, and will mainly investigate the effect of the aspect ratio of the frames. For this purpose, various tests on reinforced concrete frames of different height, width and scale are planned. The properties of the reinforced concrete frames will be the same as the frames used in the previous tests. Also, analytical approaches will be developed in order to determine design parameters.

CHAPTER 3

TEST SPECIMENS

3.1 GENERAL

The test specimens used in this experimental study are one-third scale, single-story single-bay reinforced concrete frames with hollow brick masonry infills. Figure 3.1 shows a general view of the frames. These frames resemble typical characteristics and common deficiencies of the structural frames of reinforced concrete buildings in Turkey. These weaknesses include low concrete strength, using plain bars, short lap length, insufficient anchorages, poor confinement and beams stronger than columns. The frames were divided into two groups according to their detailing type of reinforcement. Continuous reinforcement was used in some specimens, whereas, some had lap-spliced reinforcement.

All frames were infilled with hollow brick masonry walls. Masonry infill and plaster were made by ordinary workers the same way as in the standard practice. All specimens were white washed for better observation in the tests.

Figure 3.1 – General View of the Test Specimen

Except the reference specimens, all specimens were strengthened against lateral loads by means of precast reinforced concrete panels bonded on the masonry infill wall. Panels were composed of high-strength concrete (C40) and mesh reinforcement. Different types of panels and panel connections were tested. Properties of the precast panels are explained in Section 3.5. The bonding agent used for bonding the panels was SikaDur-31 epoxy mortar. This mortar is a two component adhesive with a tensile strength much higher than that of concrete. It is found to be very convenient for panel strengthening applications due to its rapid hardening rate, ease of preparation and viscosity level which makes it practical for vertical surfaces. By means of this mortar, panels were bonded to the masonry wall, frame members, foundation and each other. Welding was also used as a connection method for some specimens. Specimens were tested under a constant vertical loading and increasing cyclic lateral loading. The specimens used in this experimental research are listed in Table 3.1 below.

Table 3.1 – Test Specimens

Specimen	Reinforcement	Strengthening
CR	Continuous	Reference
CIA4	Continuous	Type A Panels
CIB4	Continuous	Type B Panels
CIC4	Continuous	Type C Panels
CID4	Continuous	Type D Panels
LR	Lap-Spliced	Reference
LIC4	Lap-Spliced	Type C Panels
LID4	Lap-Spliced	Type D Panels

A certain system of specimen designation was followed for all studies within precast panel strengthening research project. The first letter of the specimen name indicates if the specimen has continuous column reinforcement (C) or has lap-spliced bar connection at the foundation level (L). The second letter is a reference specimen (R), or strengthened with panels from the interior (I) or the exterior (E) side. The third letter denotes the panel type used for that specimen (A, B, C, D, …). The number at the end indicates that dowels were used on how many sides of the infill (1, 2 or 4). For example, specimen CIA4 has continuous column reinforcement, strengthened from the interior side with type A panels and dowels were used along four sides of the infill.

Substandard concrete strength was deliberately selected for the specimens. To represent the common practice in the existing building stock in Turkey, plain bars were used for the frame reinforcements, which have much less adherence with concrete than deformed bars.

Ductility of frame members was low, since insufficient ties were used in columns and the beam. Stirrups were $\phi 4$ bars and they were placed with a spacing of 100 mm, which is too much to provide any confinement effect. Also, beam-column joints were not confined. Confinement zones were not provided at beam and column ends. According to the Turkish Seismic Code, plastic hinge zones of reinforced concrete members should be confined more extensively, and this requirement was not met. In addition, stirrups had 90º hooks, contrary to the code specification of making 135º hooks to provide effective confinement by anchoring tie ends to the core concrete.

3.2 DIMENSIONS OF THE TEST SPECIMENS

The specimens are reinforced concrete frames consisting of two columns, one beam and a foundation beam. The columns are 100×150 mm and the beam is 150×150 mm in cross-section. The columns have a clear height of 750 mm. The beam is 1300 mm long. The foundation beam has 400 mm depth, 450 mm width and 1900 mm length. All dimensions are shown in Figure 3.2.

All specimens had hollow brick masonry infill. The bricks are also 1/3 scale and specially produced. The dimensions of a brick unit are shown in Figure 3.3. The bricks are bonded to each other by a cement-lime-sand mortar. The mix ratios and properties of the mortars are presented at Section 3.6.3. The masonry infill was covered by a plaster similar to the bonding mortar. At the interior side, only the face of the brick wall was plastered. On the exterior side, brick wall was plastered together with the beam and columns. The thickness of the plaster was about 10 mm. Lastly, the specimen was whitewashed in order to be able to distinguish the cracks and separations more clearly.

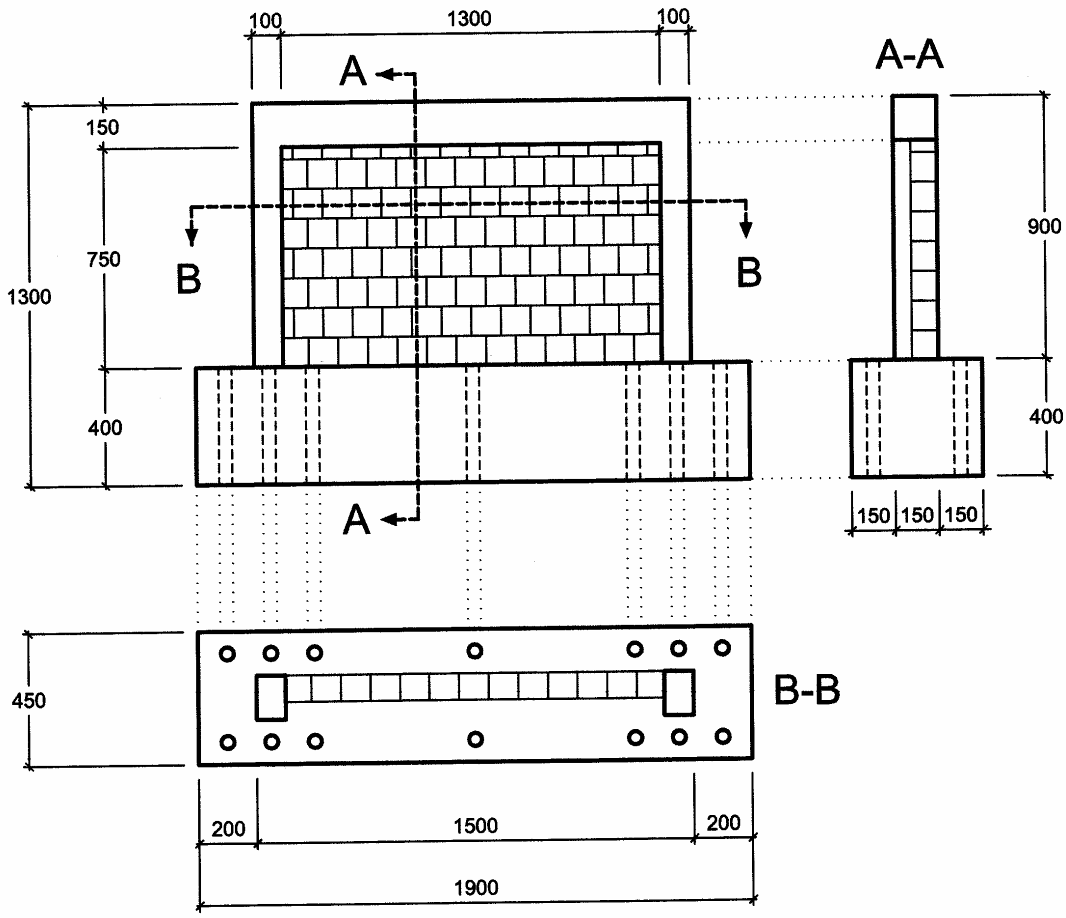

Figure 3.2 – Dimensions of the Test Specimens (dimensions in mm)

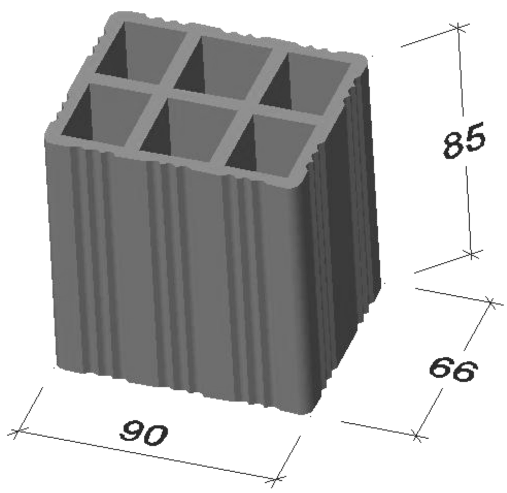

Figure 3.3 – Dimensions of the Hollow Clay Tile Bricks Used for Masonry Infill (dimensions in mm)

For the formwork, steel forms which were produced for another set of experiments were used. The forms originally belonged to similar but two-storey specimens which were also part of panel strengthening research series, and the necessary parts were used. Geometry of the formwork is given below in Figure 3.4 and Table 3.2. The assembled view of the formwork can be seen in Figure 3.5.

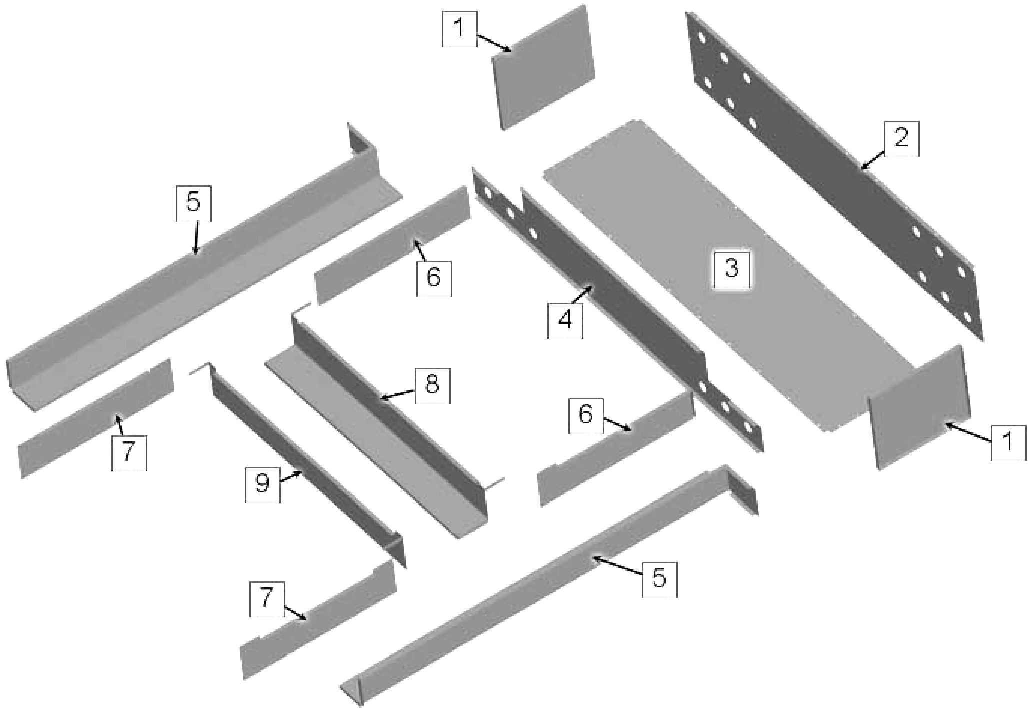

Figure 3.4 – Geometry of the Formwork

Table 3.2 – Dimensions of the Formwork Segments

Segment	Dimensions (mm)
1	450×400
2	1900×400
3	1900×450
4	1900×300
5	1800×150(100)
6	750×150
7	750×150
8	1300×150
9	1300×150

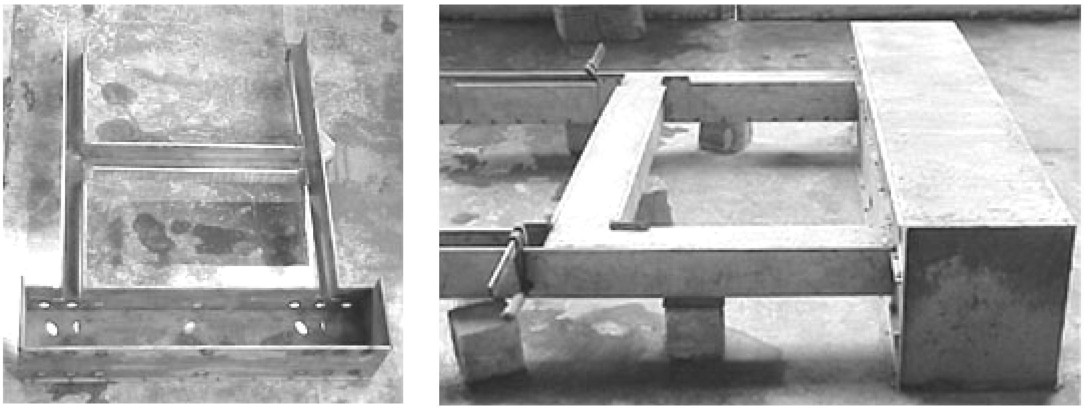

Figure 3.5 – Assembled View of the Formwork

3.3 DETAILING OF THE SPECIMENS

3.3.1 Detailing of the Foundation Beam

The foundation beam, which had been intentionally overdesigned, had a reinforcement of 5ϕ16 deformed bars at the top and 5ϕ16 bars at the bottom. Each of the longitudinal bars at the top and bottom are connected by ϕ14 bars welded to their ends. Transverse reinforcement was ϕ8 deformed bars with 150mm spacing which had 135° hooks at their ends. The foundation beam was designed to be strong enough not to cause any undesired failures during the tests. The details of the reinforcement for the foundation beam can be found in Figures 3.8 and 3.10.

3.3.2 Detailing of the Frames

a) Frames with Continuous Reinforcement

In the beam and columns, ϕ8 straight bars were used as longitudinal reinforcement. There were 6 ϕ8 bars in the beam and 4 ϕ8 bars in each column. Steel bars in columns extended to the bottom of the foundation continuously, and their ends were bended 90° for anchorage. Clear cover was 10mm. Properties of reinforcing bars are listed in Table 3.3.

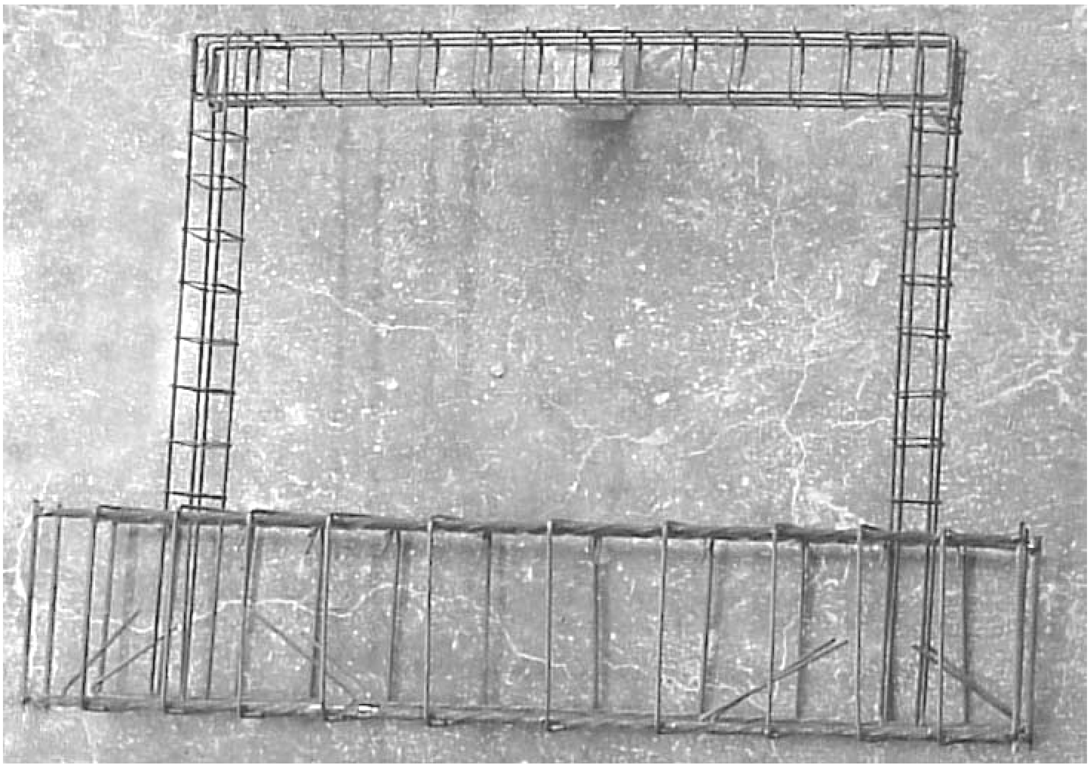

Figure 3.6 – General View of Reinforcement

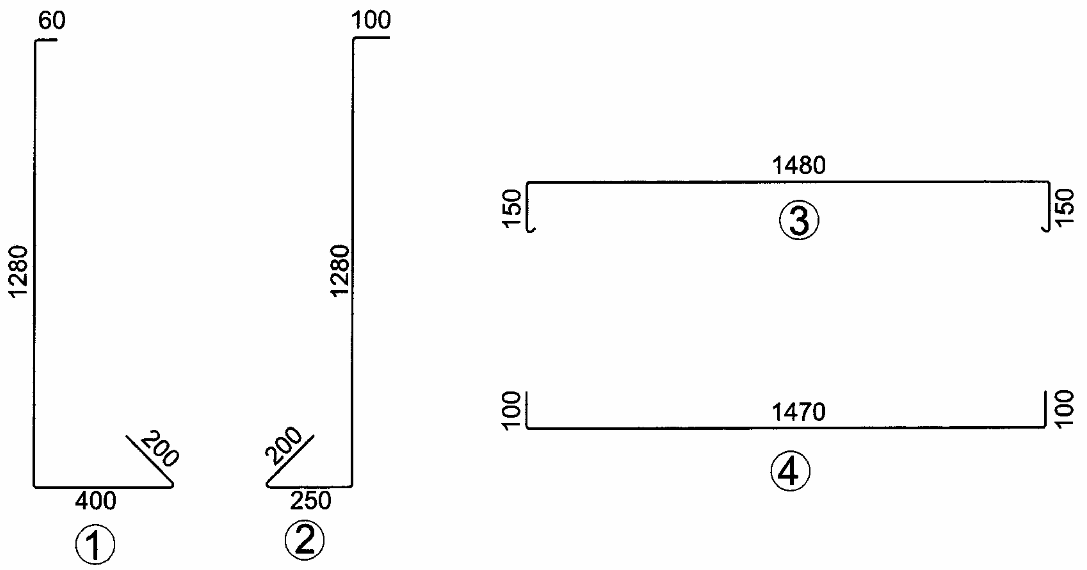

Figure 3.7 – Details of Reinforcement (dimensions in mm)

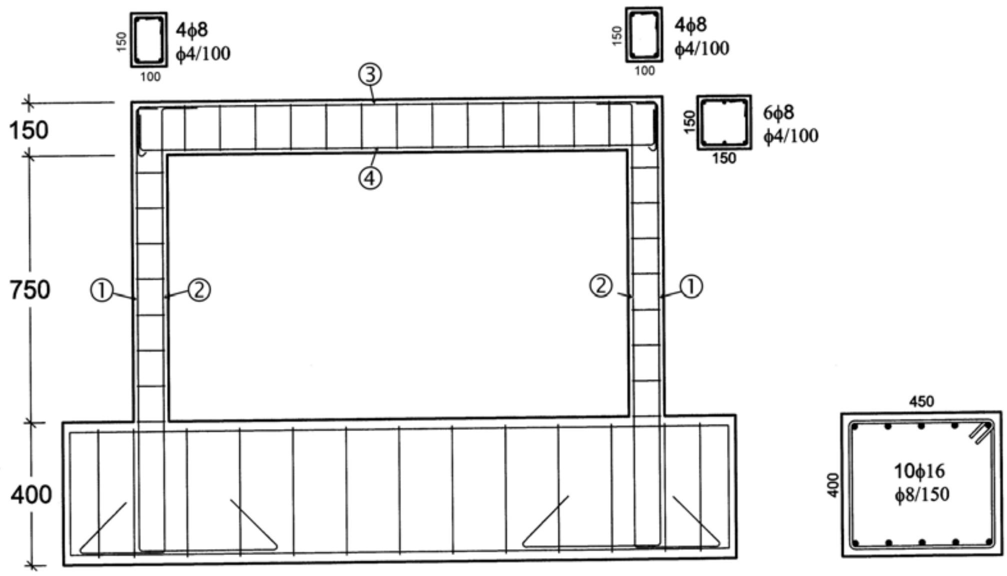

Figure 3.8 – Reinforcement Details of the Specimens with Continuous Reinforcement (dimensions in mm)

b) Frames with Lap-Spliced Reinforcement

Three specimens had lap-splices in column reinforcement in order to observe the effect of splicing on masonry infilled and strengthened frames. As in the common practice, lap splices were formed at the foundation level. Except the lap splices, the dimensions and reinforcement detailing are identical to frames with continuous reinforcement. Lap splice length was 160 mm corresponding to 20ϕ (20 times diameter of longitudinal reinforcement. A lap-spliced connection is shown in Figure 3.9.

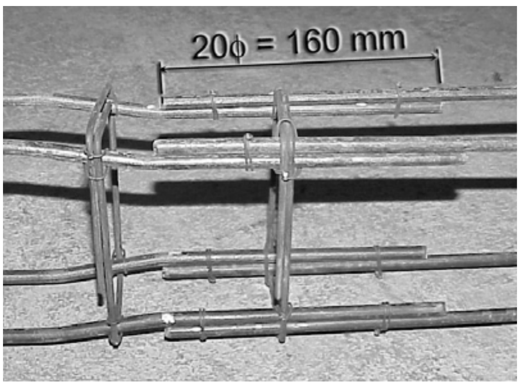

Figure 3.9 – Close View of Lap-Spliced Connection

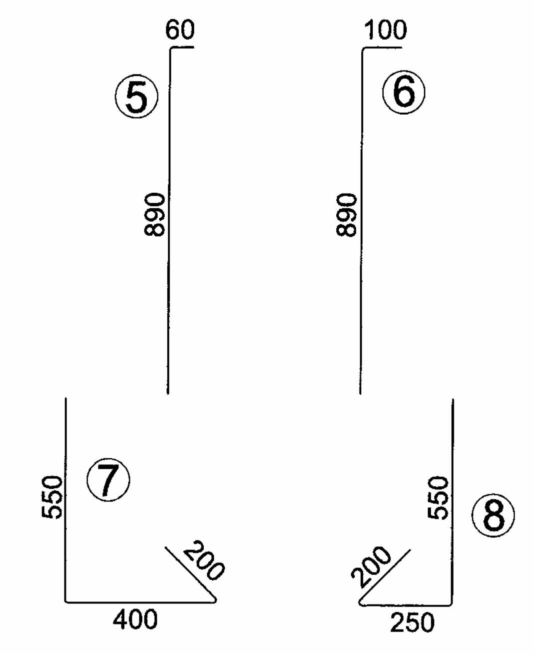

Figure 3.10 – Details of Reinforcement (dimensions in mm)

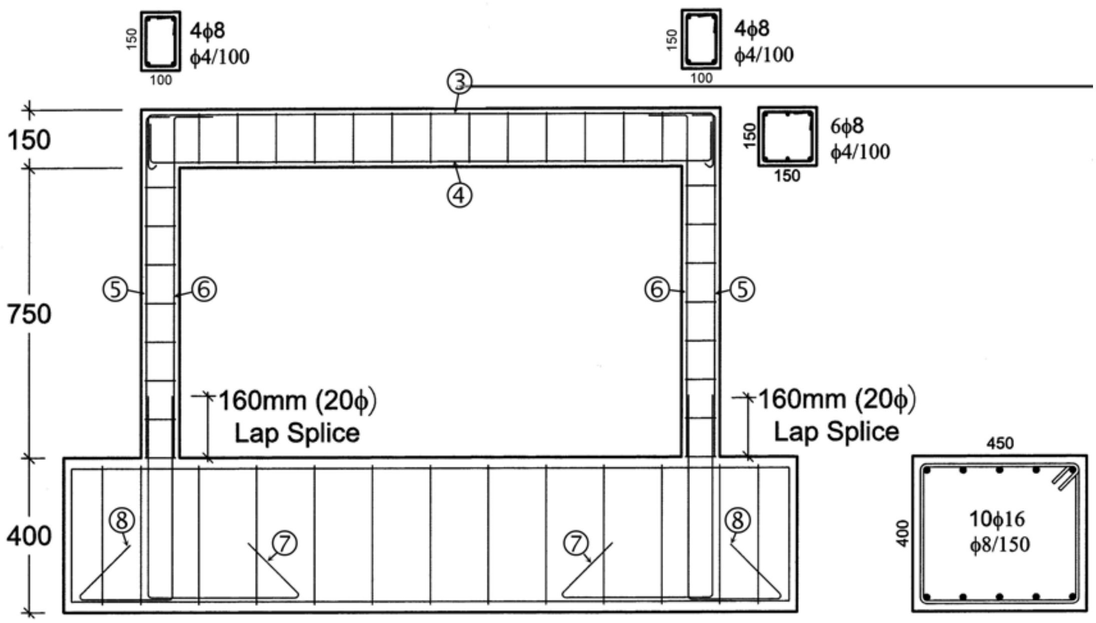

Figure 3.11 – Reinforcement Details of the Specimens with Lap-Spliced Reinforcement (dimensions in mm)

Table 3.3 – Properties of Reinforcing Bars in the Frames

Bar Location	Number of Bars	Bar Diameter ϕ (mm)	Properties	Yield Strength f_y (MPa)
Beam Longitudinal Bars	6	8	Plain	330
Column Longitudinal Bars	4	8	Plain	330
Transverse Reinforcement	–	4	Plain	220
Foundation Long. Reinf.	10	16	Deformed	420

3.4 UNIVERSAL BASE

For the test, the specimen was installed on a universal base which is fixed to the strong floor of the laboratory with steel bolts. The aim of this universal base was to prevent any lateral movement of the base of the specimen under the horizontal loading during the test.

The universal base is a reinforced concrete mat with 2950 mm length, 1500 mm width and 400 mm depth. Dimensions are given in Figure 3.12. Ready mixed concrete of 30 MPa strength was used. The concrete was self-compacting in order to eliminate vibrating.

The base was reinforced in two directions with ϕ14 and ϕ18 deformed steel bars at top and bottom. In the long direction, ϕ18 deformed bars were placed with 150 mm spacing, and in the short direction, ϕ14 bars were placed with 180 mm spacing. The longitudinal bars at the top and at the bottom were connected to each other by welding ϕ14 bars.

The strong floor in the Structural Mechanics Laboratory has a gallery underneath, and holes have been made in the floor opening to the gallery. In order to fix the foundation to the strong floor, six 60 mm diameter holes were formed in the foundation, coinciding with the holes in the strong floor. The foundation was fastened to the strong floor by 50 mm diameter prestressing bolts passing through these holes.

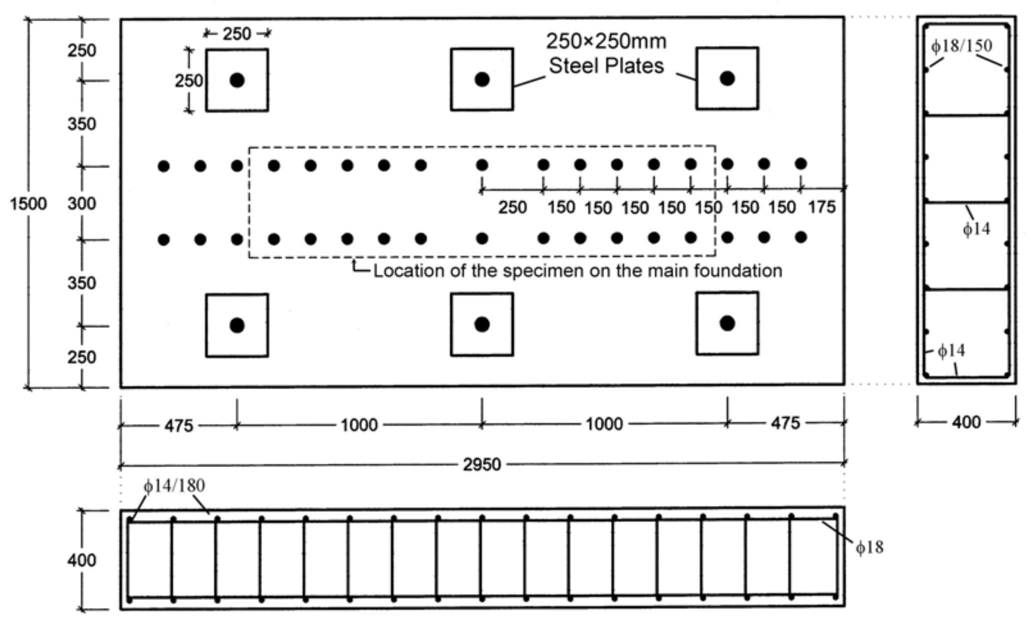

Figure 3.12 – Dimensions and Details of the Universal Base
(dimensions in mm)

In order to fasten the test specimen on the universal base, each specimen has 14 holes as was shown in Figure 3.1. The universal base was also designed to have M38 nuts corresponding to the holes of the specimens. On the foundation, 34 fastener bolt holes were arranged in order to be able to make use of it with different sized specimens.

3.5 PRECAST PANELS

3.5.1 General

Precast panel application is introduced as an innovative method of strengthening RC structures. It is proposed as an alternative to conventional strengthening techniques with its advantages like practical, fast and occupant-friendly application. Although panels of different geometry and detail are designed, they all are intended to have reasonable size and weight, so that they can be carried and installed by two workers at the most. Also, they should not be too large to pass through door openings, for applicability point of view. Therefore, the panels are proposed to be not as a single piece but smaller separate units placed side by side.

One approach is to arrange the panels in three rows and four columns, and another is to use panels having the full height of the infill in several lines. Since the infill dimensions of the ⅓–scaled test frames are 1300×750 mm, the first type of panels would be 320×245 mm, and the latter type dimensions would be 105×745 mm, considering also the thickness of the bonding material and imperfections. The two types of panel geometry are shown in detail in the following sections. The panel thickness was chosen as 20 mm. Therefore, the panels are about 3 kg in weight. This weight is for ⅓ scale panels, so the corresponding weight for the actual sized panels would be about 80 kg, which is not too heavy to restrain practical application.

The panels were produced from 1.5 mm thick forms made of steel. The forms, like the formwork for the frames, were composed of several pieces joined by bolts in order to extract the panels easily after hardening. The forms were also oiled for the same purpose. ϕ3 mesh steel with 50mm spacing was used as reinforcement. The mesh reinforcement was prepared by cutting and trimming from a larger steel mesh. 4 spacers were placed under the mesh to provide the clear cover spacing of 5 mm. A special admixture called Sikament-300 was also added to the concrete mixture of the panels for attaining higher strength, increasing workability, obtaining smooth finished surface and eliminating vibration. The details of concrete mix for precast panels and the admixtures will be described in Section 3.6.1.

The objective of precast panel strengthening method is to transform the hollow brick masonry wall into a composite and rigid infill. The performance of this lateral-load-resisting wall depends on the interaction between its two components; panels and the masonry wall, both of which has important functions. The panels provide stiffness and strength to the masonry wall and the wall holds the panels against out-of-plane deformations. Also, the composite infill should demonstrate composite action with the frame elements. Separation of the infill from the columns, beam or the base should be prevented.

Panel-to-panel connections were provided by the epoxy mortar called SikaDur-31. Type A and Type B panels also had projected steel bars at the corners to be welded to each other. Connection details are given for each type of panels in the following sections.

3.5.2 Shear Keys

Among the four types of panels, which are Type A, Type B, Type C and Type D, two of them (Type A and Type B) had extrusions called shear keys, which are intended to provide better bonding and improve shear force transfer between panels. Shear key widths are 10 mm for Type A panels and 20 mm for Type B panels. For Type A, shear key lengths changed between 61 and 78 mm, and for Type B, between 100 mm and 111 mm. Details of the shear keys are given in the following sections together with the panel details presented in the following sections.

3.5.3 Type A Panels

a) Panel Geometry

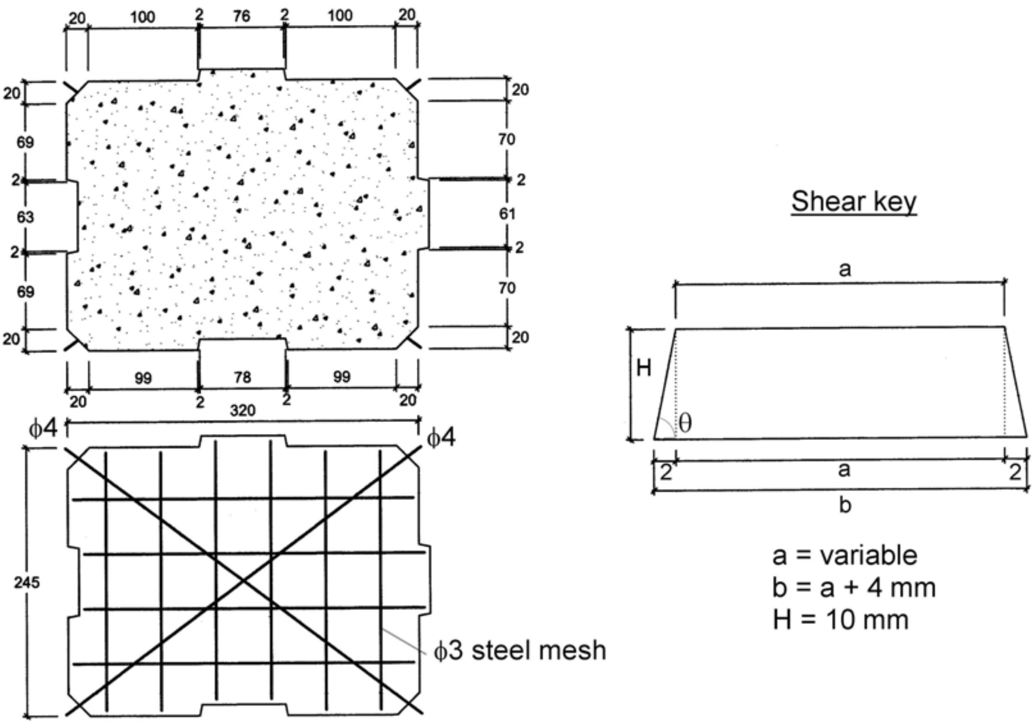

Figure 3.13 – Details of Type A Panels (dimensions in mm)

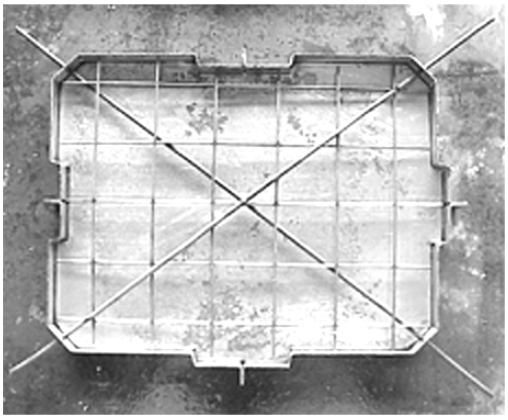

i) Panel form

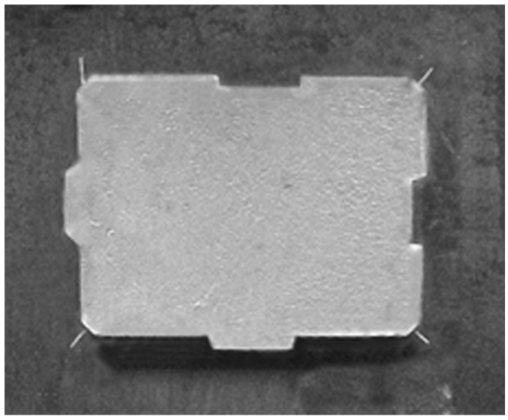

ii) Panel

Figure 3.14 – Type A Panels

Type A panels are rectangular panels of 320×245 mm and 20 mm thickness. These panels have ϕ3 mesh steel, and also, ϕ4 diagonal bars which are projected from the corners for welding with neighbouring panels. The diagonal bars were also used to weld-connect the panels to the frames by means of embedded dowels of ϕ6 deformed bars. Dowels were embedded to around 100 mm depth into the columns, beam and the base, and glued with epoxy. Type A panels also had shear keys.

b) Dowel Locations and Panel Arrangement for Type A Panels

Using Type A panels requires dowels to be embedded in the frame members and the base. The first operation of the panel application procedure is drilling ϕ8 holes 80 mm deep into the columns, beam and the foundation adjacent to the surface of the masonry wall. Dowel hole locations correspond to the corners of the panels and are shown in Figure 3.16. Then, the holes were cleaned with compressed air and wiped with moist rags. Dowel bars are ϕ6 deformed bars of about 120~130 mm in length. Their lengths had to be adjusted to match with panel steels. Epoxy was filled in the holes and the dowel bars were inserted.

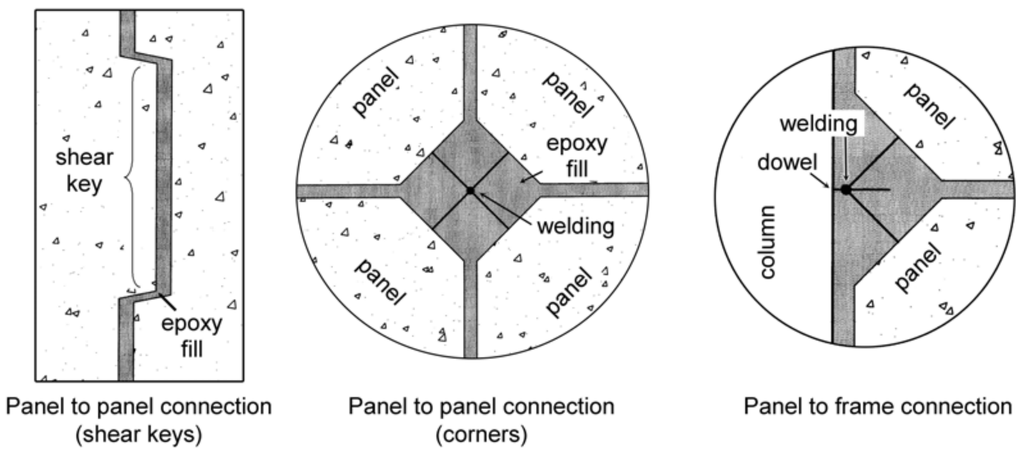

Figure 3.15 – Panel Connection Details

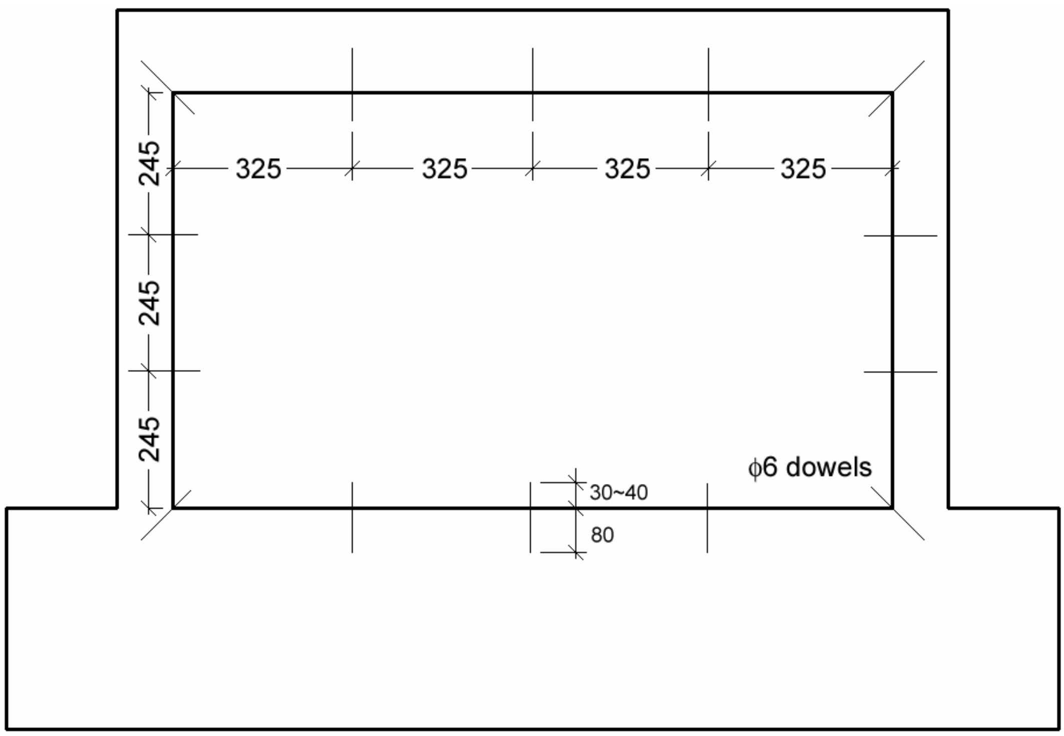

Figure 3.16 – Embedment of Dowels before Application of Type A Panels
(dimensions in mm)

After the hardening of epoxy, the dowels became ready for placement of panels. Covering one face with SikaDur-31 epoxy mortar, the panels were pasted firmly on the brick wall side by side. Interfaces with panels were also filled with epoxy layer except the corner zones. Then, the corner bars of the panels were welded to each other and the dowel bars. Lastly, epoxy mortar was again used to fill completely the corner regions. Connection details of the panels with epoxy and welding are shown in Figure 3.15 and the final layout is shown in Figure 3.17. Figure 3.18 shows some views from the application procedure.

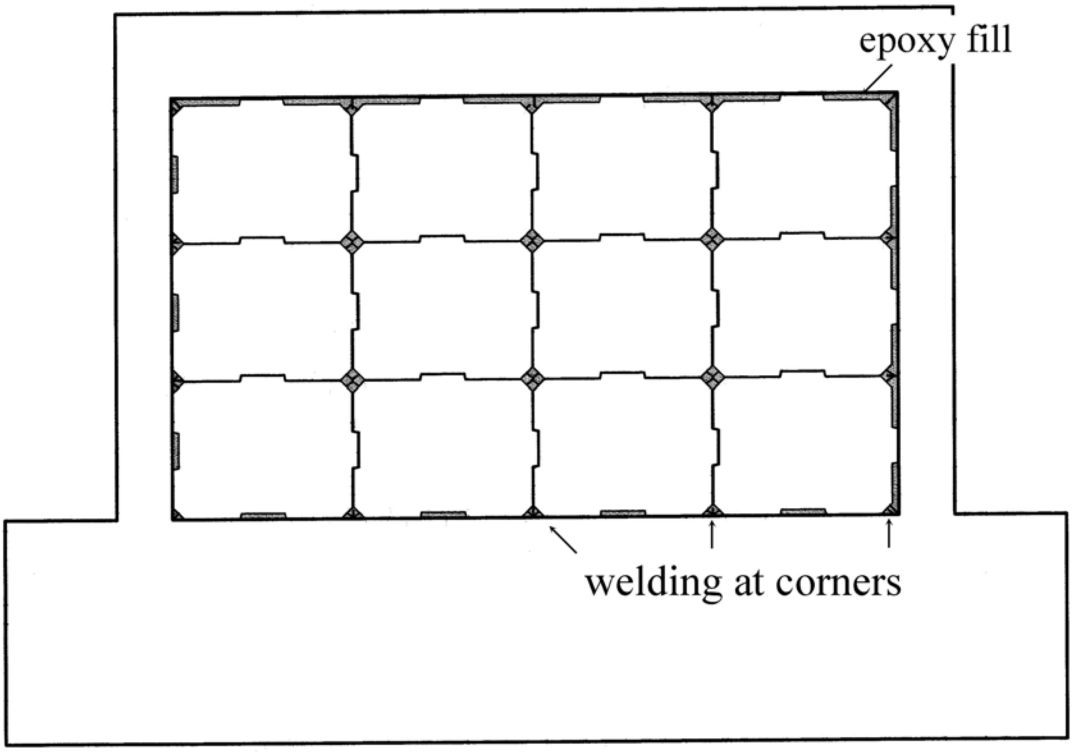

Figure 3.17 – Panel Arrangement for Type A Panels

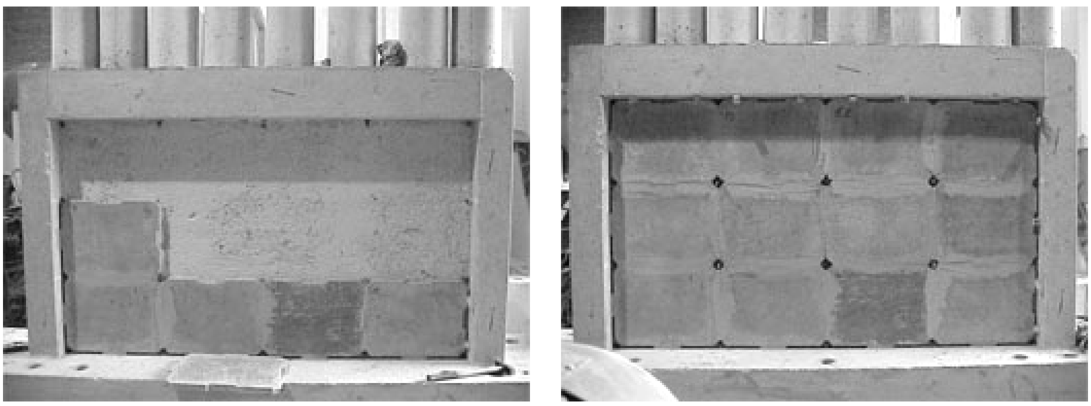

Figure 3.18 – Application of Type A Panels

3.5.4 Type B Panels

a) Panel Geometry

Type B panels are full height tall panels extending from the base to the lower face of the beam. Like Type A panels, these have shear keys and corner bars to be welded to each other. Panel dimensions are given in Figure 3.19. The geometry of Type B panels differs slightly for side and inner panels. Side panels have 3 $\phi6$ deformed bars which were designed to penetrate into the columns. $\phi6$ bars were cast together with the panels.

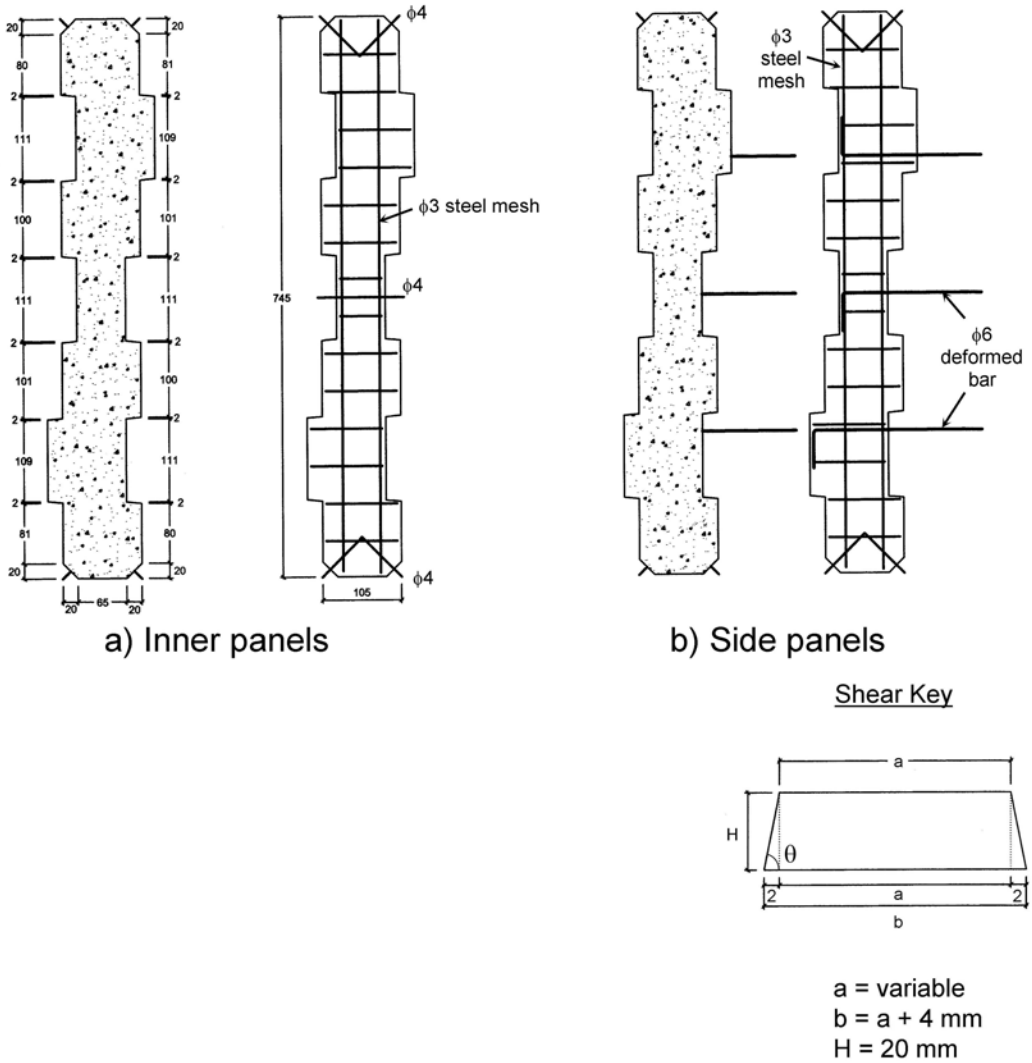

Figure 3.19 – Details of Type B Panels (dimensions in mm)

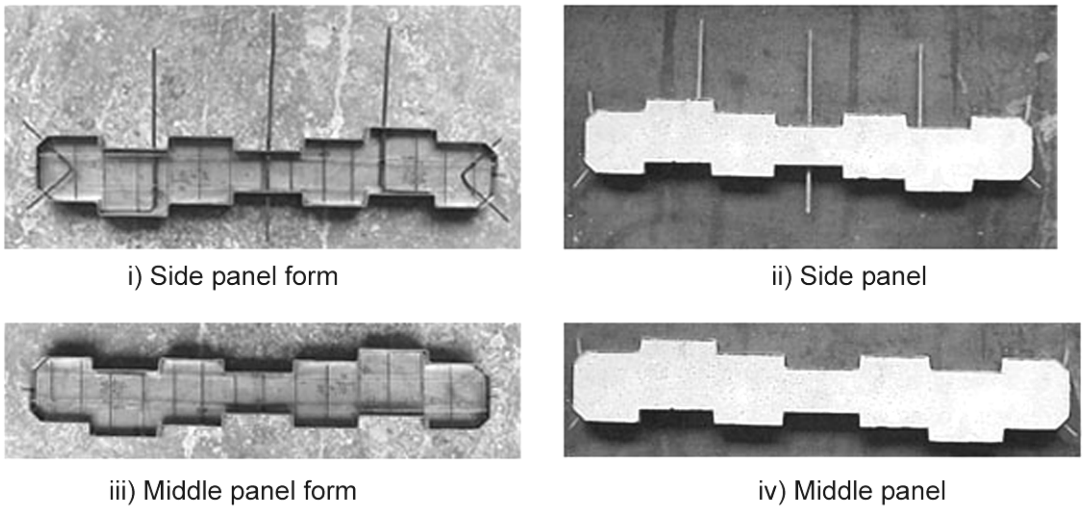

Figure 3.20 – Type B Panels

b) Dowel Locations and Panel Arrangement for Type B Panels

Application procedure for Type B panels was similar to that for Type A panels. 100 mm deep ϕ8 holes were drilled into the base and into the bottom face of the beam close to the face of the masonry wall, with 105 mm spacing, as shown in Figure 3.21. In each column, three similar holes were also made for the side panels. Holes were cleaned and the dowels were epoxy-glued to the holes at the top and at the bottom. Dowel bars in the side panels were also covered with epoxy and placed in the side holes together with the panels. Side panels were fixed to the masonry wall by the epoxy mortar at the same time. Other panels were then placed and fixed. After the corner bars were welded to each other, the remaining gaps were filled and finished with the epoxy mortar. Arrangement of the panels is shown in Figure 3.22.

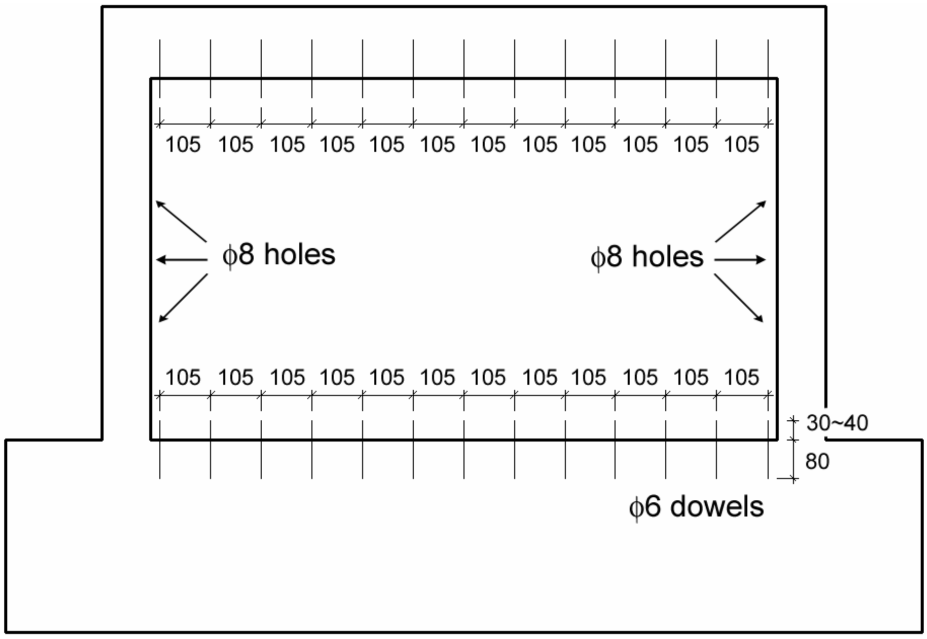

Figure 3.21 – Embedding of Dowels before Application of Type B Panels (dimensions in mm)

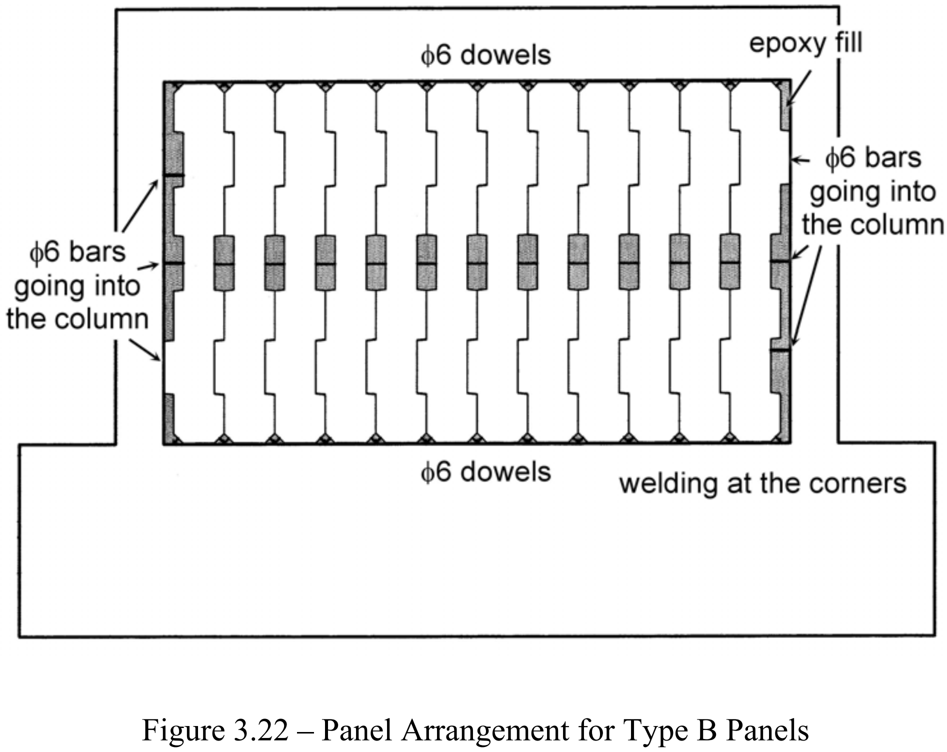

Figure 3.22 – Panel Arrangement for Type B Panels

3.5.5 Type C Panels

a) Panel Geometry

Type C panels are similar to Type A panels in general shape, except having no shear keys and corner bars. They are the simpler forms of precast panels. No welding is required and placement is easier. Dowel bars were again embedded in frame members and the base. In order to fit to the dowel bars, minor modifications were made in the geometry of perimeter panels. These are shown below in Figure 3.23 and Figure 3.24.

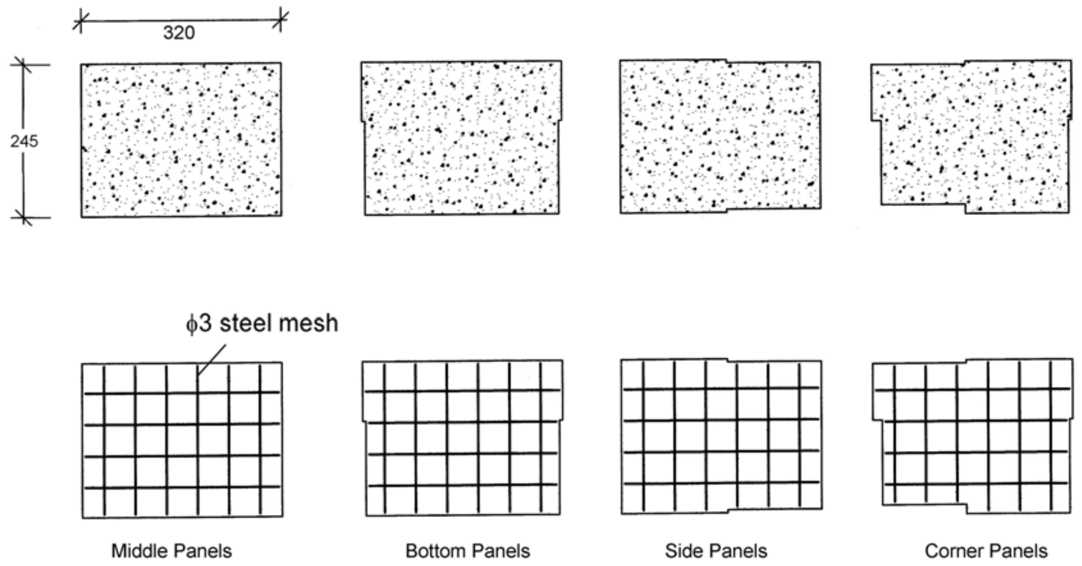

Figure 3.23 – Details of Type C Panels (dimensions in mm)

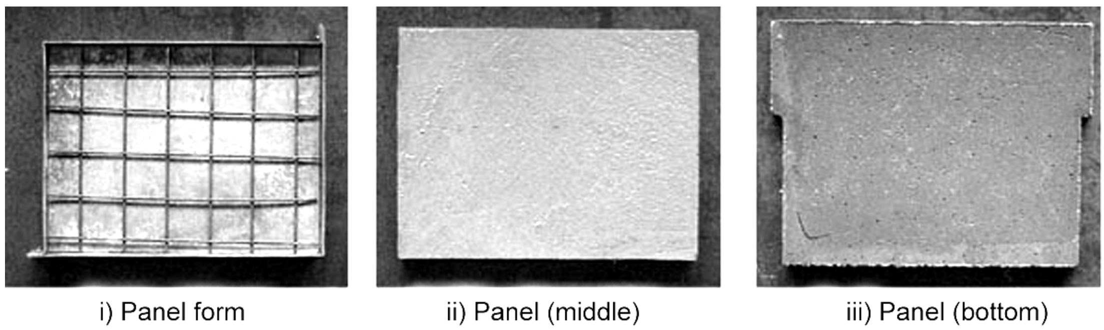

Figure 3.24 – Type C Panels

b) Dowel Locations and Panel Arrangement for Type C Panels

In this type of panels, dowels were not welded, but they were put between the panels and connection to the panels was provided only by epoxy. ϕ8 deformed bars were driven 100 mm in ϕ10 holes and 150 mm length was left outside. Dowel bars were fixed into the holes with epoxy. Then, the panels were installed over the masonry wall, covering back and side faces of each panel with the epoxy mortar. Figure 3.25 and Figure 3.26 present details of the application.

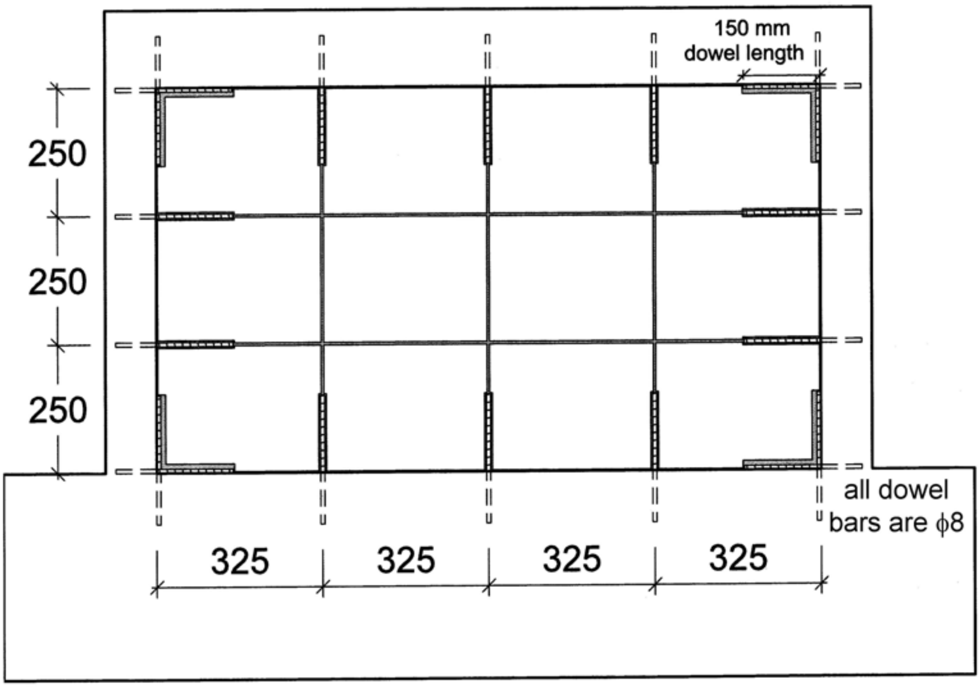

Figure 3.25 – Arrangement of Type C Panels (dimensions in mm)

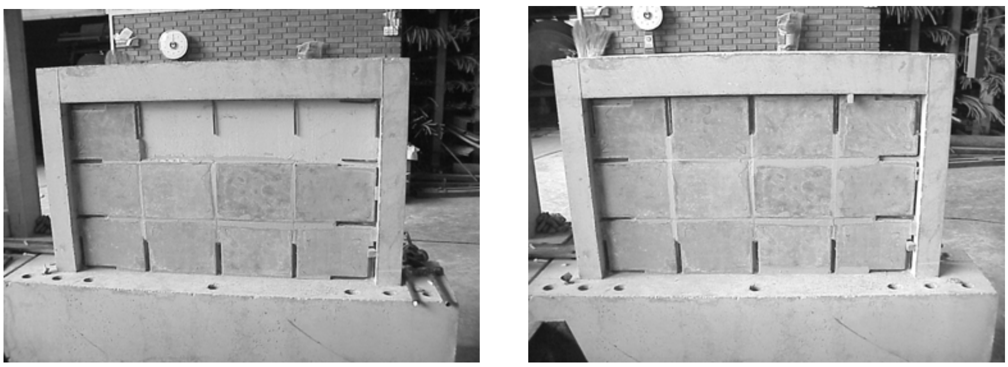

Figure 3.26 – Application of Type C Panels

3.5.6 Type D Panels

a) Panel Geometry

Type D panels are the simpler equivalents of Type B panels. Shear keys and corner bars are not present. Welding is not used for connection. Dowel bars were placed from top and bottom. Dowel bars were ϕ8 deformed bars and had 100 mm length inside the concrete and 150 mm length outside. In order to provide anchoring from all sides, the side panels were specially designed to have 3 ϕ6 deformed steel bar extensions. These extensions were inserted to corresponding holes in the columns and fixed with epoxy. Regular and side panel details are shown in Figure 3.27 and Figure 3.28.

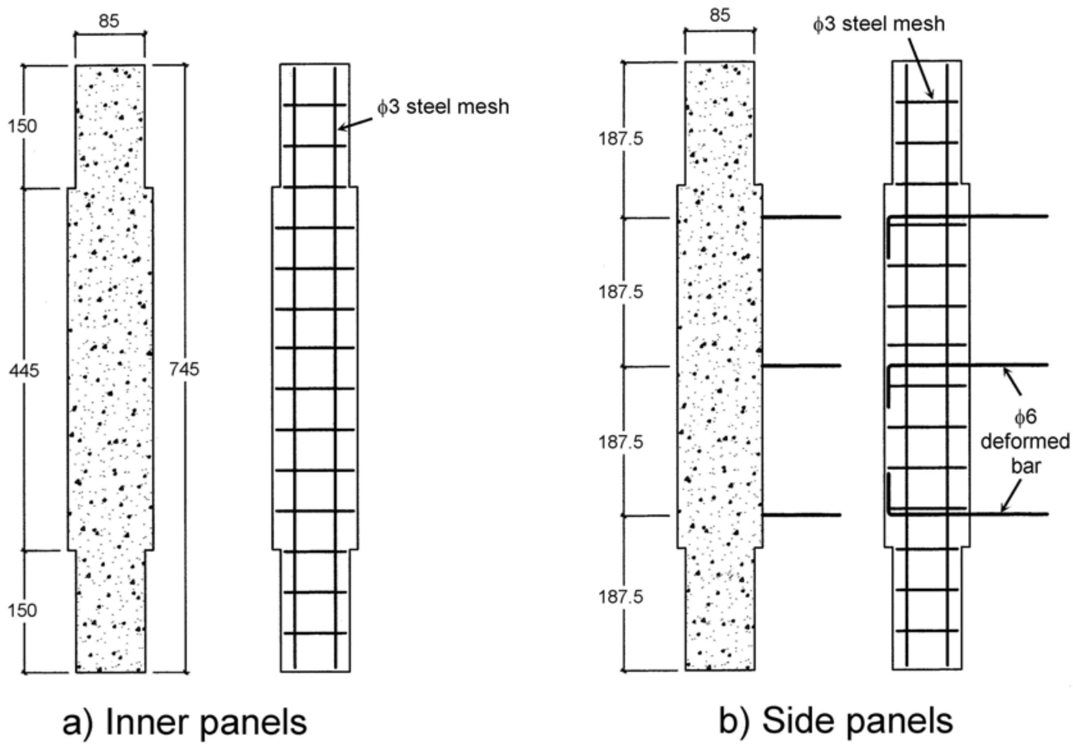

Figure 3.27 – Details of Type D Panels (dimensions in mm)

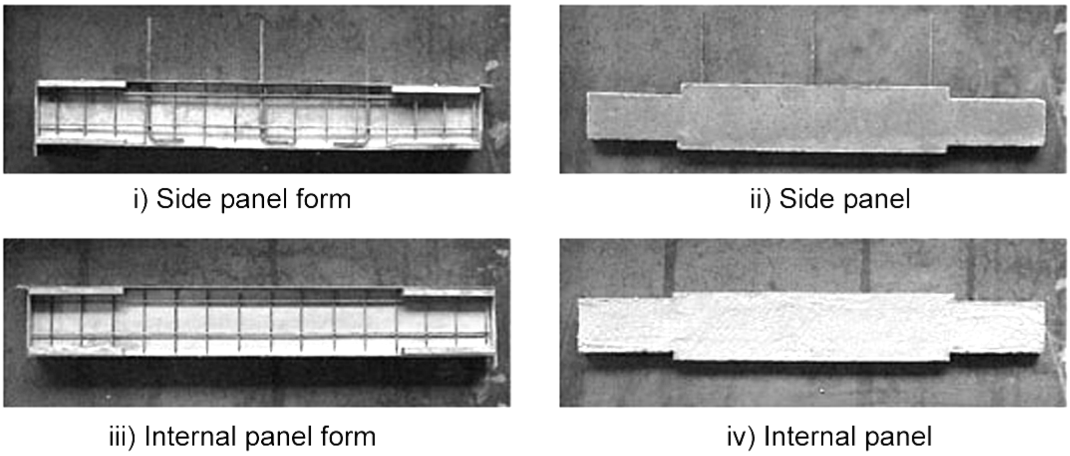

Figure 3.28 – Type D Panels

b) Dowel Locations and Panel Arrangement for Type D Panels

Dowel application was similar to the previously explained methods for other panel types. Panel arrangement can be seen in Figure 3.29. Panels were assembled the same way as Type B Panels.

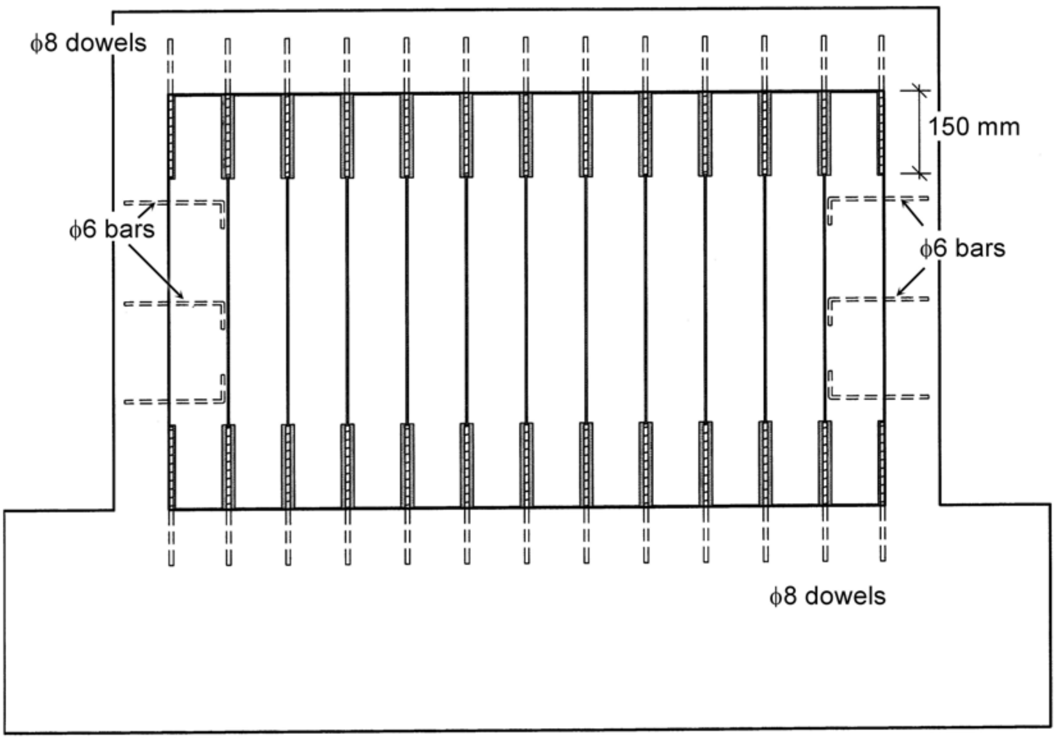

Figure 3.29 – Arrangement of Type D Panels (dimensions in mm)

3.6 MATERIALS

3.6.1 Concrete

a) Concrete used in the frame

The target concrete strength of the frame was 12 MPa, which is approximately the average grade for the existing reinforced concrete buildings in Turkey. The proportions of cement, aggregate, sand and water in the mixture is shown in Table 3.4. The concrete used for the frames were about 0.40 m^3. A total of 1050 kg concrete was mixed for each casting. Concrete was mixed in the mixer machine in the laboratory, and in two batches. Vibrator was used during casting.

Table 3.4 – Frame Concrete Mix Proportions (for 1 m^3 of concrete)

	Weight (kg)	Weight (%)
Cement	267	12
0 – 3 Aggregate	422	19
3 – 7 Aggregate	844	38
7 – 15 Aggregate	444	20
Water	245	11
Total	2222	100

In order to determine the compressive strength of the concrete, samples were taken during casting. Together with each casting, six cylinder samples were taken from the concrete. Cylinders were standard sized, with 150 mm diameter and 300 mm height. Samples were taken according to standard sampling procedures. The cylinder samples were kept near the specimens and in the same conditions. At the test date, the cylinders were capped and tested for axial compression. Results of the cylinder tests are provided in Table 3.5.

After casting, the specimens were unmoulded in the following 4 or 5 days. Concrete was cured for 7 to 14 days by covering the specimens with wet burlap. The moisture of the concrete was maintained and heating was applied if necessary.

Table 3.5 – Results of Cylinder Tests for Frame Concrete (MPa)

Specimen	Cylinder						f_{cm} (average)
	1	2	3	4	5	6	
CR	14.2	18.1	14.0	18.2	13.2		15.6
CIA4	21.6	15.7	16.3	18.5	21.1		18.7
CIB4	11.9	13.3	11.6	11.8	12.7		12.2
CIC4	15.6	13.1	16.3	13.4	13.0	14.2	14.2
CID4	9.8	10.7	11.6	8.8	16.6	9.5	11.1
LR	9.2	9.7	9.7	9.8	9.9	10.0	9.7
LIC4	15.5	13.8	13.4	16.8	17.6	17.2	15.7
LID4	9.7	10.1	10.1	10.1	10.5	9.8	10.1

b) Concrete used in the panels

In panels, relatively high strength concrete was used. Concrete grade of the panels was C40. The mix proportions of panel concrete are given in Table 3.6. A water reducing admixture called Sikament-300 was added to the concrete mix in order to:

– Achieve high strength,
– Increase workability with less w/c ratio,
– Eliminate vibration,
– Have an accelerated rate of hardening,
– Reduce voids in the concrete, and
– Obtain a good surface finish.

Table 3.6 – Panel Concrete Mix Proportions (for 1 m^3 of concrete)

	Weight (kg)	Weight (%)
Cement	501	19
0 – 3 Aggregate	994	38
3 – 7 Aggregate	857	33
Water	276	10
Sikament300	4	0.15
Total	2632	100

Each panel had about 1565 cm^3 (1.565×10^{-3} m^3) volume. In a few days, the panels were taken out of the forms and kept submerged in the water in the curing pool until usage. 6 cylinder samples were taken from the concrete for each batch and they were tested in the testing day. The results of compressive strength tests of panel cylinders are presented in Table 3.7.

Table 3.7 – Results of Cylinder Tests for Panel Concrete (MPa)

Panel	Cylinder No.						f_{cm} (average)
	1	2	3	4	5	6	
Type A	39.0	41.0	30.8	27.6			34.6
Type B	46.1	42.5	47.7	49.9			46.5
Type C	37.6	34.2	40.7	39.6	39.7	37.3	38.2
Type D	45.6	44.2	45.6	46.0	46.5	42.5	45.1

3.6.2 Steel

Steel reinforcement of various type and dimensions were used in the specimens. Frame longitudinal bars were $\phi 8$, frame transverse reinforcement was $\phi 4$, foundation longitudinal reinforcement was $\phi 16$ and foundation transverse reinforcement was $\phi 8$ bars. In the frame, plain bars were used, but the reinforcement in the foundation was deformed bars. List of reinforcing bars and their properties are given in Table 3.8 below. $\phi 6$ deformed bars were used as anchor dowels for panel types A and B, and dowels of $\phi 8$ deformed bars were used for types C and D.

Table 3.8 – Properties of Reinforcing Bars

Bar Diameter, ϕ	Property	Yield Strength, f_y (MPa)
$\phi 4$	Plain	220
$\phi 6$	Deformed	378
$\phi 8$	Plain	330
$\phi 8$	Deformed	330
$\phi 16$	Deformed	420

Other than these listed, $\phi 3$ mesh steel and $\phi 4$ plain bars were used inside the panels. $\phi 6$ deformed bars were also placed in some of the panels.

3.6.3 Masonry Infill

Masonry infill walls of the frames were made by using specially produced ⅓-scale hollow brick units. Geometry and dimensions of the bricks are given in Figure 3.3. The compressive strength of the brick units had been tested by Duvarci [1] and given in Table 3.9.

Table 3.9 – Results of Compression Tests of Brick Tiles (MPa) [1]

Tile No.	Failure Load (kN)	Compressive Strength (Net Area)	Compressive Strength (Gross Area)
1	46.1	14.55	7.76
2	55.9	17.65	9.41
3	42.2	13.32	7.10
4	42.2	13.32	7.10
5	59.8	18.88	10.07
6	53.0	16.73	8.92
Average	49.87	15.74	8.39

Masonry wall was produced by binding the brick units with cement-lime-sand mortar. The mix proportions of the ingredients of this plaster are found in Table 3.10. The same mixture was used for plastering the masonry infill on both sides. Plaster was applied approximately 1 centimeter. At the interior side, only the surface of the masonry wall was plastered, but at the exterior side, both the wall and the frame members were covered by plaster. Small sized cylinder samples were taken from the mortar. 3 samples were taken from each mortar mix. Sample cylinders had 75 mm diameter and 150 mm height. The samples were tested to obtain the compressive strength of the mortar and the plaster. Compressive test results of mortar samples are given in Table 3.11.

Table 3.10 – Mix Proportions for Plaster and Mortar

	Weight (%)
Cement	10
Sand	65
Lime	10
Water	15
Total	100

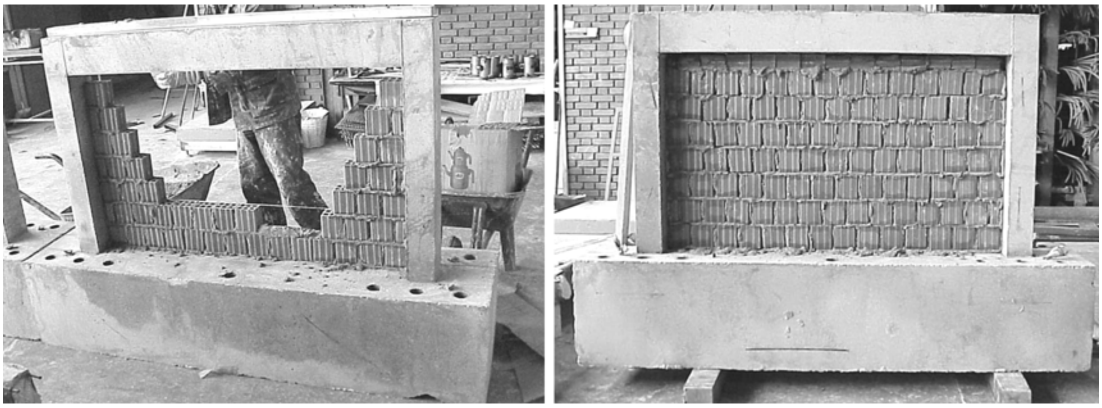

Figure 3.30 – Construction and Final View of the Masonry Infill (without plaster)

Table 3.11 – Results of Cylinder Tests for Mortar and Plaster (MPa)

Specimen	Cylinder No.			f_{mm} (average)
	1	2	3	
CR	6.4	5.5	6.4	6.1
CIA4	3.8	4.0	6.0	4.6
CIB4	2.8	3.6	3.9	3.4
CIC4	5.6	4.5	5.6	5.2
CID4				
LR	5.1	4.1	5.5	4.9
LIC4				
LID4	3.2	3.1	3.5	3.3

3.6.4 Epoxy Mortar

SikaDur-31 epoxy mortar was used for bonding the panels to the masonry wall, to frame elements and to each other. SikaDur-31 is a two component epoxy adhesive generally recommended for reinforced concrete repair works. It is obtained by mixing the two components with a ratio of 1:3 and mixing. The material properties of SikaDur-31 epoxy adhesive are given in Table 3.12. This material was preferred due to its advantages such as:

– Easy application and preparation, and good workability
– Thixotropic* consistency allowing application for vertical surfaces
– Suitability for dry or damped environments
– Suitability of its material properties (strength, adhesion)
– Relatively inexpensive price

Table 3.12 – Properties of Sikadur-31 (as given in the catalog)

Compressive Strength	65 MPa
Tensile Strength	20 MPa
Adhesion (Steel)	20 MPa
Adhesion (Concrete)	3.5 MPa

* Thixotropic : the property of various gels of becoming fluid when disturbed (as by shaking)

CHAPTER 4

TEST SETUP AND PROCEDURE

4.1 TEST SETUP

The test setup is built in METU Structural Mechanics Laboratory. The setup consists of a universal base, test specimen, a steel frame around the specimen to control out-of-plane displacements, loading system and a reaction wall (Figure 4.1). The Laboratory has a strong floor of 600 mm thickness. This slab also includes holes with 150 mm diameter which are used to prestress the specimens to the floor. The main foundation was fixed to the strong floor by six 50-mm diameter high-strength steel bolts. The specimens were fixed on top of the main foundation by fourteen 45-mm bolts.

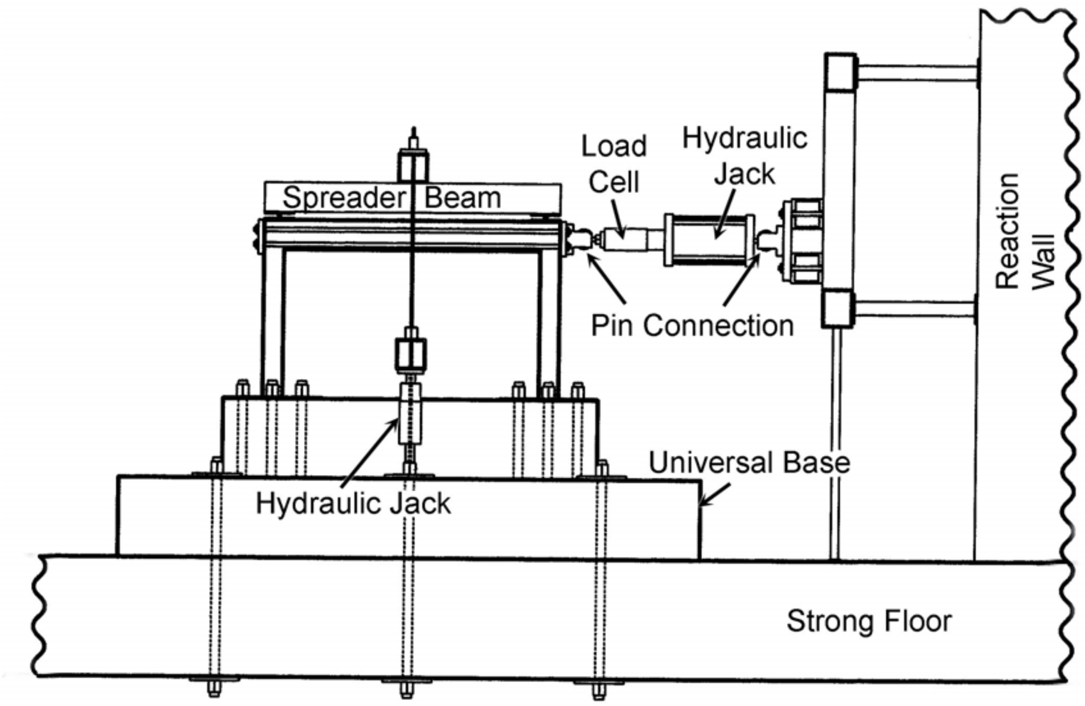

Figure 4.1 – Test Setup

For applying lateral loads a 4.5-meter high reaction wall had been constructed. This reaction wall is also prestressed to the strong floor by means of bolts. Holes are present on the vertical face of the wall for installing lateral loading mechanisms. Details of the loading mechanism will be given in Section 4.2.

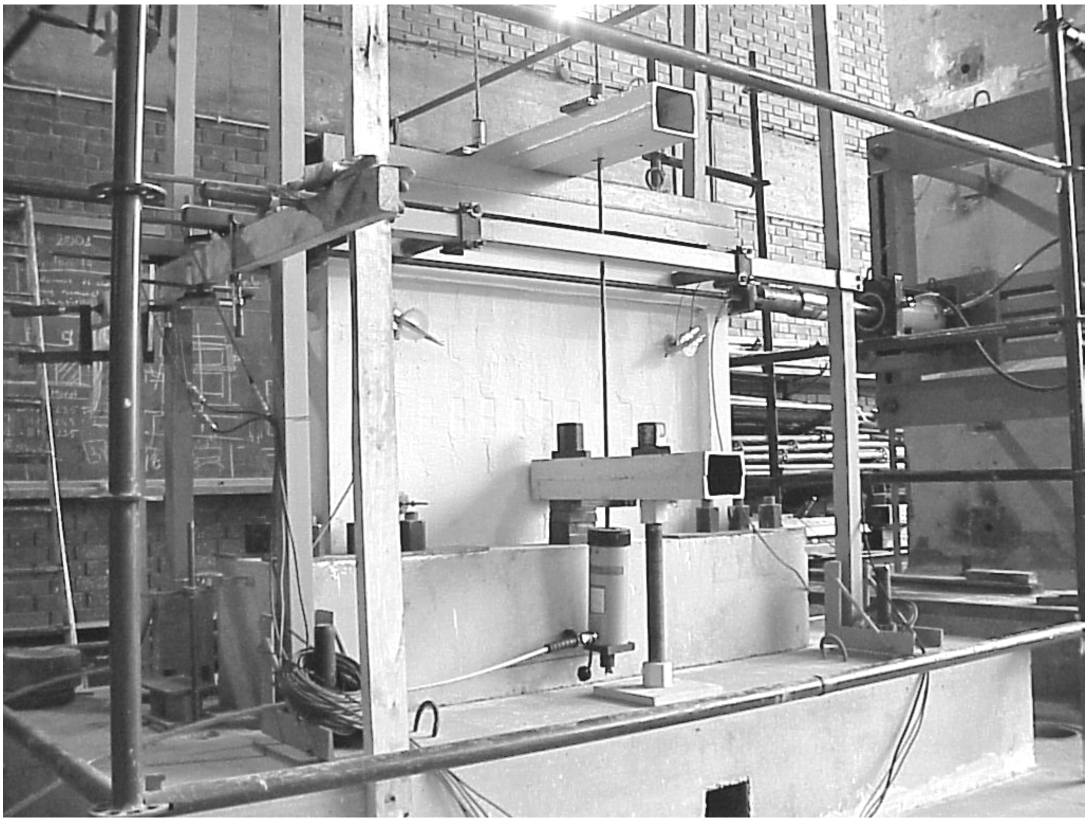

Figure 4.2 – Specimen in the Test Setup

As seen in Figure 4.2, specimens were placed on top of the main frame and inside a steel frame which was fixed to the main frame. The steel frame was also supported by the laboratory wall by L-section steel bars. Since the masonry infill and panels were placed on the back side of the specimen, this produced some eccentricity with respect to the loading axis. In the preliminary tests with this setup, twisting of the specimen was observed [1]. Therefore, this steel frame was intended to prevent out-of-plane deformations, i.e., torsion of the specimen by providing lateral support to the beam with rollers. These are called ball transfer units and a close-up view is given in Figure 4.6. Ball bearings have an axial load capacity of 2.5 kN and functioned effectively in all tests.

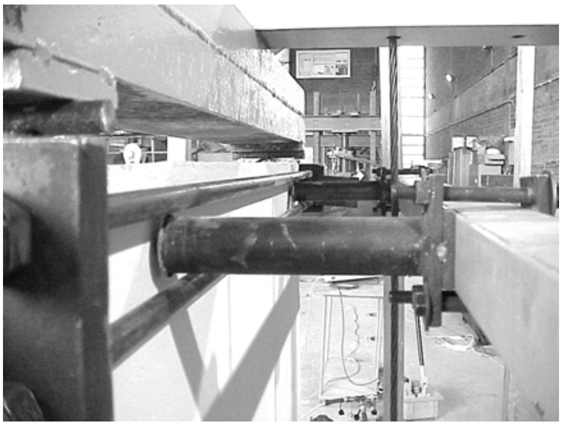

Figure 4.3 – Ball Bearings

4.2 LOADING SYSTEM

a) Vertical Loading

During the test, a constant axial load was applied to the specimens. The load was applied by two hydraulic jacks on two sides and as seen from Figure 4.1, the load is transferred to the cross beam by cables. The cross beam was connected to the center of the spreader beam, so the load was distributed equally by means of a spreader beam. The spreader beam and the cross beam are both steel box sections welded to each other.

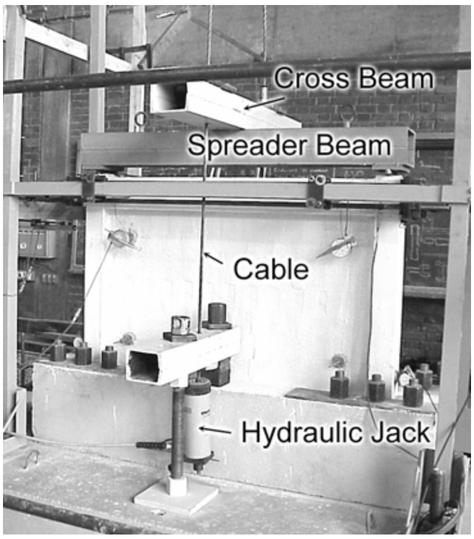

Figure 4.4 – Elements of the Vertical Loading System

The axial load level on the columns was kept constant throughout the test. Axial load was different for specimens with continuous and lap-spliced reinforcement. The axial load values used for each specimen are given in the Test Procedure Section (Section 4.4)

b) Horizontal Loading

The specimens were tested with hysteretic lateral loading for modelling ground motion effect. A sketch of the lateral loading system is shown in Figure 4.5. The system consists mainly of an adjustable steel frame attached to the reaction wall, a load cell, a hydraulic pump and pin connections at either end of the loading column consisting of the jack and load cell.

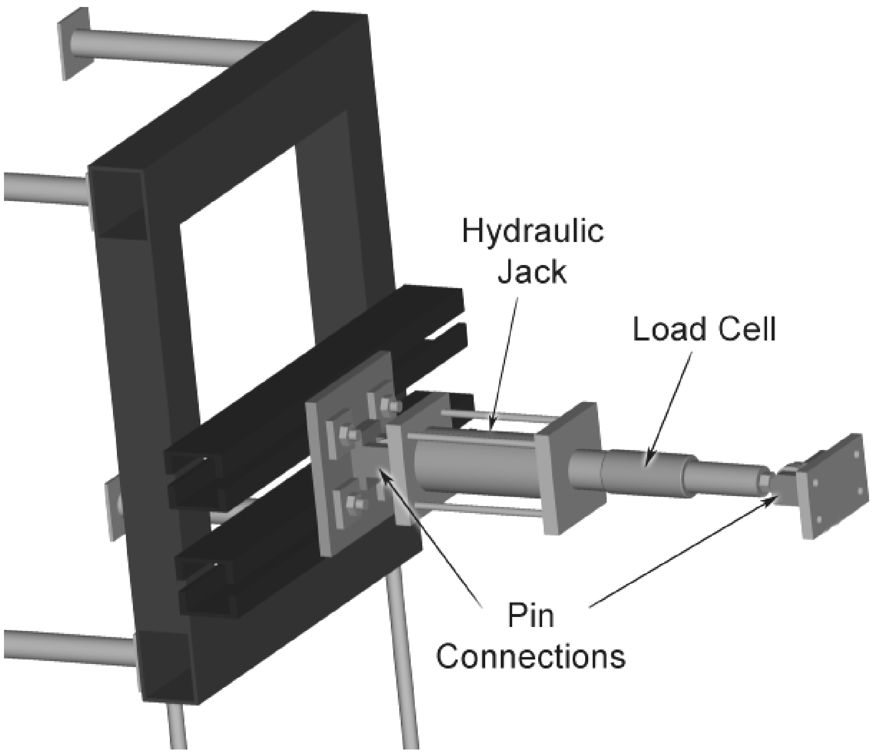

Figure 4.5 – Lateral Loading System

Loading was applied by the assemblage of a hydraulic jack and a load cell with pin connections at the ends. Figure 4.6 shows a detailed view of this assembly. The pin connections at the ends provide the system to create axial stress only. The pin connections can be seen in detail in Figure 4.7.

The hydraulic jack has a capacity of 600 kN in under tension and 450 kN under compression. The load cell used in the test was able to record up to 600 kN force and it was calibrated in the Structural Mechanics Laboratory before the tests.

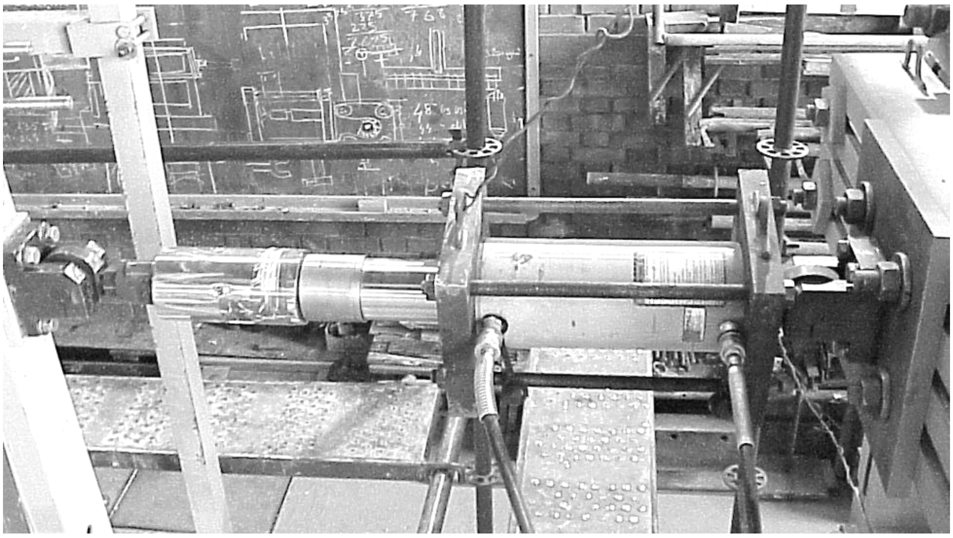

Figure 4.6 – Lateral Loading System

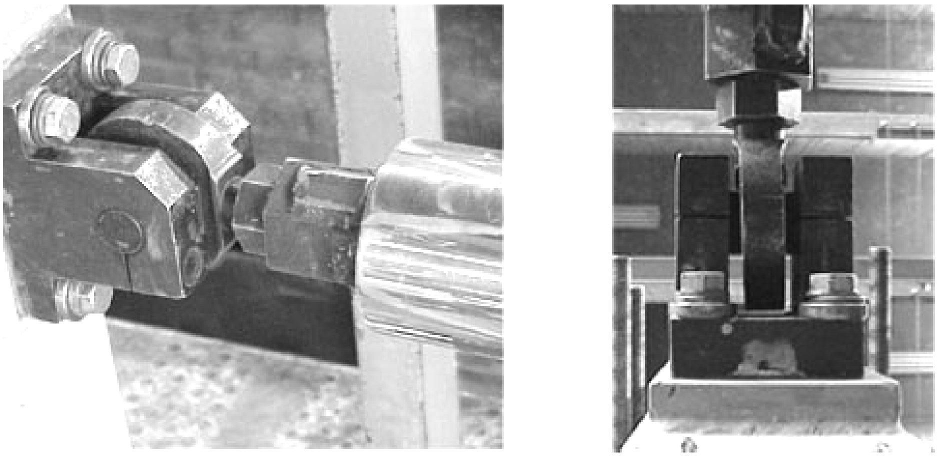

Figure 4.7 – Close View of the Pin Connections

The lateral load was planned to act in two directions; pushing and pulling. To achieve this aim by a loading system at one side, steel plates were attached to both ends of the beam with four steel bars. This way, it became possible to apply the load in two directions from one side. The steel bars connecting the plates were loosely clamped not to cause a confining effect.

Lateral load was applied from the top of the frame. The axis of the pump was aligned to the centroid of the beam section. In the tests, the loading was applied in cycles. Each load level was repeated in reverse direction before proceeding to the next load level. The loading schemes are given in Section 4.4.

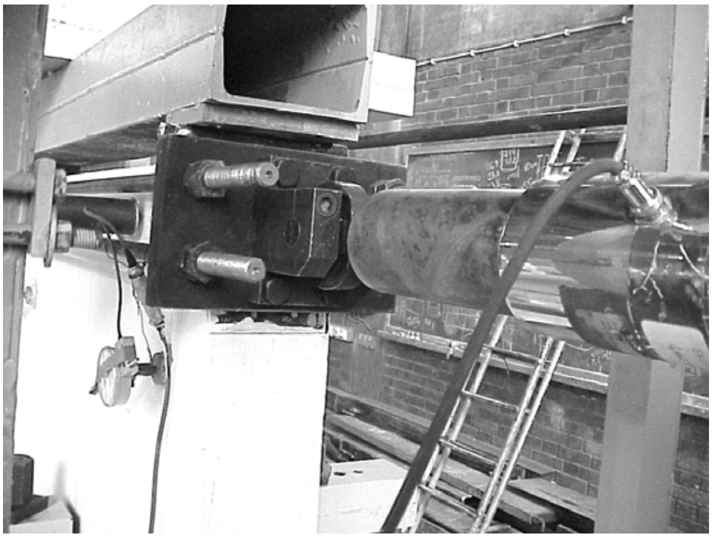

Figure 4.8 – Steel Plates for Loading in Two Directions

4.3 INSTRUMENTATION

In order to record deformations, linear variable displacement transducers (LVDT) and dial gauge type measurement devices were used. The positions of the gauges are shown in Figure 4.9. The lateral load was also being recorded by a load cell throughout the tests. The data were continuously collected by a data logger attached to a personal computer.

4.3.1 Dial Gauges

A total of six dial gauges were used. Four of the dial gauges were located on the specimen (1, 2, 3 and 4 in Figure 4.9) and connected to the data acquisition system. The other two dial gauges were measuring the relative displacement of the foundation beam with respect to the main foundation (gauge 9 in Figure 4.9) and the relative displacement of the main foundation with respect to the floor (gauge 10 in Figure 4.9), and these were read directly. These last two gauges were installed in order to insure that no slip would occur, and they showed almost zero measurements in all of the tests.

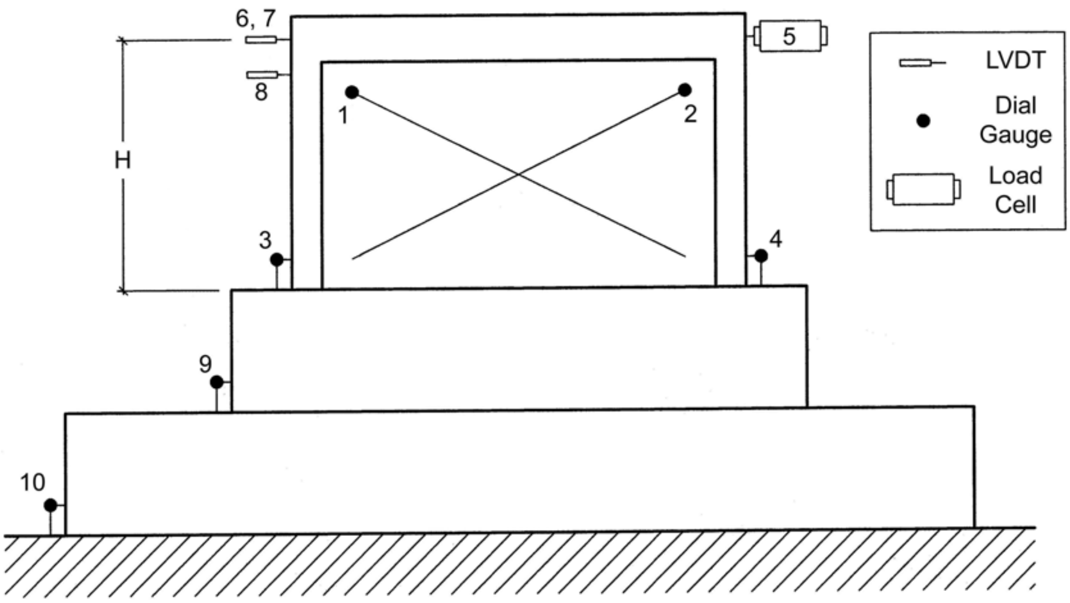

Figure 4.9 – Instrumentation

Two dial gauges were arranged to measure the diagonal displacement between the opposite corners of the infill (gauges 1 and 2). These 20-mm gauges took measurements on the cable attached to thin bars fixed on the infill wall surface. Two 50-mm gauges were placed at the lower ends of the columns (gauges 3 and 4) in order to measure the variations in the column-base rotations, and also cracking under tension and crushing under compression.

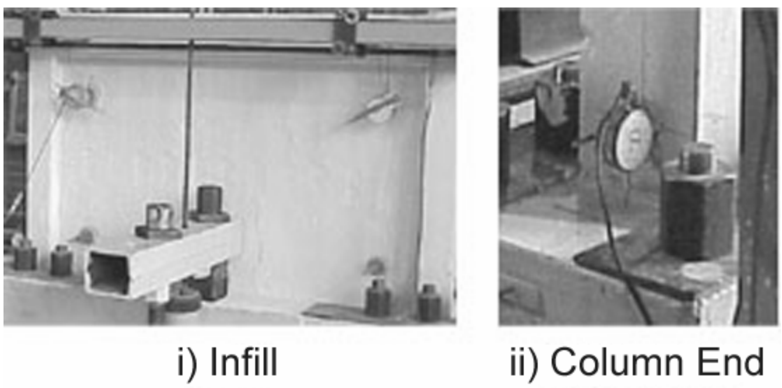

Figure 4.10 – Dial Gauge Positions

4.3.2 LVDTs

The LVDT (also known as Linear Variable Differential Transformer) is a measurement device that produces an electrical voltage proportional to the displacement of a movable magnetic core.

LVDT type displacement measurement devices were used for lateral displacements. Two LVDTs (6 and 7) were positioned at the beam level, aligned with and opposite to the loading axis. They were put as a pair to obtain a more accurate recording by taking their average. Another LVDT device (8) was installed below LVDTs 7 and 9 aligned to the column center-line. LVDT devices used in the specimen are shown in Figure 4.11. All LVDTs had a measurement capacity of 200 mm.

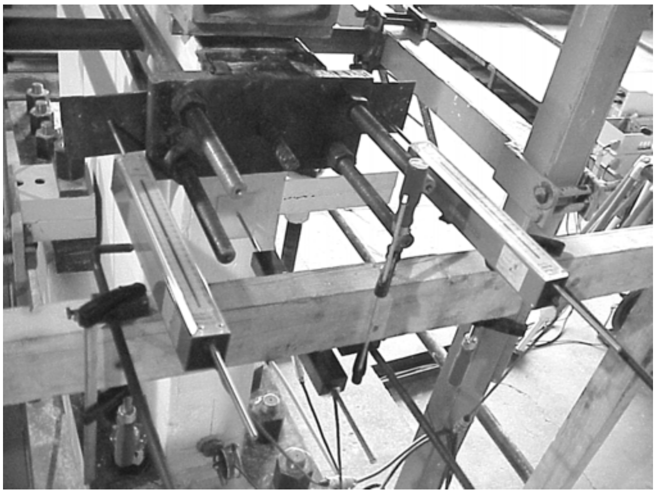

Figure 4.11 – LVDTs

4.3.3 Load Cells

A load cell was attached to the lateral loading system (See Figures 4.5 and 4.6) and used to measure the input lateral load. This load cell had a measurement capacity of up to 600 kN both in tension and compression.

Also, another load cell was used in order to monitor the axial load level on the columns, which was supplied by a separate loading system (Section 4.2-a).

4.3.4 Data Acquisition System

The data acquisition system was composed of a data logger unit, a PC and software. The voltage signals delivered from the gauges and LVDTs were continuously received by a collector unit, and then converted to displacement values by a personal computer. The data was recorded and load vs. displacement graph was simultaneously displayed by the software developed and used previously in the Structural Mechanics Laboratory.

4.4 TEST PROCEDURE

When the curing periods of the test specimens were finished, they were moved into the test setup and carefully positioned to their exact location on the main foundation. Their alignments and horizontality were checked in order to eliminate any undesirable effects due to eccentricity. After the adjustments, specimens were tightly fixed to their final locations by fastening to the main foundation by bolts. Before the experiment, standard cylinder tests were performed in order to obtain the compressive strength of the concrete and mortar in the specimen and the panels.

Instrumentation was installed on the specimens as explained in Section 4.3. After finishing the necessary connections, calibrations of the gauges were checked.

Axial load was applied on the columns by using the vertical loading system. The vertical load was different for specimens with continuous reinforcement and lap-spliced reinforcement. For specimens with continuous reinforcement, each column was applied 60 kN axial compressive force which corresponds to 22 % of the axial load capacity ($N = 0.22\ N_o$). Since the adverse effect of a lap-splice is greater for lower axial load values, lap-spliced specimens were applied less vertical load. Each column of lap-spliced specimens was under 30 kN compressive force corresponding to 11 % of its axial load capacity ($N = 0.11\ N_o$). The total vertical loads and column vertical loads were given in Table 4.1. The axial loads were kept constant during the tests.

Table 4.1 – Axial Load Levels in the Tests

Specimens	Total Axial Load (kN)	Axial Load per Column (kN)
Continuous	120	60
Lap-Spliced	60	30

The experiments were commenced by applying lateral load. The loading was in-plane and reversed cyclic. Lateral load was applied up to a predetermined level and unloaded, which makes a half cycle loading. For each half cycle, cracks were marked and necessary notes and photographs were taken. Each loading was repeated in the opposite direction in order to complete the cycles. Load level was increased gradually at each cycle. During the test, top displacement versus lateral load graph was monitored. The load level was kept in the elastic range in the first few cycles, but with increasing load levels, plastic response was seen. Once the response of the specimen became non-linear, the loading was controlled by the top story displacement.

CHAPTER 5

TEST RESULTS

5.1 GENERAL

Test results of the eight specimens in this experimental study are presented in this chapter together with the experimental observations. Critical observations are listed and photographs are also provided for interpreting the observations during the tests. In the observations section, forward cycle term is used for pushing the hydraulic jack which means loading towards south. The directions are illustrated in Figure 5.1. Loading histories are also shown for each specimen in Figure 5.2.

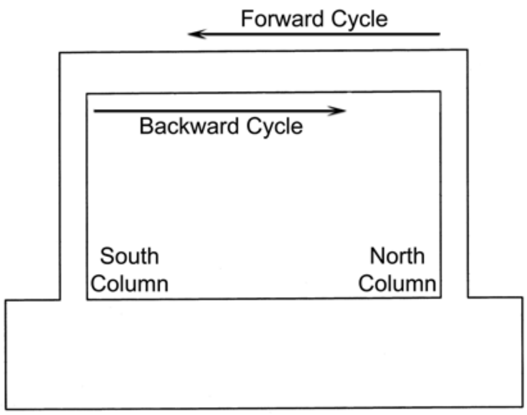

Figure 5.1 – Directions and Names Used for Describing the Observations

5.2 SPECIMEN CR

The specimen CR was the reference specimen and was not strengthened. It was a single-story single-bay frame with brick masonry infill and was planned to be used for comparison. The loading history for this specimen is given in Figure 5.2a. The maximum lateral load that this specimen could carry was 86.6 kN at 3.01 mm lateral deformation, corresponding to 3.5% story drift ratio.

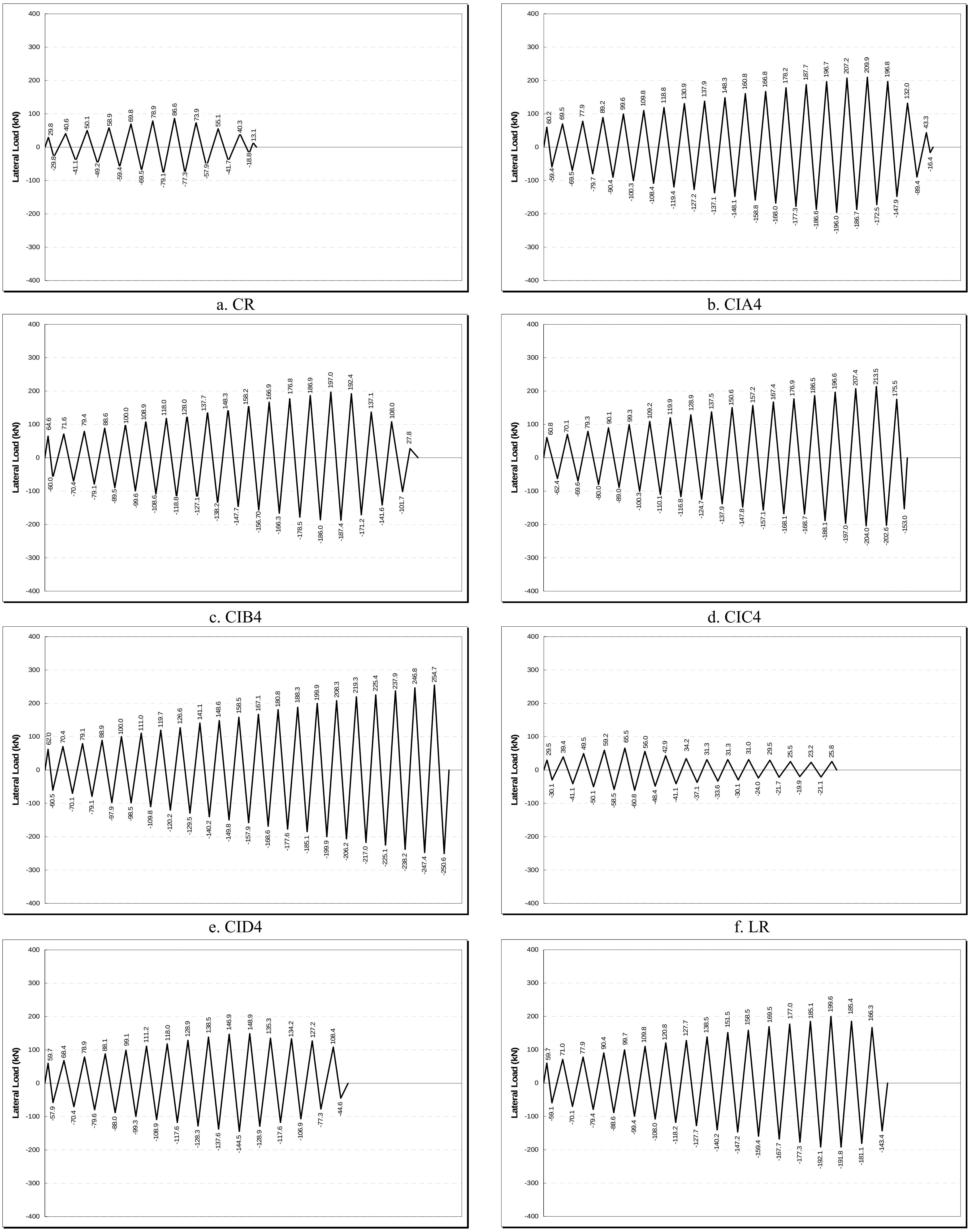

a. CR
b. CIA4
c. CIB4
d. CIC4
e. CID4
f. LR
g. LIC4
g. LID4

Figure 5.2 – Loading Histories of Test Specimens

In the diagram shown in Figure 5.4, lateral load was plotted against lateral displacement measured from the top of the frame. Following the maximum load, the curves in the load-displacement diagram started to become rounded and the peaks started to decrease gradually at each following cycle.

Load vs. column deformation at the base graphs were obtained by using the data from the dial gauges at the column bases. These dial gauges were installed at some distance from the outer faces of the columns; therefore, their measurements include the rotation of columns at the foundation level. Figure 5.3 illustrates the displacement of the dial gauge with deformation at the south column base. It must be kept in mind that these measurements are also affected by column base cracking and by column base crushing at later stages. In Figure 5.6 and Figure 5.7, column deformations at the base were plotted against lateral load.

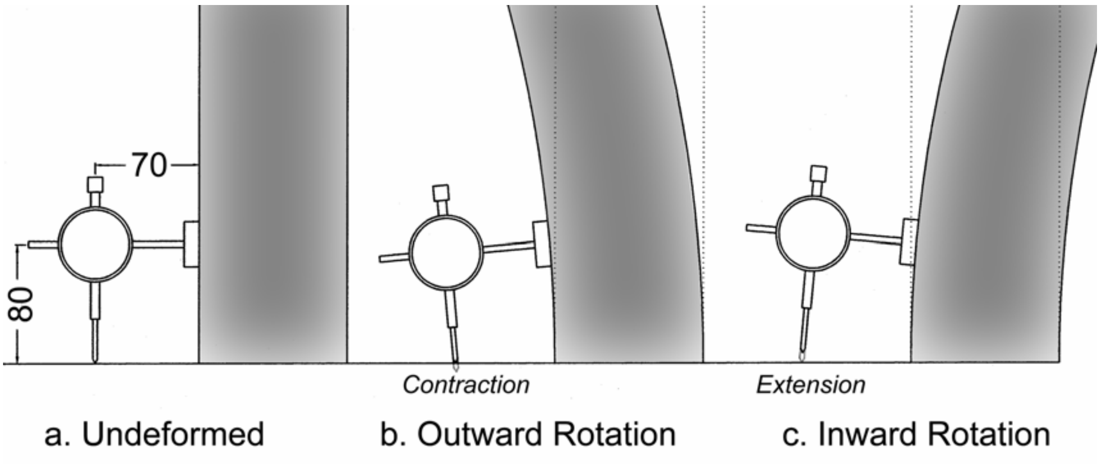

Figure 5.3 – Measurement of South Column Deformation at the Base (units in mm)

Loading in forward direction (as indicated in Figure 5.1) caused the south column to rotate outwards and the north column to rotate inwards with respect to the infill. Loading in backward direction caused deformation in the opposite directions. Contraction of the dial gauges record positive displacement and extension records negative displacement. Accordingly, positive displacement in Figure 5.6 and Figure 5.7 means rotation of columns away from the infill as in Figure 5.3b, and negative side shows rotation in the opposite direction as in Figure 5.3c.

In the graphs of load vs. column deformation at the base for specimen CR, curves are more significant at one side, according to the loading direction. The curves for both columns are wider at the positive side of the graphs. This means that, column bases experience much more deformation towards the opposite direction of the infill, since the infill provides a local restraint reducing column base rotation. These graphs also indicate the starting stage of infill crushing as significant increase in displacements in the negative direction. Column bases rotate in both directions without significant restraint after crushing of the infill. This rotational freedom at column bases indicates a frame behavior and loss of effectiveness of the infill.

Figure 5.5 shows shear deformation characteristics of the infill. The diagram shows mainly linear behavior until the crushing of the brick masonry infill, which started in early stages. After crushing of the infill, the dial gauges could no longer obtain accurate data, and this is the reason of the jump in the diagram. This data suggests that the brick masonry infill keeps its stiffness until its lateral load resistance capacity, which is relatively low, is reached. This graph implies the brittle behavior of the masonry infill.

Important observations of the behavior of the test specimen during the experiment are listed below:

- No cracks were formed in the first three load cycles.
- The infill was separated from the north column with a thin crack from the base to the middle height of the column in the fourth forward half cycle. At this cycle, the maximum lateral load was 60 kN. At the fourth backward half cycle, a symmetrical crack was formed at the connection of the south column and the infill.

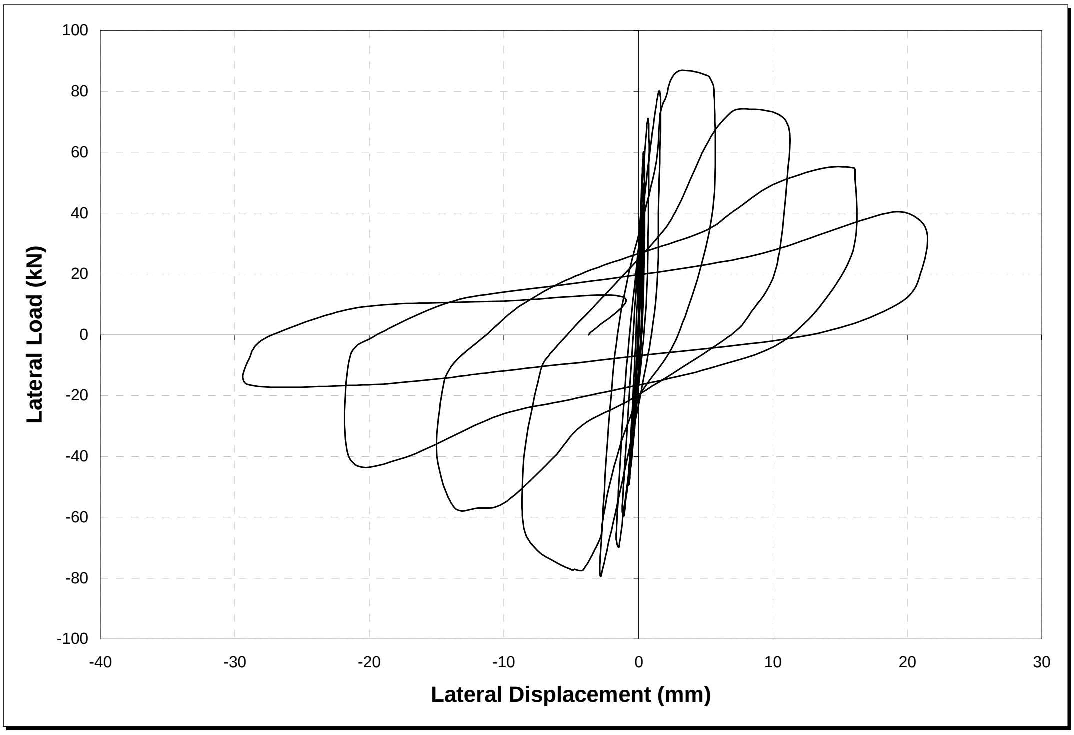

Figure 5.4 – Lateral Load - Lateral Displacement Curve of Specimen CR

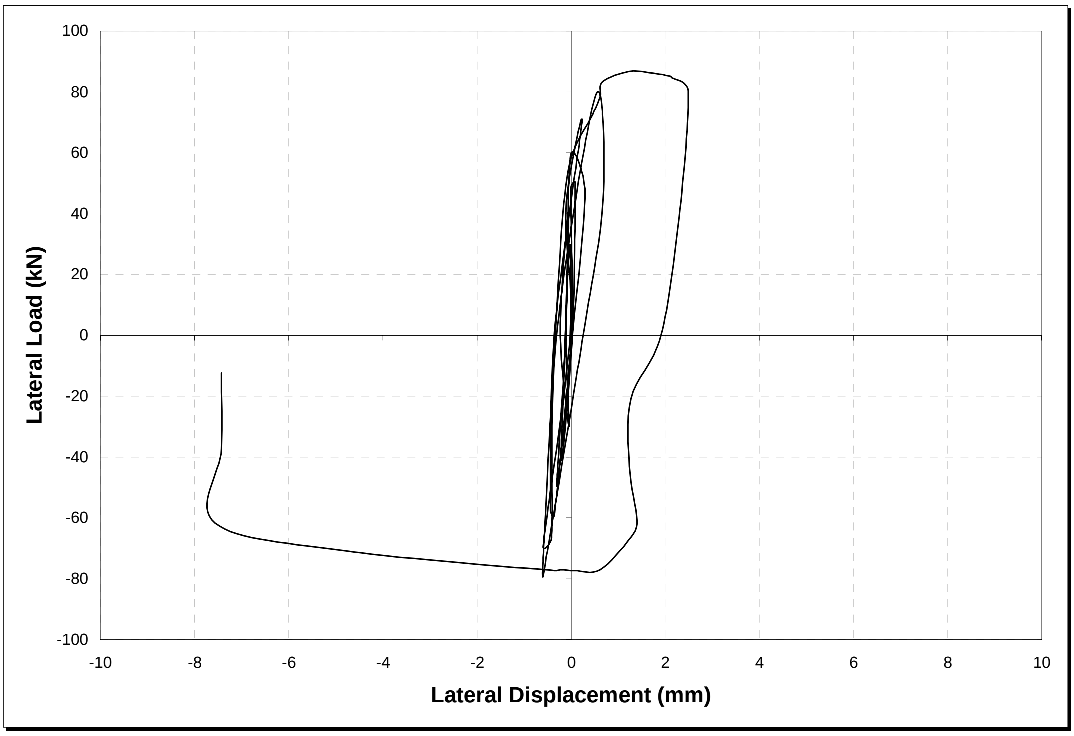

Figure 5.5 – Lateral Load - Shear Deformation Curve, Specimen CR

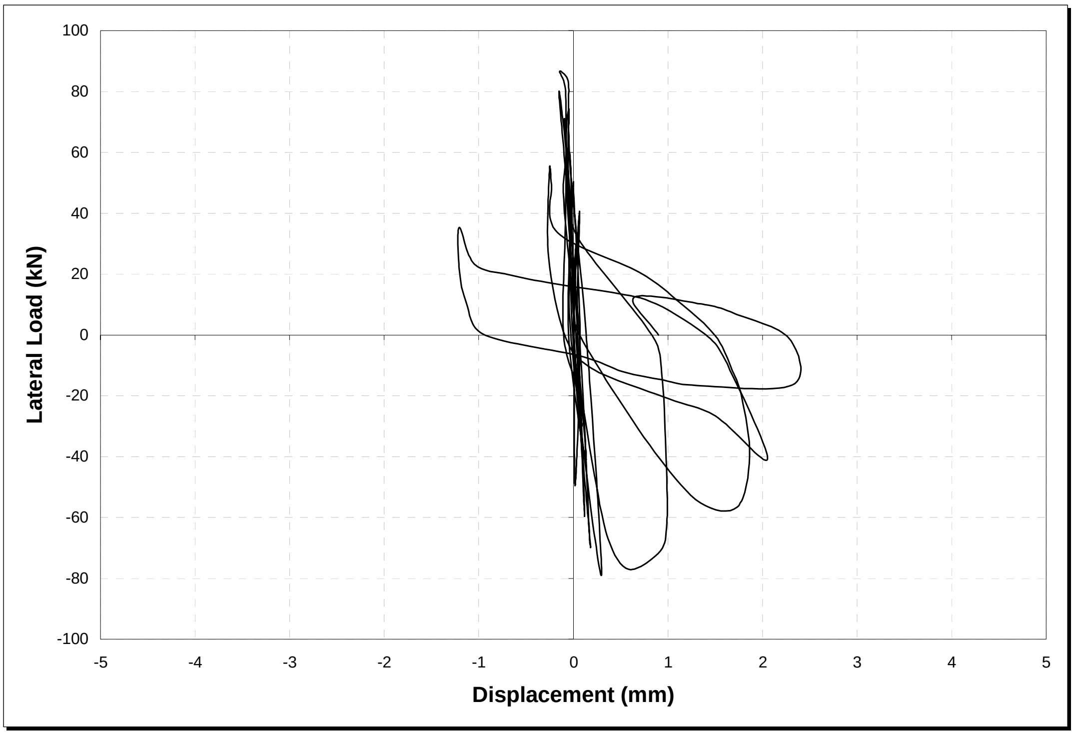

Figure 5.6 – Lateral Load-North Column Deformation at the Base, Specimen CR

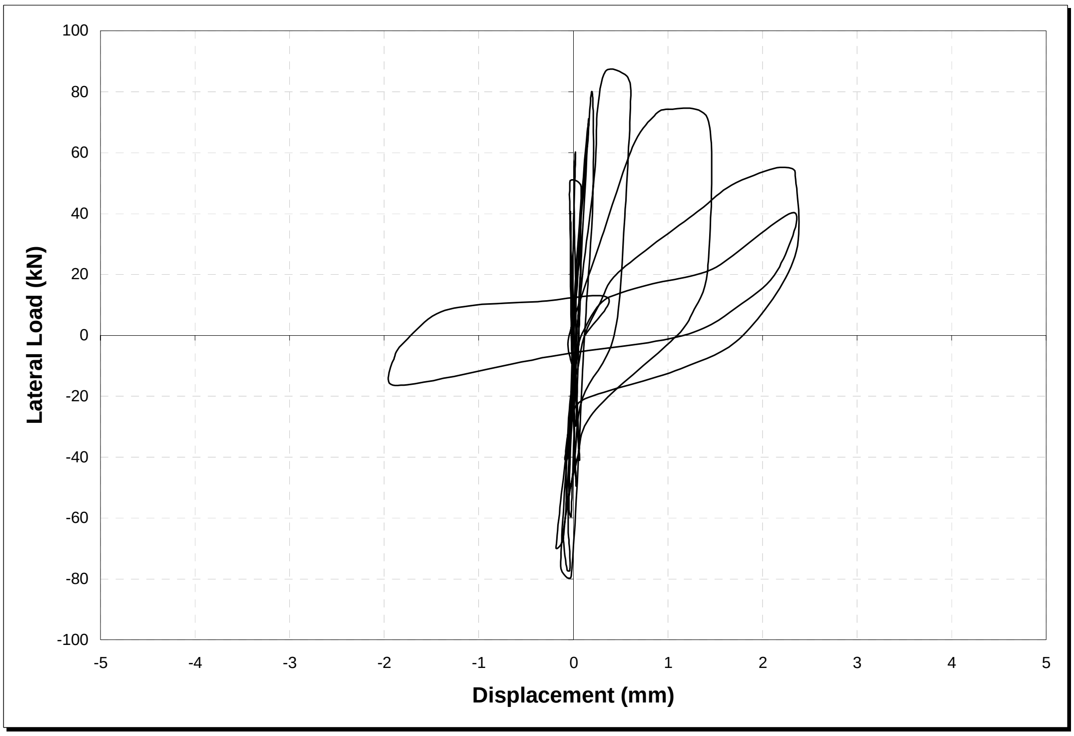

Figure 5.7 – Lateral Load-South Column Deformation at the Base, Specimen CR

- Hairline cracks appeared at the north beam-column joint in the sixth forward half cycle. In the next load stage, which was the sixth backward half cycle, similar cracking was seen at the opposite joint. Also, at this stage, the plaster on the rear surface started to separate from the frame and the separation cracks of the infill from the north column grew to as much as 4 mm (Figure 5.8). At the seventh forward half cycle, separation was observed on the infill near the south beam-column joint. At this cycle, the maximum load of 86.6 kN was reached before the displacement started to increase without increasing the load. While approaching this load level, the load-deformation curve experienced a significant loss of slope (Figure 5.4). After this point, linearity of the curves is lost and the frame carried the increasing loading with much reduced stiffness in the following cycles. From this stage on, displacement controlled cycles were applied to the frame.
- Bending cracks developed on the outer surface of the north column in the eighth forward half cycle. One crack was at the mid-span, and there were two others at 100 mm above and 200 mm below this crack. At this cycle, load was applied up to 10 mm displacement and the maximum load level was 74.2 kN. The infill started to crush at the top corner on the south side. Diagonal cracks were observed on the infill and at the plaster on the rear side of the frame. With the destruction of the infill and damage in the columns, column bases started to experience large rotations, as can be observed from the load-column base deformation graphs in Figure 5.6 and Figure 5.7. In these graphs, it can also be seen that the columns deformed more towards the opposite side of the infill, since they have already separated. Crushing of the infill made the dial gauges mounted on it inaccurate, so the load-shear deformation curve given in Figure 5.5 is not reliable after the maximum load level.
- In the eighth backward cycle, bending cracks were observed on the south column and intense cracking appeared on the plaster over the column at the rear side. At the south beam-column joint, additional cracks were formed and existing ones progressed further. The plaster started to fall down at large pieces.

- In the ninth forward half cycle, the separation of the infill and the frame increased so much that it was possible to see the other side of the frame. Crushing started at the mid-span of the south column due to bending (Figure 5.9). The plaster was completely wiped off from the column faces. Dial gauges on the infill dropped down. The load-displacement curve also progressed with very small slope in this cycle.
- In the tenth cycle which was the last, the corners of the infill were completely crushed. There was severe damage in the columns and beam-column joints. The effect of crushing of the infill can be seen in the load-column base crack diagrams as the last curves indicating deformation of the column towards the infill. The stiffness of the frame dropped to very low levels indicating that the frame was almost transformed into a sway mechanism. The load displacement curve was almost horizontal in the last cycle and the frame virtually had no stiffness any more. The final view of the specimen can be seen in Figure 5.10 and Figure 5.11.

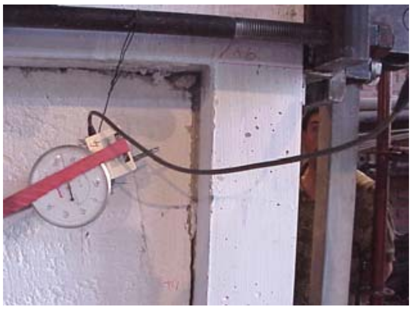

Figure 5.8 – Separation in the Sixth Cycle, Specimen CR

Figure 5.9 – Damage in the South Column in the Ninth Cycle, Specimen CR

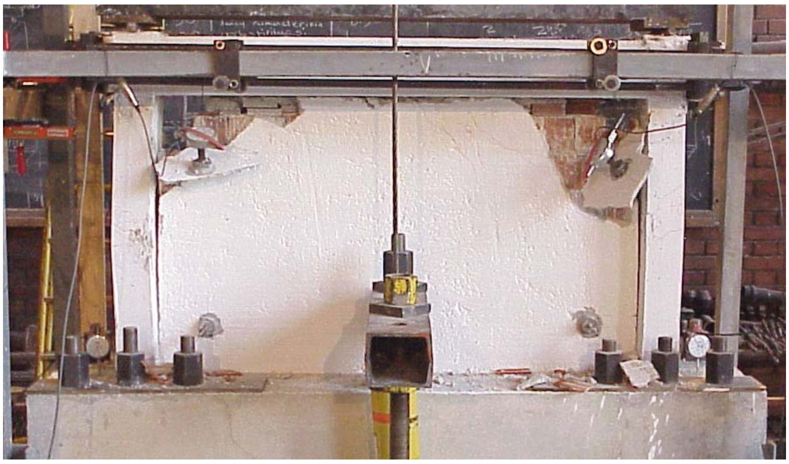

Figure 5.10 – General View of Specimen CR after the Test (front)

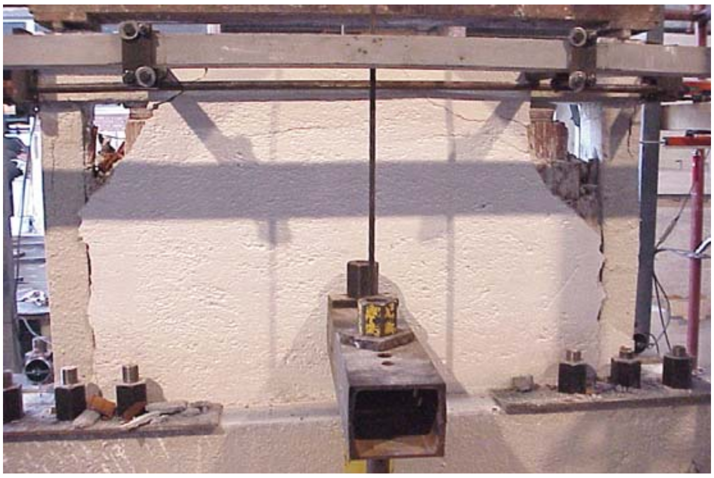

Figure 5.11 – General View of Specimen CR after the Test (back)

5.3 SPECIMEN CIA4

This specimen was the identical of the reference specimen CR except that it had been strengthened by Type A precast panels bonded over the hollow brick masonry infill. The panels were weld-connected at the corners to each other and to the dowels along four sides. Longitudinal reinforcement in the columns was continuous. In the test, a constant axial load of 60 kN was applied on each column, corresponding to 25% of their nominal axial load capacity. The lateral loading was applied as shown by the loading history chart in Figure 5.2b.

The load-displacement curve given in Figure 5.12 suggests that the behavior is positively affected by the strengthening of the infill, since the lateral load capacity was increased, and little capacity drop was observed between the cycles.

Load-column deformation at the base diagrams in Figure 5.14 and Figure 5.15 indicate deformation in a single direction, as expected, signing to effective contribution from the infill, as explained for the specimen CR. Contrary to the reference test, deformations stayed linear in the opposite direction even in the final cycles. This shows higher local restraint from the infill preventing column base rotation towards the infill, which indicates greater contribution of the infill.

Load-shear deformation graph in Figure 5.13 shows a stiff and linear behavior for the infill before diagonal cracking starts on the panels. Then, deformation increases with increasing diagonal crack widths.

Important observations during the test are as follows:

- In the first four loading cycles, no cracking has occurred.
- In the fifth forward half cycle, plaster at both sides of the frame started to separate along the north column-infill joint, up to 300 mm from the base.
- In the ninth forward half cycle, a thin crack was observed on the north column base at the tension side. The base crack is shown in Figure 5.16. The south column base cracked in the tenth backward half cycle. Base cracks on the infill started in the tenth forward half cycle at the north side.
- Loading plate failed in the very early stages of the fifteenth backward half cycle. The test was continued after the loading plate was replaced with a stronger one.
- Diagonal cracking started on the infill panels in the sixteenth cycle, as shown in Figure 5.17. With the start of panel diagonal cracking, load-shear deformation curve lost its linearity. Also, north beam-column joint cracked significantly. Another diagonal crack appeared on the north column a little below the joint. South beam-column joint cracked significantly in the backward half cycle.

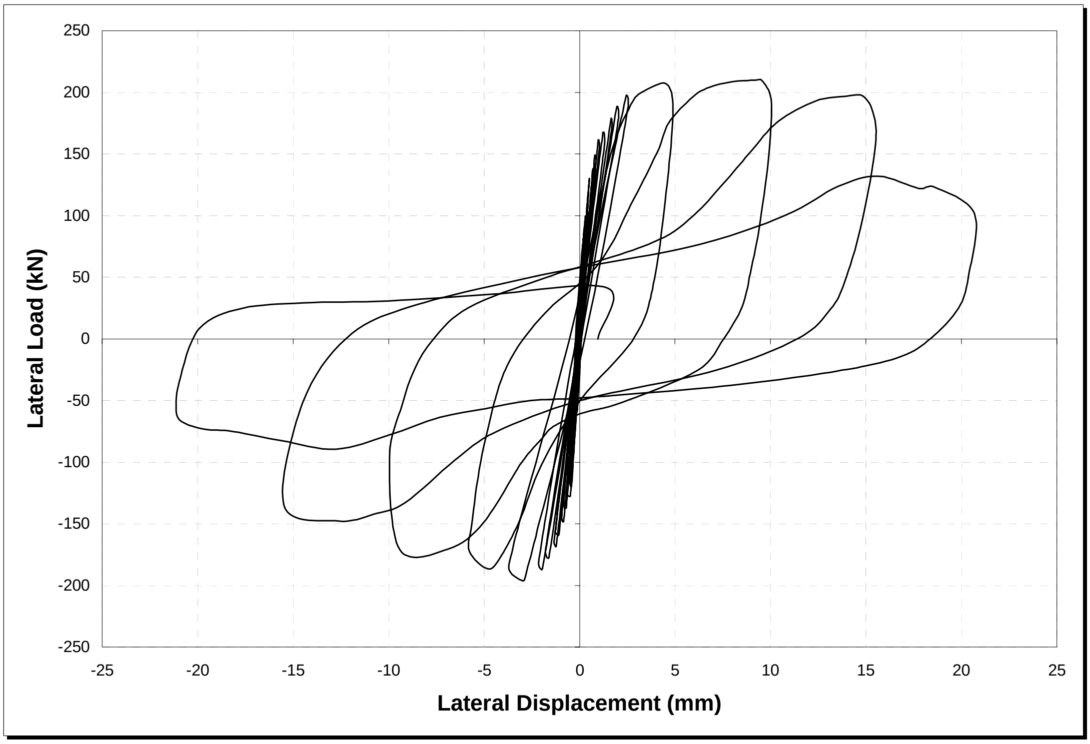

Figure 5.12 – Lateral Load - Top Displacement Curve, Specimen CIA4

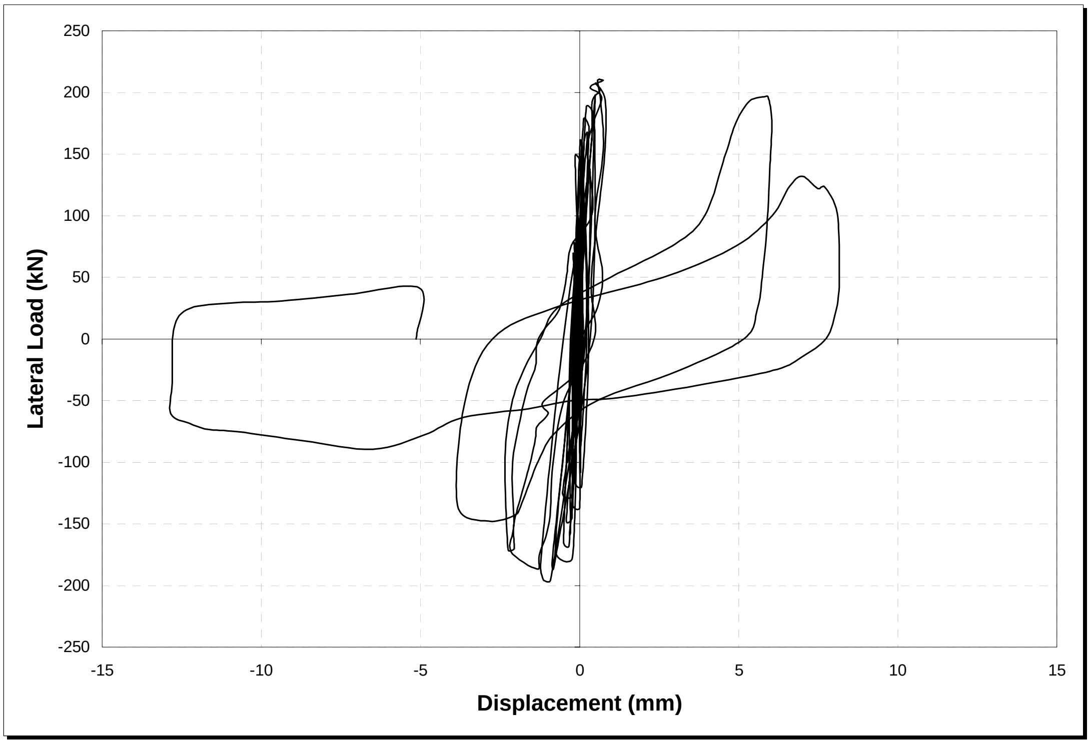

Figure 5.13 – Lateral Load-Shear Displacement Curve, Specimen CIA4

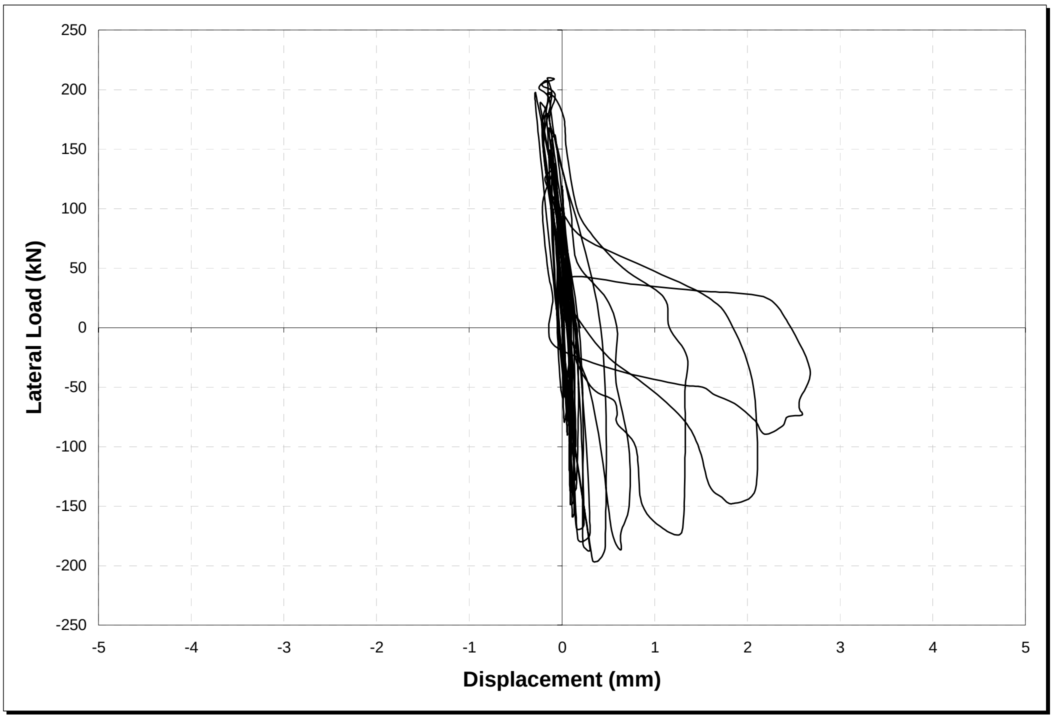

Figure 5.14 – Lateral Load-North Column Deformation at the Base, Specimen CIA4

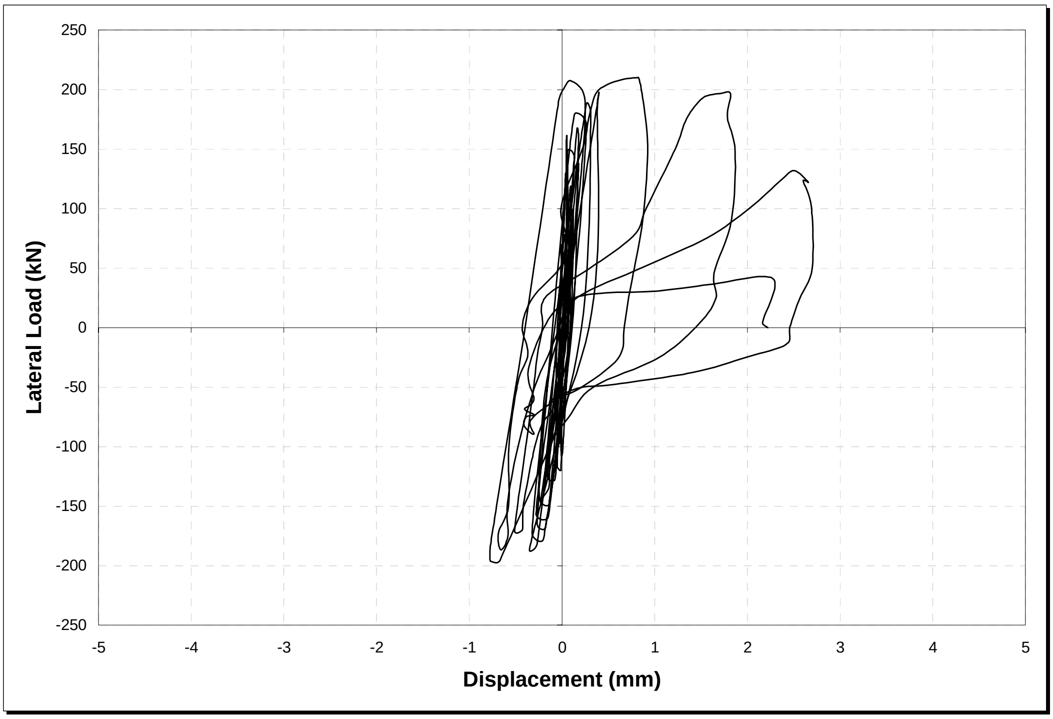

Figure 5.15 – Lateral Load-South Column Deformation at the Base, Specimen CIA4

- Maximum lateral load of 209.9 kN was reached at the seventeenth cycle in the positive direction at 9.2 mm top level displacement. Similar to the previous test, the load-deformation curve (Figure 5.12) became non-linear and started leaning down. The load-column base crack curves started to have significant non-linearity after this point.
- Crushing started at the north beam-column joint in the eighteenth forward half cycle. Severe crushing was observed at the south beam-column joint in the eighteenth backward half cycle (Figure 5.18). Large diagonal cracks developed on the infill. The damage on the infill is shown in Figure 5.19 and the effect of this damage to the load-shear displacement curve can be seen in the related figure (Figure 5.13) as significant non-linear behavior. At the same time, although showing large displacements, the peak of the load-displacement curves did not go lower. The curves also did not indicate significant loss of strength.
- Since the frame members were damaged and the specimen lost its load carrying capacity, the experiment was discontinued after the nineteenth cycle. The final view of the specimen from front and back is given in Figure 5.20.

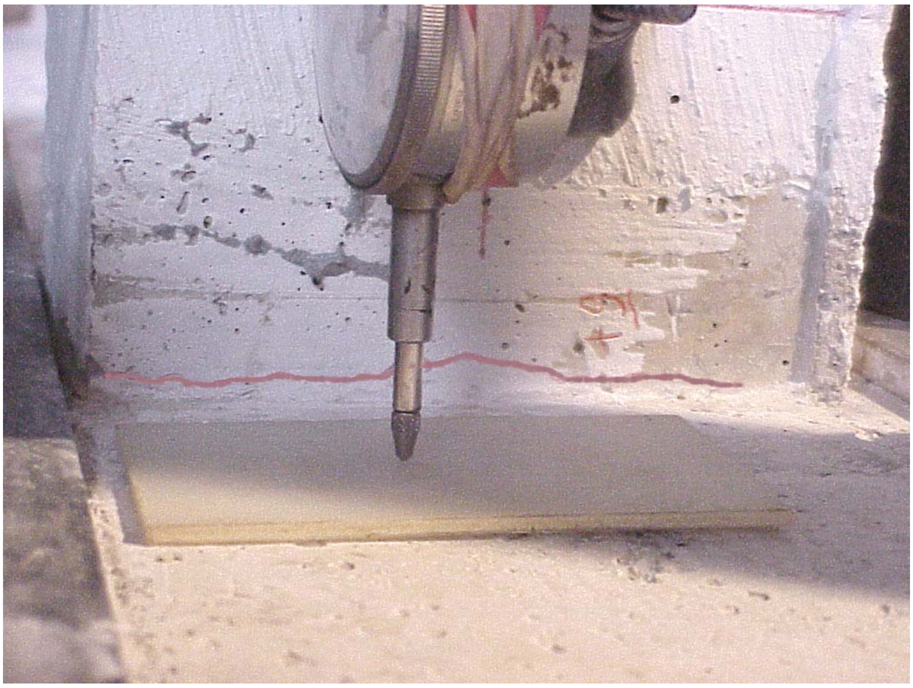

Figure 5.16 – Column Base Crack in the Nineteenth Cycle, Specimen CIA4

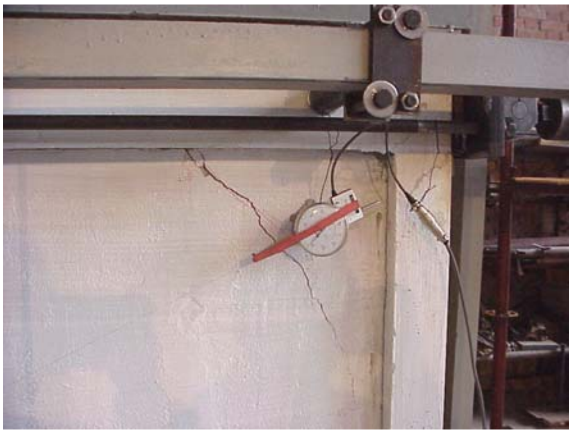

Figure 5.17 – Diagonal Cracking on the Infill in the Sixteenth Cycle, Specimen CIA4

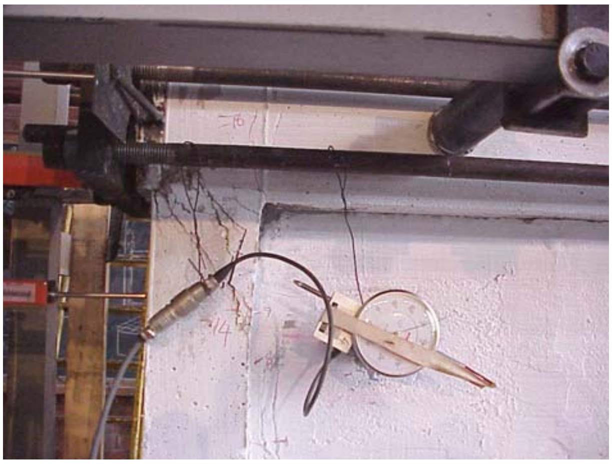

Figure 5.18 – Damage in the South Beam-Column Joint, Specimen CIA4

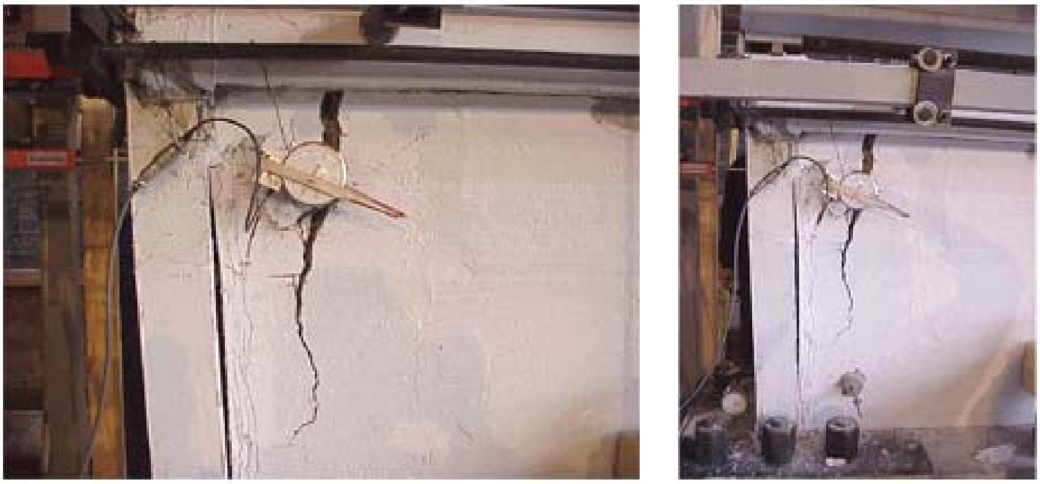

Figure 5.19 – Damage on the Infill, Specimen CIA4

Figure 5.20 – Specimen CIA4 at the End of the Test

5.4 SPECIMEN CIB4

This specimen was strengthened by Type B panels bonded on the brick masonry infill and welded to the dowels at the bottom and top. The longitudinal reinforcement used in this specimen was continuous. This specimen was tested under a constant axial load of 60 kN applied on each column ($N/N_o = 0.25$).

The load-displacement diagram of this specimen is shown in Figure 5.21. This graph shows similar increase in the load carrying capacity as for the specimen CIA4 compared with the reference specimen CR. Also, the successive curves in the post-linear stage maintain considerable stiffness.

Figure 5.22 and Figure 5.23 show lateral load plotted against the column deformation at the base, and these graphs show significant deformation in one direction only, according to the direction of loading. The asymmetric shape of the curves is most possibly due to local restraint provided to column bases by the infill. By inspection of these graphs, column deformation at the base in the inward direction seems to be prevented by the infill, in contrary to the reference specimen CR. They also show that the strengthened infill has much more lateral stiffness than the brick masonry infill and it still provides significant restraint to columns even after diagonal cracking.

The load-shear displacement curve in Figure 5.24 shows large shear deformation through the non-linear stage in one direction only and very elastic behavior in the other direction. The reason for this shape is that a major diagonal crack formed in one direction and no major diagonal cracks occurred in the other direction. Load-displacement curve agrees with this asymmetry with lower lateral load levels in the forward direction.

The important observations noted down during the experiment are given below:

- Base crack was observed on the outer surface of the north column in the second forward half cycle. South column base cracked in the third backward half cycle.
- Infill started to separate from the north column with a hairline crack forming in the second forward half cycle. In the fourth backward half cycle, separation between the infill and the south column was observed.

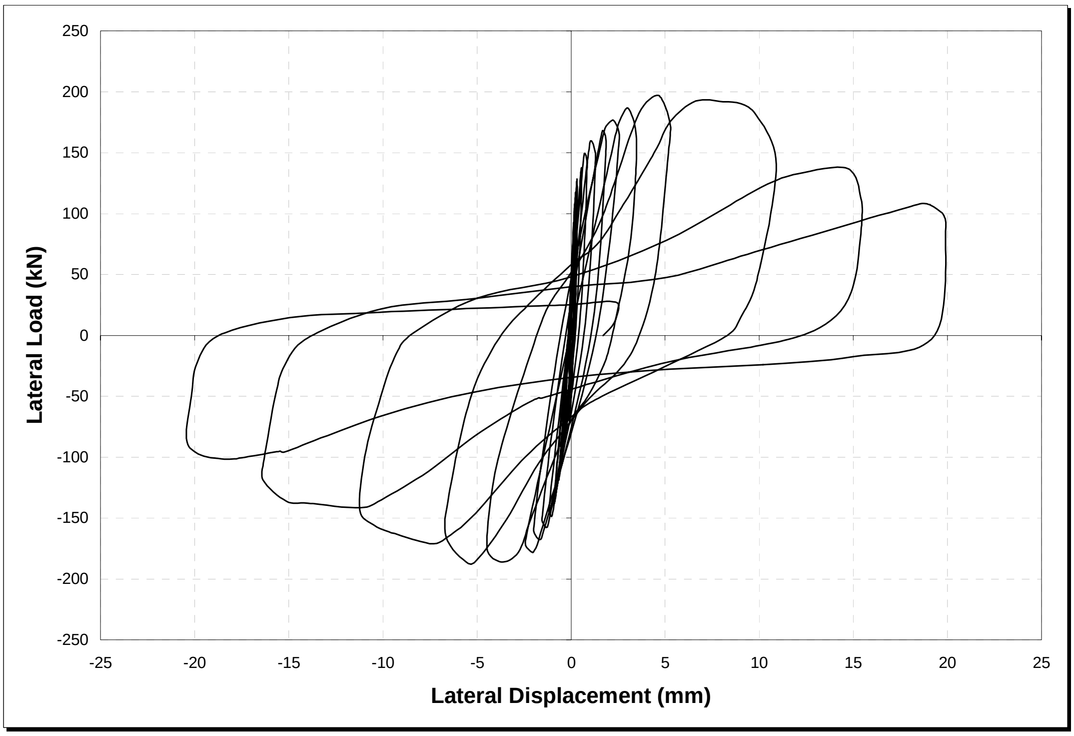

Figure 5.21 – Lateral Load - Top Displacement Curve for Specimen CIB4

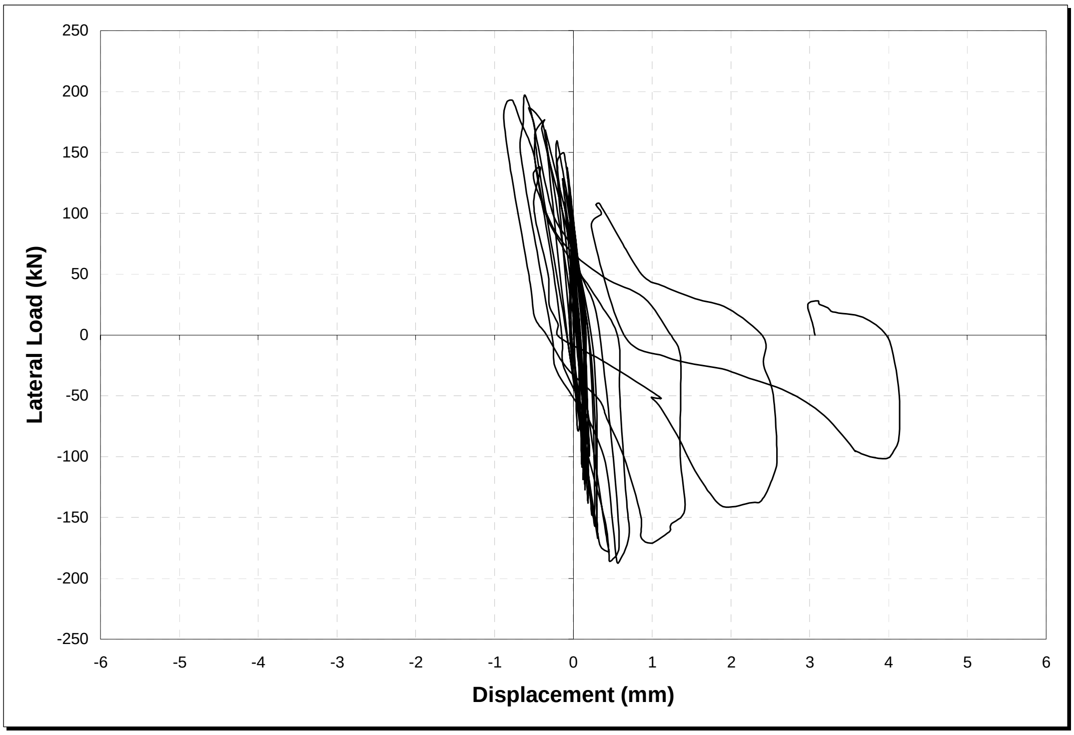

Figure 5.22 – Lateral Load - North Column Deformation at the Base, Specimen CIB4

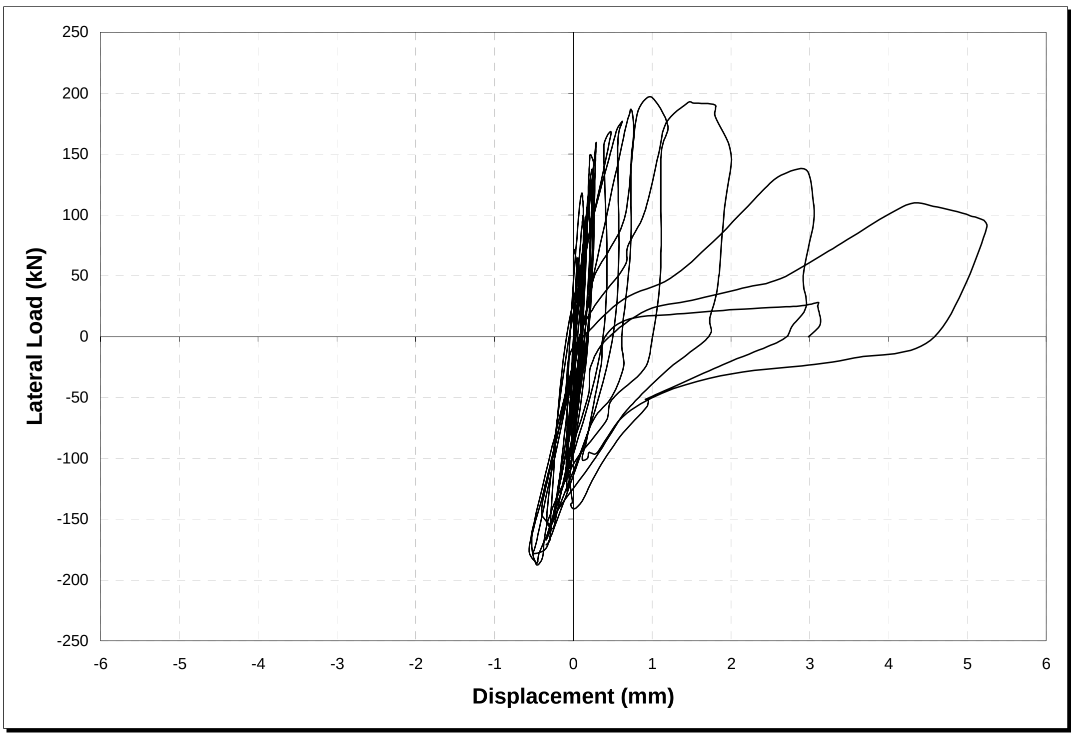

Figure 5.23 – Lateral Load - South Column Deformation at the Base, Specimen CIB4

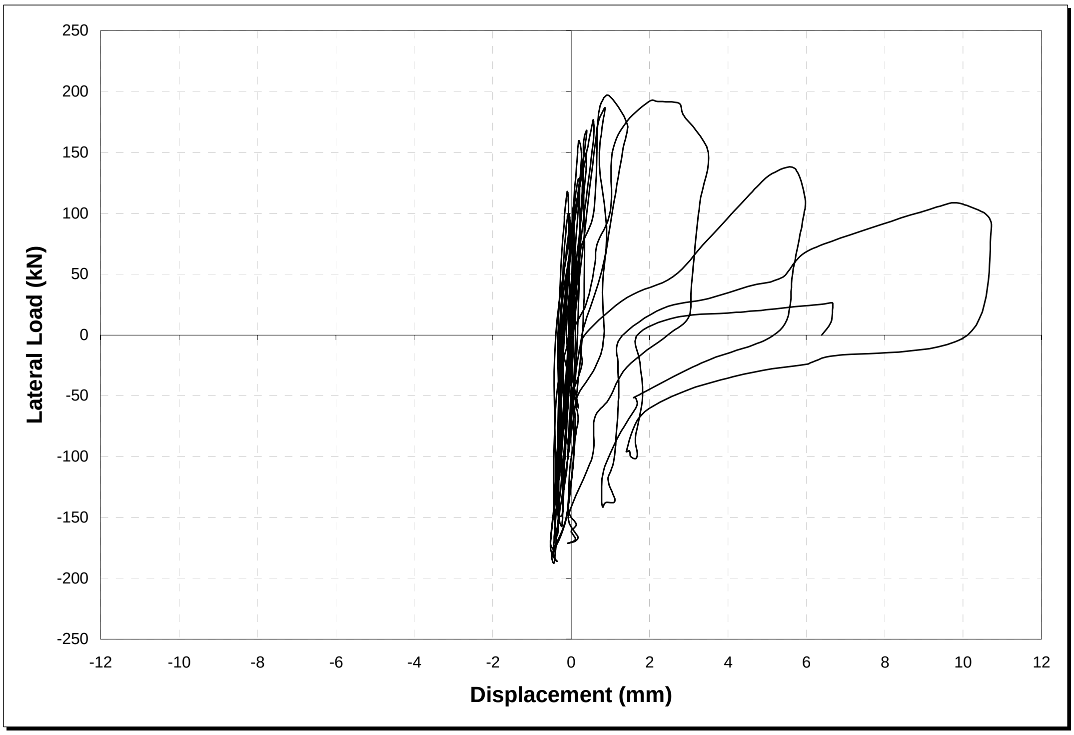

Figure 5.24 – Lateral Load - Shear Displacement Curve, Specimen CIB4

- North beam-column joint cracked in the sixth forward half cycle. In the backward loading of the same cycle, south beam-column joint cracked. Joint crack shapes may be seen in Figure 5.25. Another diagonal crack appeared at the north beam-column joint just below the first crack in the eighth forward half cycle.
- Cracking appeared at the base of the infill in the seventh forward half cycle. Also, bending cracks were observed at the north column in this cycle and in the ninth. Two more cracks were formed on the south column in the negative eighth half cycle. Load-displacement curves slowly started to lose some stiffness starting from this cycle.
- Significant diagonal joint cracks were observed in the eleventh forward half cycle at the north beam-column joint and in the twelfth backward half cycle at the south beam-column joint.
- Panels started to crack diagonally starting from the top of the infill in the fourteenth forward half cycle. The direction of this diagonal crack can be seen in Figure 5.26. Together with this crack, the shear displacement curve indicated

large deformation in the infill for loading in the forward direction, showing the opening and closing of this crack according to the cyclic loading (Figure 5.24). In backward loading, the diagonal crack on the infill closed and the shear curve showed linear and stiff infill behavior in that direction. After this crack, the load-displacement curve also has lower strength peaks for forward loading, compared with loading in the other direction.

- In the fifteenth cycle, the maximum load of 197.0 kN was recorded for this specimen. In this cycle, new cracks were observed at the joints and on the infill. The slope of the load-displacement curves decreased due to the enlargement of the diagonal crack on the infill.
- Starting from the sixteenth cycle, the infill was separated from the frame and the displacement started increasing more rapidly. Reduction of infill stiffness attracted more load on the frame members. As a result, beam-column joints suffered considerable damage and column base cracks opened further (Figure 5.27). The behavior of the system transformed into a frame behavior.
- At the end of the eighteenth cycle, the test was ended due to heavy damage and loss of stiffness. The final view of the specimen after the test is given in Figure 5.28.

Figure 5.25 – Joint Cracks in the Sixth Cycle, Specimen CIB4

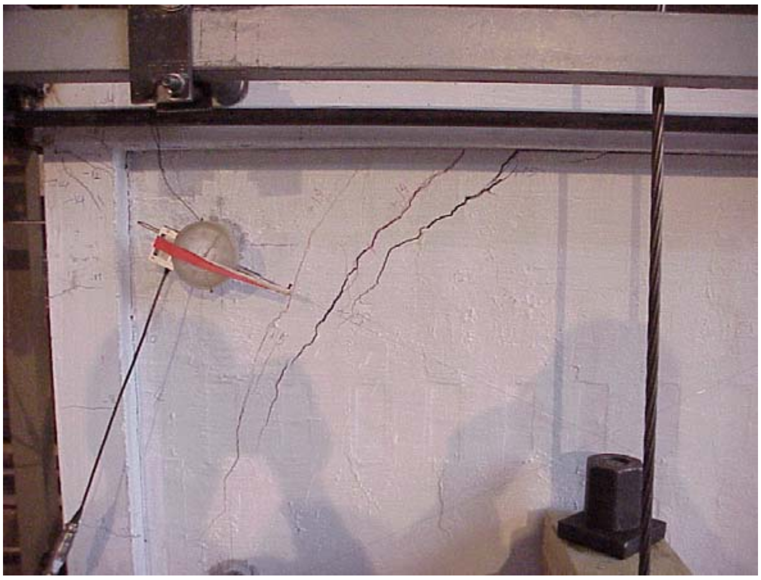

Figure 5.26 – Cracking on the Infill in the Fourteenth Cycle, Specimen CIB4

Figure 5.27 – Damage at the Joints, Specimen CIB4

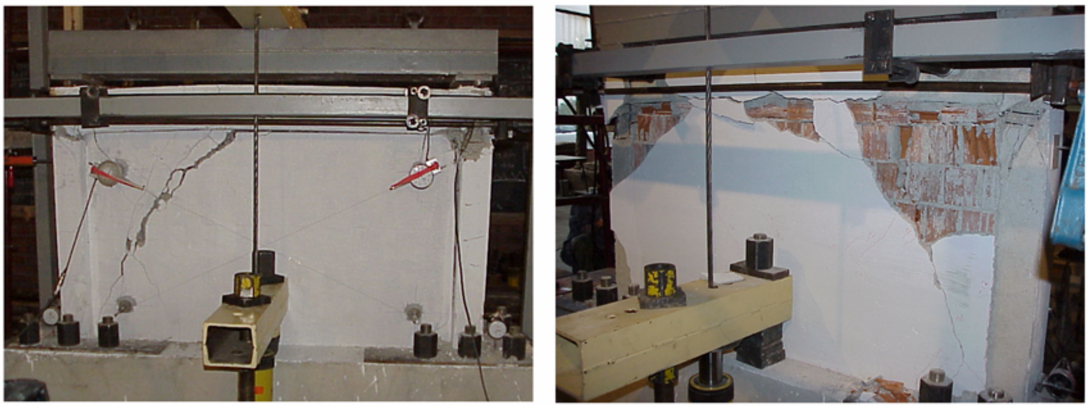

Figure 5.28 – General View of Specimen CIB4 after the Test

5.5 SPECIMEN CIC4

Specimen CIC4 had a continuous reinforcement. This specimen was strengthened with Type C panels connected to the frame by dowels along four sides. 60 kN constant axial load was given to each column ($N/N_o = 0.25$) during the experiment.

This specimen also has a significantly increased lateral load capacity, and the load level is maintained in the curves beyond the elastic range, by inspection of the load-displacement curve in Figure 5.29. The maximum load recorded for this specimen was 213.5 kN, and the top displacement was 8.74 mm at that point.

Lateral load-column deformation at the base diagrams in Figure 5.30 and Figure 5.31 reflect the common behavior of the columns in tests of specimens CIA4 and CIB4, as they have specific directions. These graphs can be similarly commented as showing the restraining effect of the infill on the columns.

The load-shear displacement diagram (Figure 5.32) shows deformation in both directions, because two major diagonal cracks were formed on the infill. Loading in forward direction caused the diagonal crack on the left to open and the one on the right to narrow, and vice-versa for loading in the backward direction. This behavior is clearly observed from the load-shear displacement graph. Also, the graph suggests that opening of the diagonal crack is greater in the forward direction loading, which means that the diagonal crack on the left should be more significant than the diagonal crack on the right. This interpretation agrees with the observed behavior of the specimen in the test, as can be seen in the observed behavior section for specimen CIC4.

Critical observations in this test were summarized and presented in the items given below:

- In the first forward half cycle, hairline separation cracks appeared on both sides of the frame at the connection of the north column and the infill. Symmetrical separation was formed separating the south column and the infill in the reverse half cycle.

- In the second forward half cycle, hairline bending cracks were observed on the outer surface of the north column at the foundation level. Same cracking was seen in the second backward half cycle.
- In the seventh forward half cycle (maximum load of 120 kN), the plaster at the back side of the frame started to separate at the north side. The separation of the plaster also became visible at the south side in the seventh backward half cycle.
- North beam-column joint cracked in the eighth forward half cycle. South beam-column joint cracks were noted in the backward loading of the same cycle (Figure 5.33). Also, several short inclined cracks were formed on the infill at the back side in this cycle.

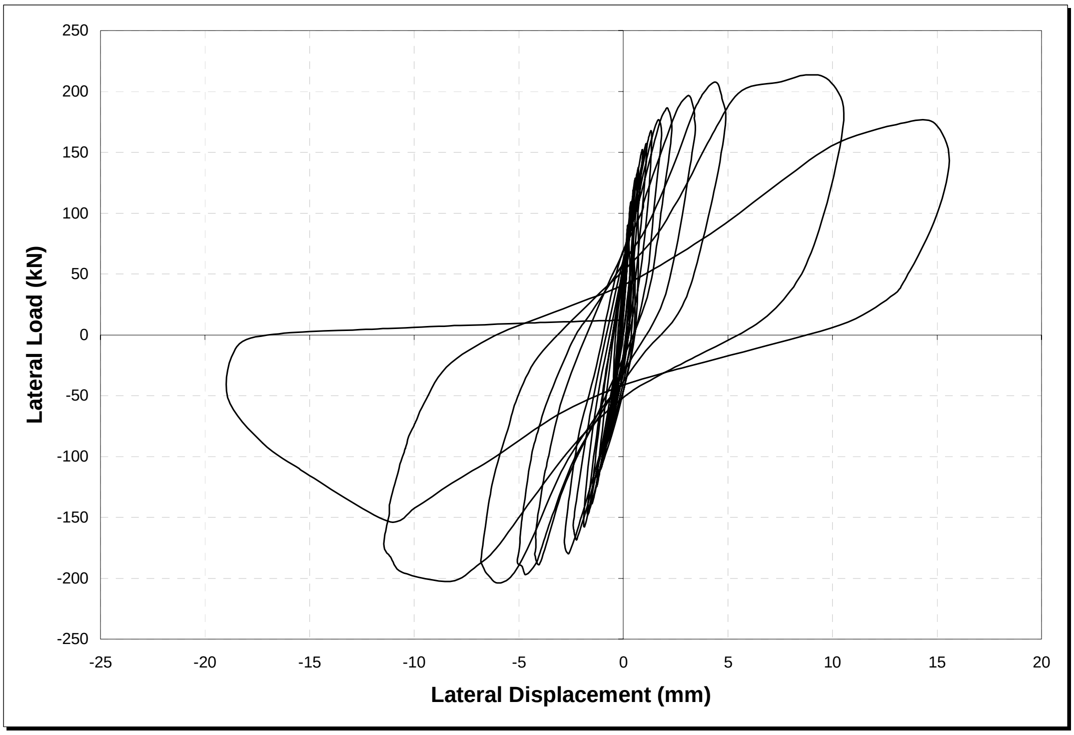

Figure 5.29 – Lateral Load - Top Displacement Curve, Specimen CIC4

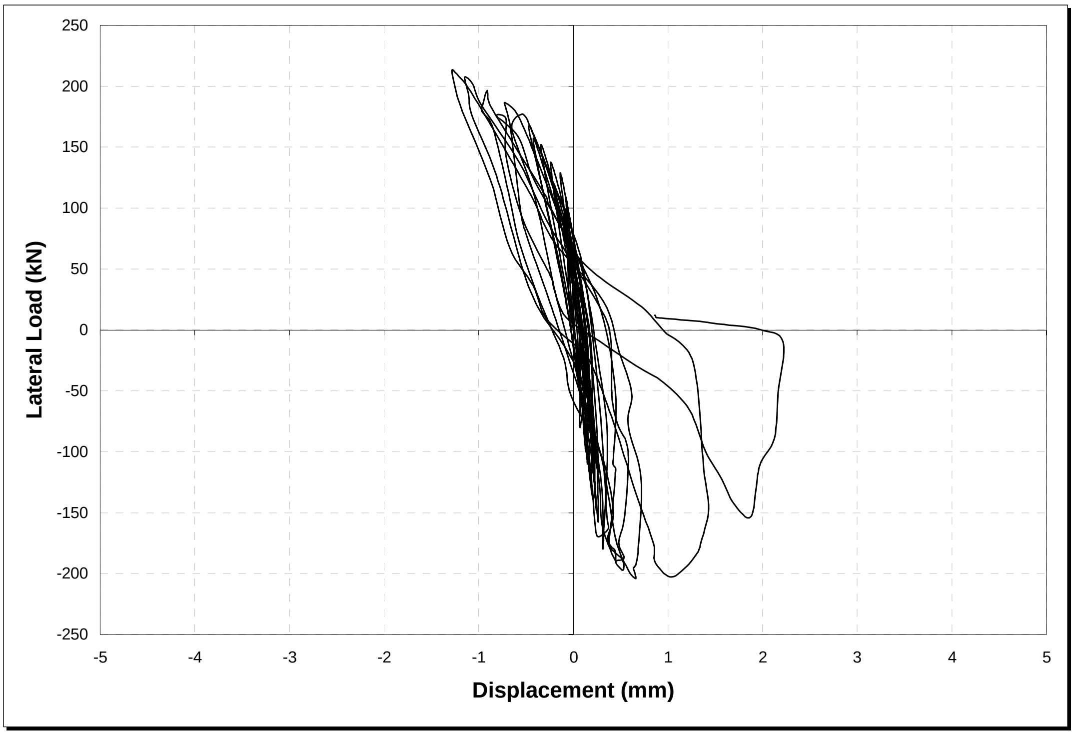

Figure 5.30 – Lateral Load-North Column Deformation at the Base, Specimen CIC4

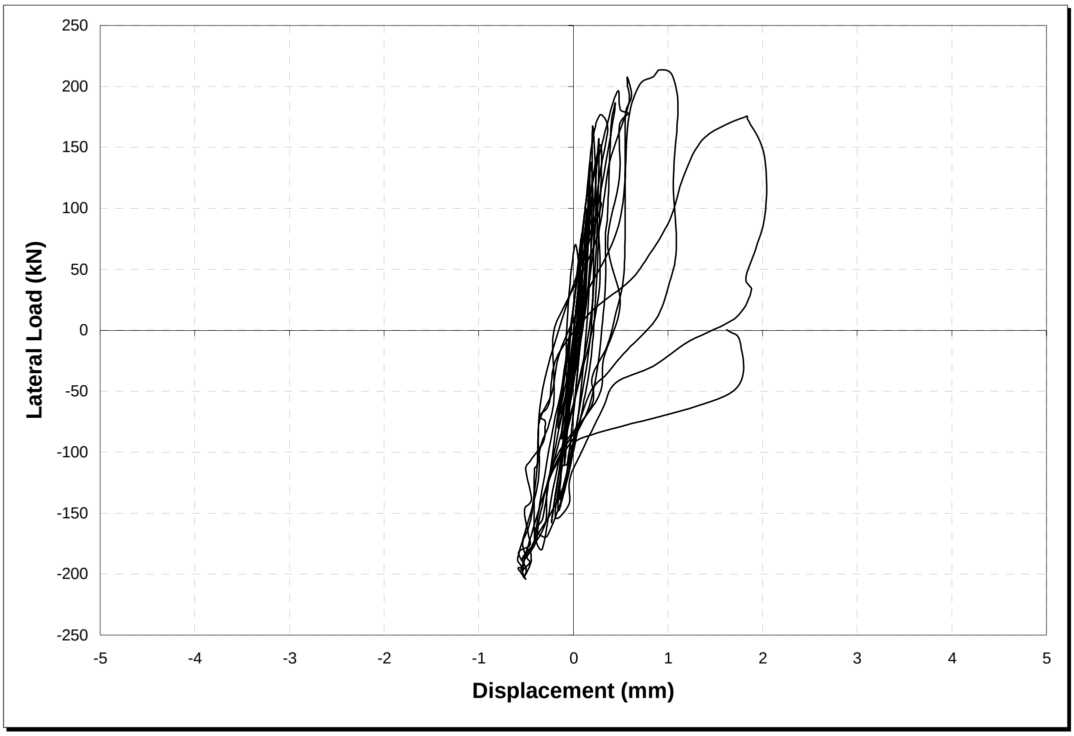

Figure 5.31 – Lateral Load-South Column Deformation at the Base, Specimen CIC4

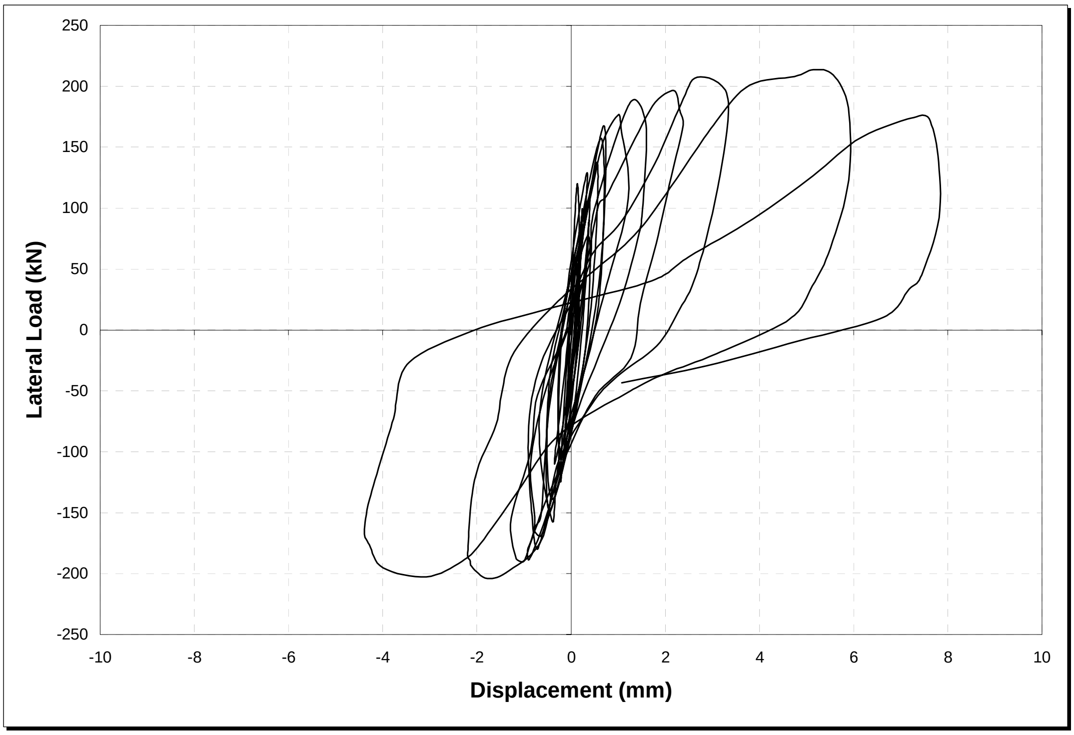

Figure 5.32 – Lateral Load-Shear Displacement Curve, Specimen CIC4

- In the ninth forward half cycle, a significant diagonal crack was formed on the north column slightly below the beam-column joint. In the backward half cycle, a similar crack was observed on the south column. Also, in this cycle, the infill separated along the foundation level at the south side. This separation turned upwards towards the south corner of the infill and merged with the separation between the south column and the infill.
- Diagonal cracks were formed on the infill panels in the tenth forward half cycle. These cracks were observed mostly on the north side of the infill, as can be seen from Figure 5.34. The direction of the cracks was from upper right to lower left corner of the panels. In the tenth backward half cycle, a few diagonal cracks were observed on the panels close to the south side. These cracks had a direction perpendicular to the cracks formed in the previous half cycle. However, no indication of stiffness loss was observed from the load-displacement curve. The behavior was still very close to linear. Panel diagonal cracks increased and spread in each following cycle.

- In the twelfth backward half cycle, a large crack was observed on the beam span.
- In the thirteenth cycle, panel diagonal cracks increased and intensified. Diagonal cracks appeared at the back side also. Another joint crack was formed in the south beam-column joint in the backward half cycle.
- From the thirteenth cycle to the sixteenth cycle, diagonal cracks on the panels increased in number and length. Some diagonal cracks grew as wide as 3 to 4 mm and as long as 250 mm. Infill cracks in this stage of the experiment are shown in Figure 5.35. Also, many cracks were observed on the columns in the fifteenth and the sixteenth cycles. Load-displacement curves started to shift from the elastic action, but not significantly. Increasing lateral load in the thirteenth to fifteenth cycles was carried by the specimen without much loss in stiffness. Load-column deformation at the base and load-shear displacement diagrams were showing slight indications of softening.
- The maximum capacity of 213.5 kN was reached in the seventeenth forward half cycle. In this cycle, the infill started to crush at the corners and crushing started in the columns just below the joint. The load-displacement curve started progressing horizontally at this point. Excessive deformation made it necessary to stop loading below 220 kN. Loading was stopped at 10-mm top displacement. Major diagonal cracks of 7~8 mm width were observed at both sides of the frame and they extended from the top to the bottom of the infill. The following cycles were carried on by controlling the displacement in 5-mm increments.
- In the eighteenth backward cycle, the south column completely crushed a little below the joint at 11.3-mm top displacement. Due to crushing, the column was torn apart from the beam and the frame lost its stiffness abruptly, making the load-displacement curve make a sharp turn and jump to 19 mm displacement with load dropping to zero suddenly. Together with crushing, column reinforcement bars buckled. The top panel at the south corner was also completely crushed. Many panels suffered damage due to severe cracking. Views of the frame at the end of the test are shown in Figure 5.36 and Figure 5.37.

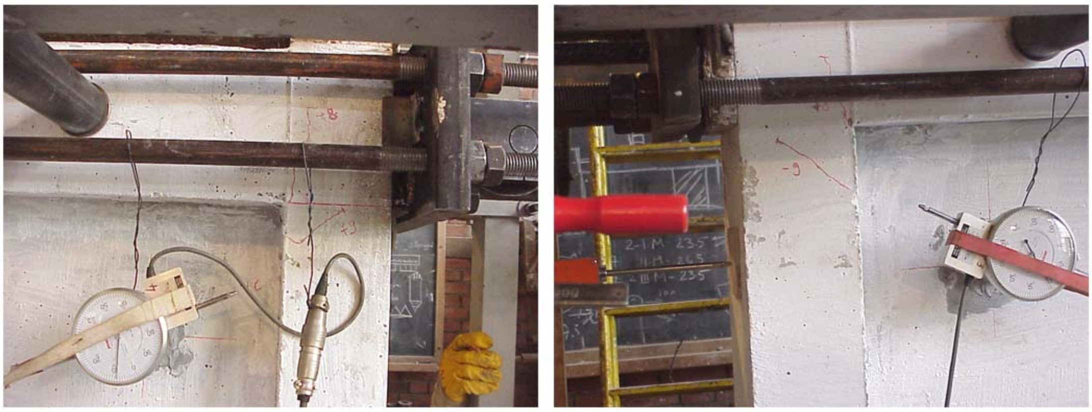

Figure 5.33 – Joint Cracking in the Eighth Cycle, Specimen CIC4

Figure 5.34 – Infill Cracks in the Tenth Cycle, Specimen CIC4

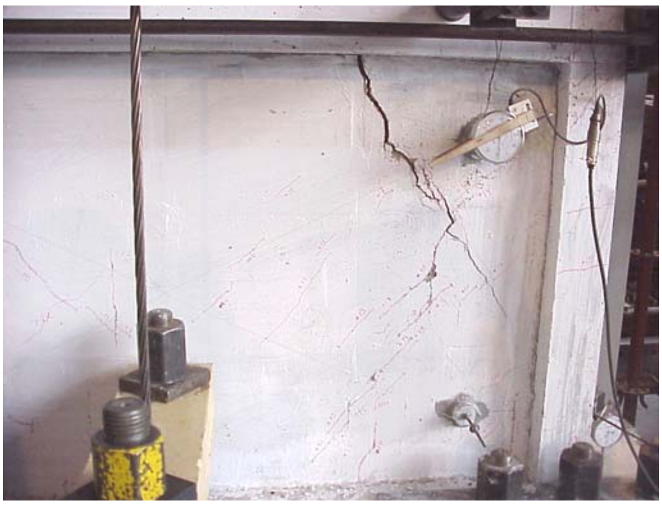

Figure 5.35 – Infill Cracks in the Seventeenth Cycle, Specimen CIC4

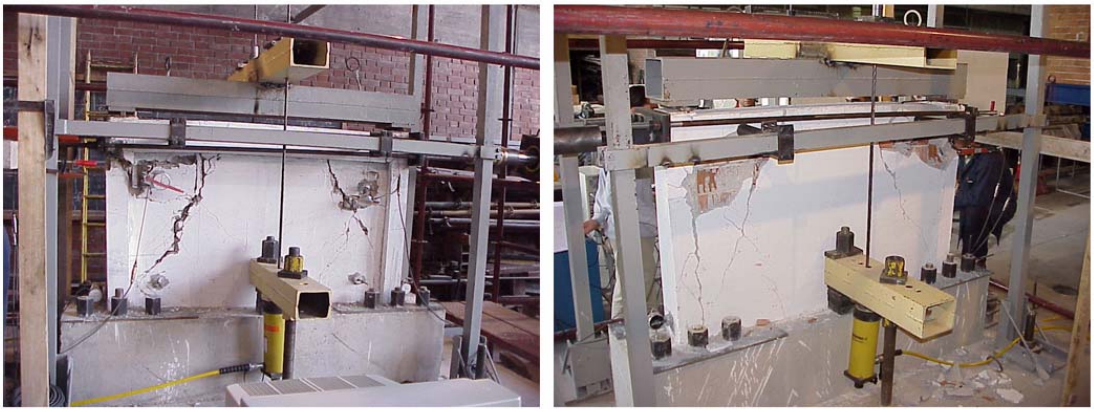

Figure 5.36 – General View of Specimen CIC4 after the Test

Figure 5.37 – Damage in the Beam-Column Joints after the Test, Specimen CIC4

5.6 SPECIMEN CID4

This specimen was a frame with continuous reinforcement strengthened with Type D panels and dowels along four sides were employed. Continuous bars were used for column longitudinal reinforcement. Specimen CID4 was tested under a constant axial load of 60 kN ($N/N_o = 0.25$) on each column.

Lateral load-lateral displacement graph given below in Figure 5.38 shows that the specimen CID4 carried the increasing cyclic load with little loss in its lateral stiffness, until the final cycle. The curves are quite symmetric and similar, reflecting the even distribution of infill cracks during the experiment.

Lateral load-shear displacement curve in Figure 5.39 is also very similar to this curve. These two curves indicate very successful load transfer and redistribution between panel, frame and connecting members. Especially symmetry and neatness of load-shear diagram is an indicator of the infill's robust behavior.

Load-south column deformation at the base diagram (Figure 5.41) has the expected one-directional behavior of the south column. However, the diagram for the north column base (Figure 5.40) indicates widening of the north column base crack or rotation towards the infill during loading in the forward direction, which would not normally be expected due to the support from the infill. However, this kind of deformation is possible if the column lost its restraint from the infill. There was a 10-mm thick epoxy layer between the column and the side panel for Type D panel application. In the test, the epoxy layer had been separated from the panel, and together with the separation of the column from the infill, the column base must have gained freedom for rotation and cracking under tensile stress from overturning. This large separation at the corner can be observed in Figure 5.45. However, rotation and cracking at the north column base does not seem to affect the desirable behavior of the frame, and does not disturb the symmetry of the load-displacement curve. This capacity of the infill was much higher than the frame members of this specimen, so upon failure of the infill, the frame could not carry this excessive load and failed in a brittle manner.

The critical observations for the testing of specimen CID4 are given below according to the loading cycle:

- In the second forward half cycle (70 kN), the plaster at the back side started to separate at the north side. Separation was observed at the back side of the frame along the column-infill connection at the north side. In the following backward half cycle, separation was seen at the column-infill connection at the south side, symmetrical to the separation in the previous half cycle. This separation crack was on both sides of the frame. In the third forward half cycle, separation was observed along the south column infill connection at the front side.

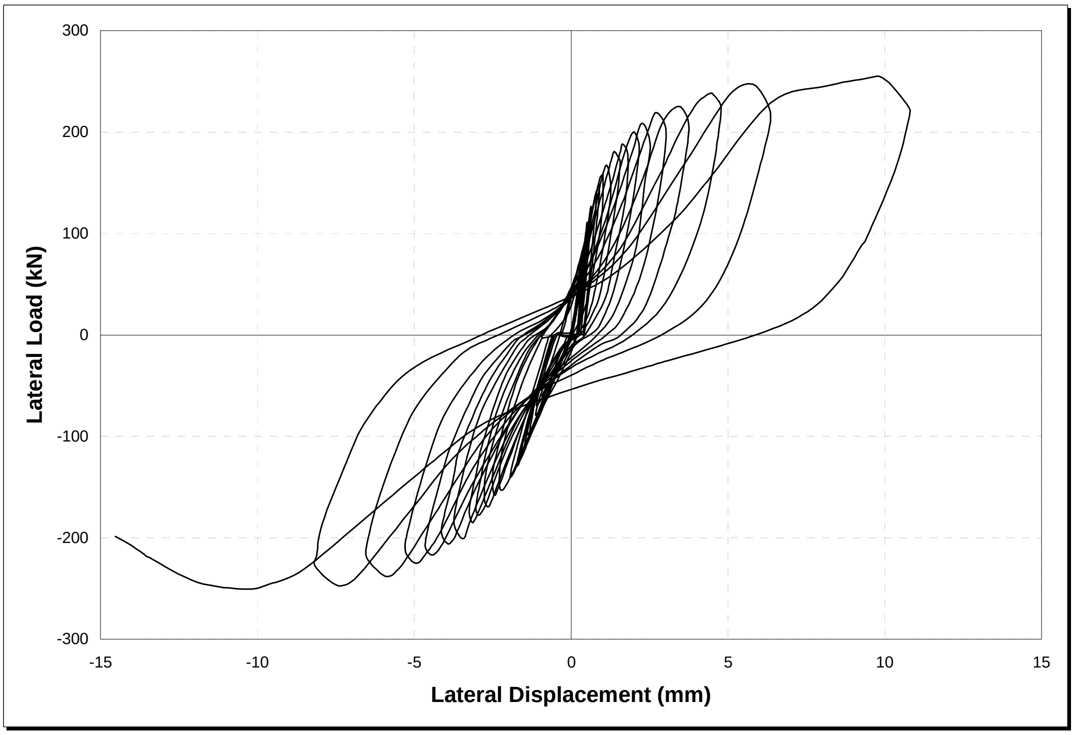

Figure 5.38 – Lateral Load - Top Displacement Curve, Specimen CID4

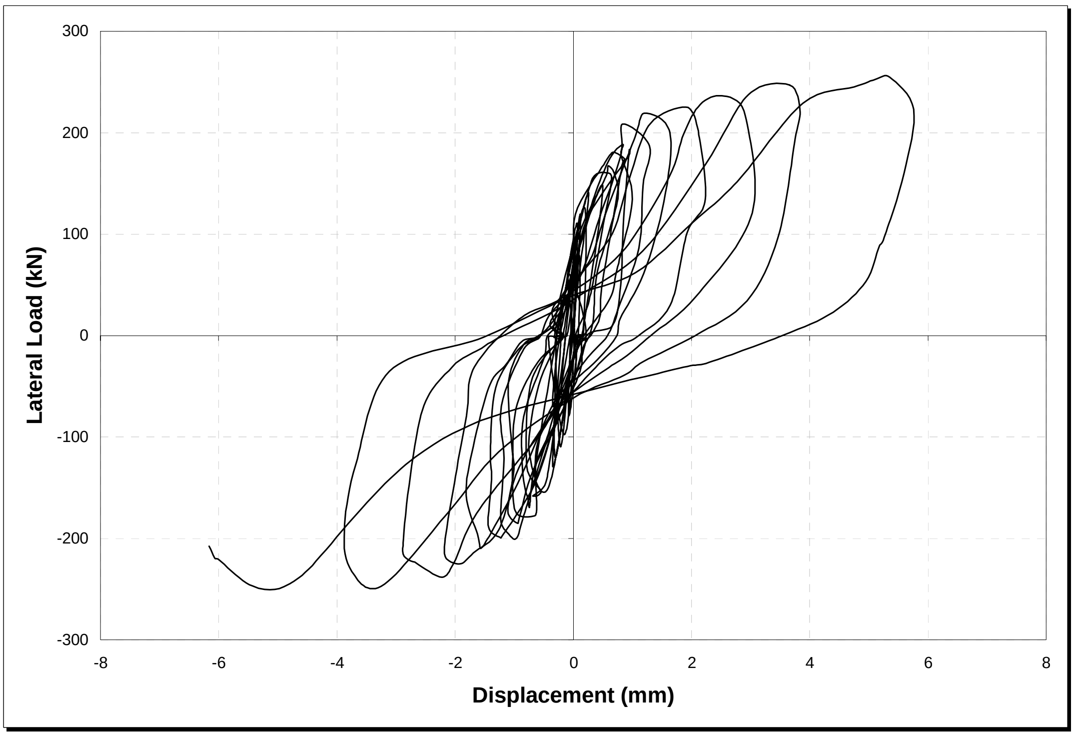

Figure 5.39 – Lateral Load - Shear Displacement Curve, Specimen CID4

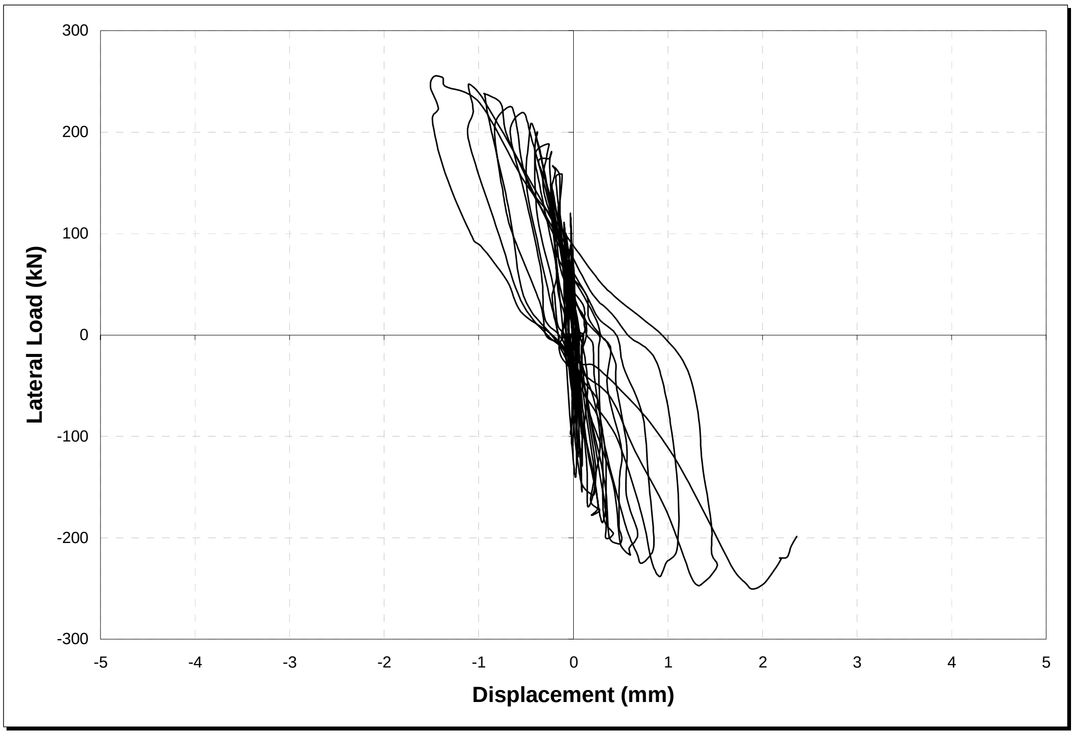

Figure 5.40 – Lateral Load-North Column Deformation at the Base, Specimen CID4

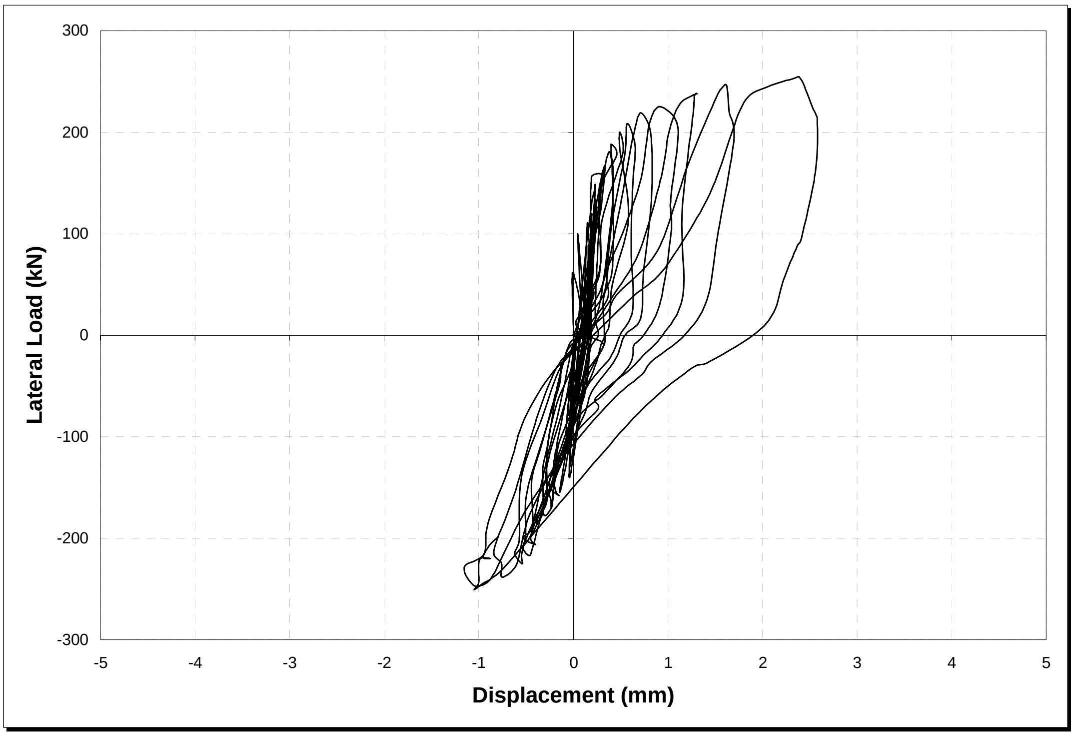

Figure 5.41 – Lateral Load-South Column Deformation at the Base, Specimen CID4

- In the seventh forward half cycle, a separation crack appeared at the foundation level of the infill at the north side, extending about 200 mm from the corner. This separation followed the edge of the epoxy layer and significantly split the column from the infill. Another separation crack at the foundation level was formed at the south corner of the infill in the seventh backward half cycle.
- In the eighth cycle, the separation at the foundation level extended at the north side and the south side in the forward and backward half cycles, respectively.
- A few thin diagonal cracks were formed on the panels close to the north side in the ninth forward half cycle. These diagonal cracks had a direction from the top north corner towards the bottom south corner of the infill (Figure 5.42). In the next half cycle, some thin cracks perpendicular to the previous diagonal cracks were formed on the panels close to the south side. A bending crack was observed at the bottom end of the south column and another small crack was noted at the joint of the south column with the beam.
- In the tenth forward half cycle, the north column cracked from bending at the foundation level. Also, small cracks appeared at the north beam-column joint.
- In the cycles ten through eighteen, diagonal cracks on the infill increased in number and length, and some major diagonal cracks of widths greater than 5 mm were formed. Some diagonal cracks extended following the connection surfaces between the panels vertically. The distribution of the cracks on panels increased to cover all over the infill surface with each consequent cycle.
- In the nineteenth forward and backward half cycles, significant cracks were formed on the north column and south column, respectively. Especially, the diagonal crack at the bottom of the south column, which is shown in Figure 5.44, seemed to be critical.
- In the twentieth backward half cycle, crushing started at the bottom end of the south column. Until this stage, load-deformation curve continued similarly at each cycle, with small stiffness change and shifting horizontally.
- In the twenty-first forward half cycle, the maximum capacity of the frame, which was 254.7 kN, was reached. In this half cycle, cracks on the north column increased and the major diagonal crack on the infill widened. At this

stage, the load-displacement curve started turning towards the horizontal and went through a large displacement.

- In the twenty-first half cycle, excessive deformation took place and the loading was stopped at 250.6 kN with 10.3 mm top deformation. After the loading was stopped, the deformation still continued increasing and diagonal cracks kept on progressing until the south beam-column joint failed suddenly. Column reinforcement bars buckled, panels at the corner crushed. Since the load carrying capacity of the specimen deteriorated, the test was terminated. The final view of the frame is given in Figure 5.47.

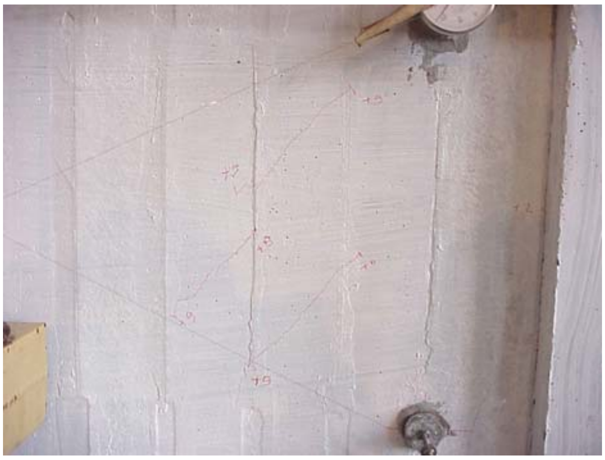

Figure 5.42 – Panel Cracks in the Ninth Cycle, Specimen CID4

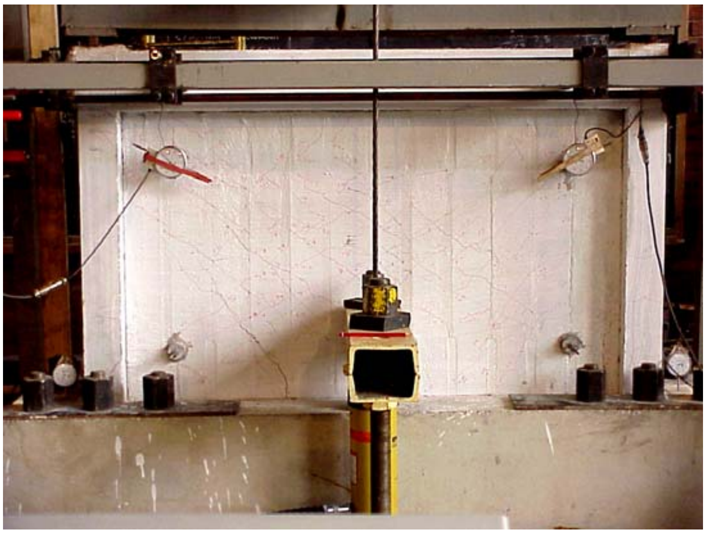

Figure 5.43 – Cracking on the Infill in the Sixteenth Cycle, Specimen CID4

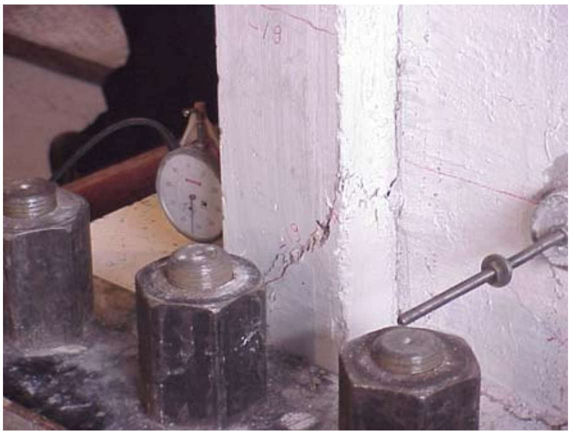

Figure 5.44 – Column Base Damage in the Nineteenth Cycle, Specimen CID4

Figure 5.45 – Separation of the Column from the Infill, Specimen CID4

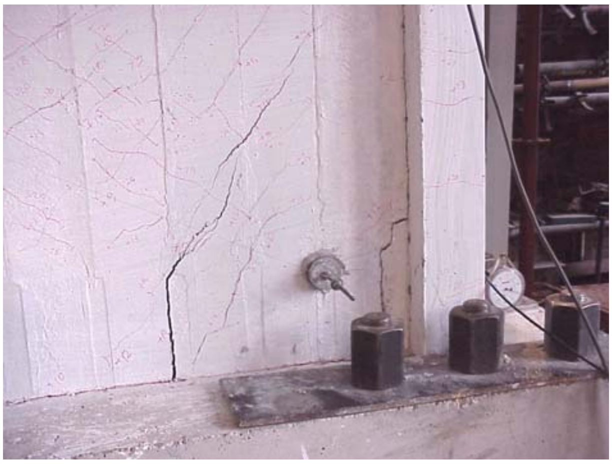

Figure 5.46 – Infill Cracking, Specimen CID4

Figure 5.47 – General View of Specimen CID4 after the Test

5.7 SPECIMEN LR

Specimen LR was an unstrengthened, brick masonry infilled frame having lap-spliced connections at column reinforcement bars at the foundation level. Lap-splices were 20ϕ, which equals 160 mm, in length. This test frame was constructed for acting as a reference for lap-spliced specimens strengthened with Type C and Type D precast panels. In the test, each column of this frame was applied 30 kN axial load (N/N_o = 0.13). Axial load applied on the columns of lap-spliced specimens was less than that of specimens with continuous reinforcement because adverse effects of a lap-spliced connection are expected to increase under a lower axial load.

The load-displacement diagram in Figure 5.48 shows relatively low lateral load capacity which drops rapidly after lateral load capacity is reached. Shear pinching is very significant in the curves. The main reason for the pinching effect seems to be reinforcement slip at the lap-spliced connection. When the bars slip, the load-displacement curve progresses almost horizontally and drops suddenly with removal of load, since the bars slide back into their place. In this specimen, column bases suffered greater damage than specimens with continuous reinforcement at the same lateral load levels, and this is also an indication of lap-splice effect. Also, cracks were observed on the columns at the lap-splice level.

The graph in Figure 5.50 showing the load vs. north column deformation at the base displays large displacement in both directions with relatively low stiffness. The displacement in the positive direction is the result of bending outwards with respect to the infill. Dial gauges show approximately 7 mm displacement where it was 2.3 mm for the reference specimen with continuous column reinforcement (Specimen CR). Negative side displacement is seen to be greater than the positive side, and is influenced both by bending and wide cracks forming by slipping of lap-spliced column reinforcement. Extension of dial gauges is about six times that for the specimen CR. These large deformations show both the lack of contribution from the infill wall to restrain the base region of the column and formation of extensive cracks at the lap-splice region. It also deserves attention that the bottom corners of the infill had been crushed; giving more rotational freedom to the column bases. Figure 5.51 is a similar graph showing the deformation characteristics of the south column at the base. The only difference is that deformations in two directions are not much different from each other. Same comments can be made for this graph. This graph implies that the behavior of the specimen is very similar to bare frame behavior.

Load-shear deformation graph in Figure 5.49 does not seem to be very helpful for drawing results, since the data from the dial gauges stopped when the infill crushed quickly. It can be said that the infill performs a linear behavior for a few cycles before jumps appear on the graph. The behavior of the brick masonry infill seems to be very brittle according to this graph.

Experimental observations for specimen LR are given below:

- In the first forward half cycle, hairline separation cracks were formed at the bottom north corner of the infill, along the foundation level and the column edge. The plaster cover at the rear surface of the frame started to separate at the top north edge. In the negative half cycle, the same pattern of separation was observed at the south edge of the infill.

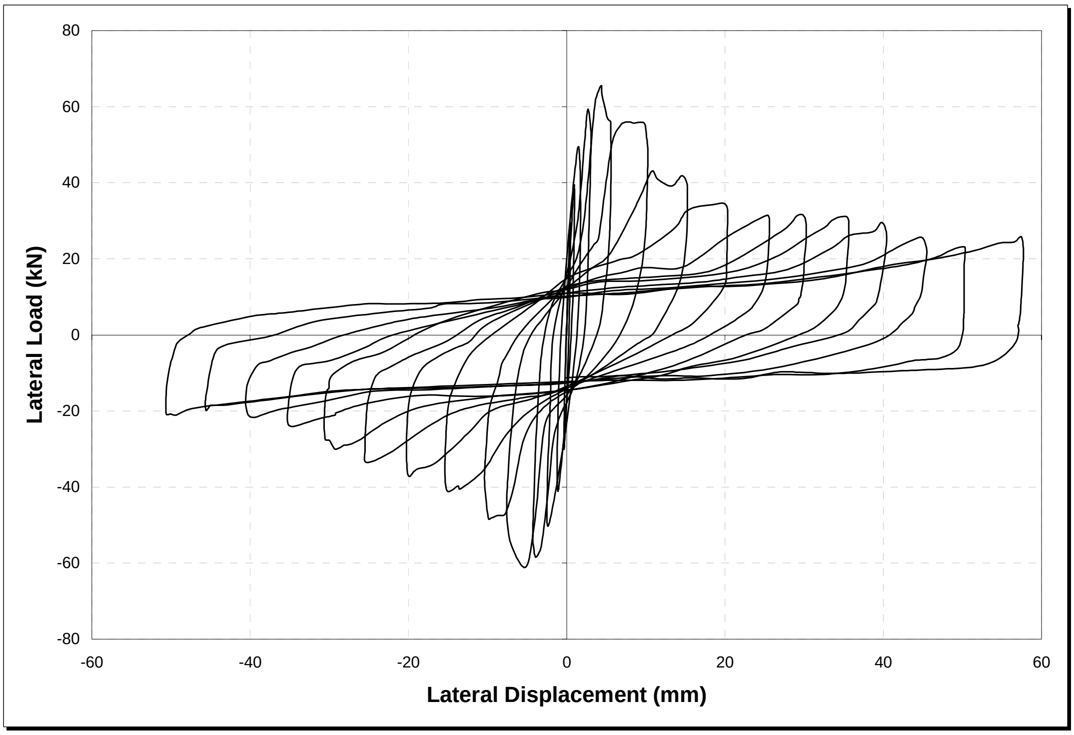

Figure 5.48 – Lateral Load vs. Top Displacement Curve, Specimen LR

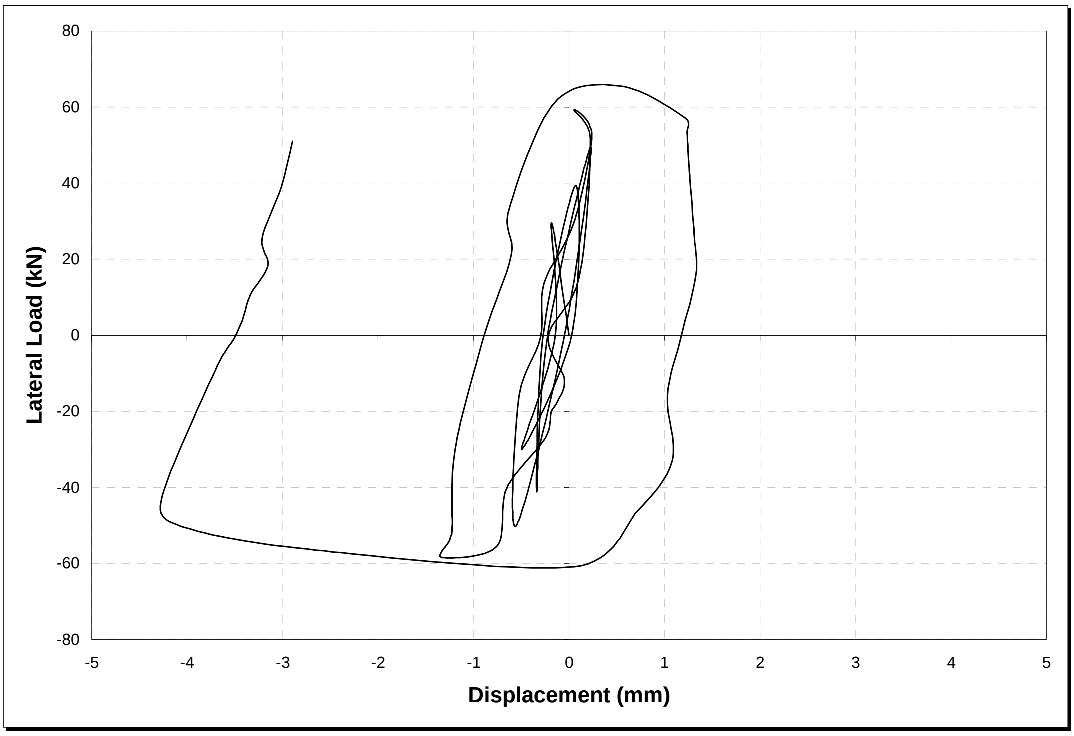

Figure 5.49 – Lateral Load - Shear Displacement Curve, Specimen LR

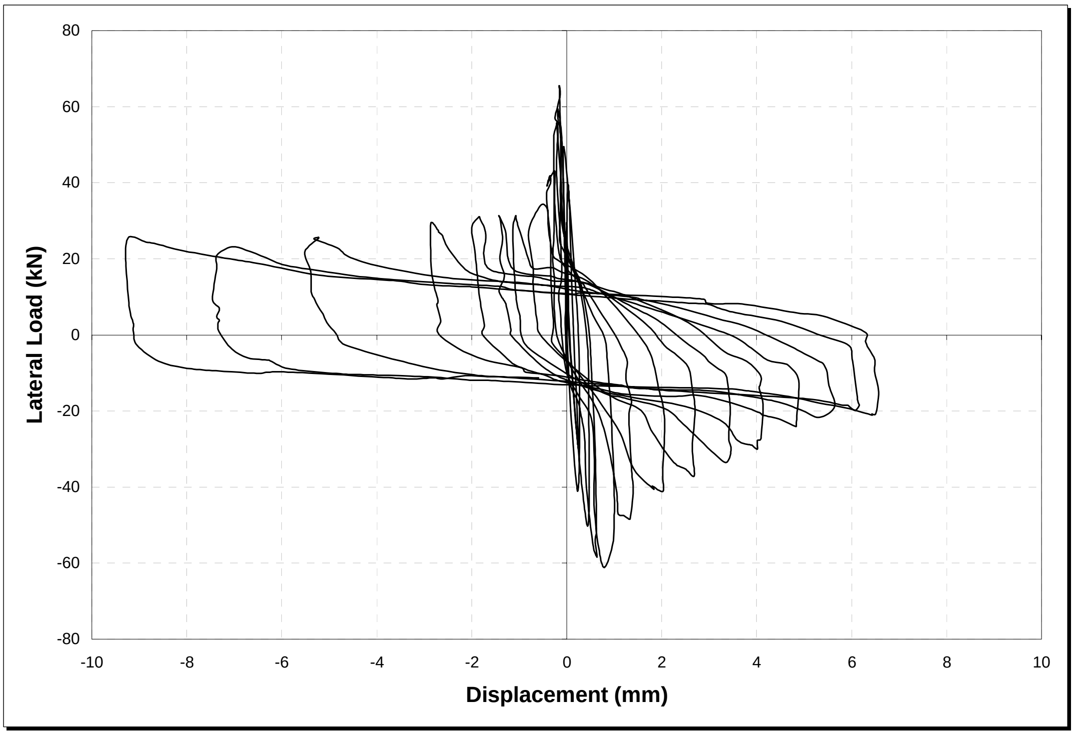

Figure 5.50 – Lateral Load-North Column Deformation at the Base, Specimen LR

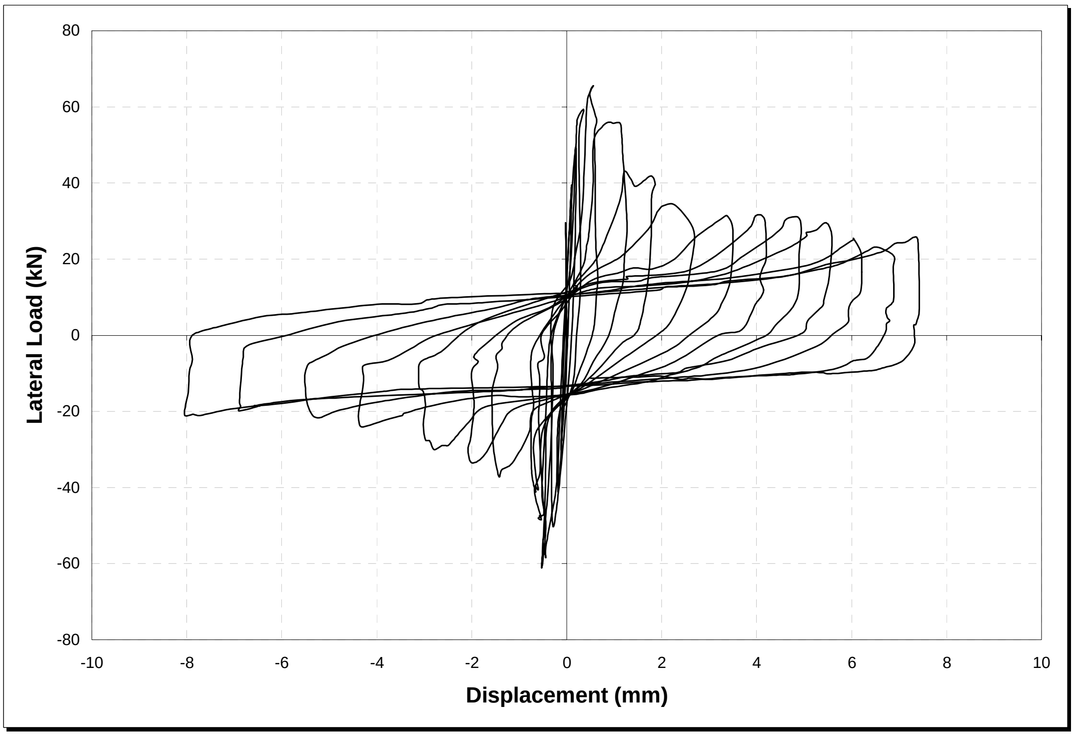

Figure 5.51 – Lateral Load-South Column Deformation at the Base, Specimen LR

- Infill base has separated completely in the second cycle. In the forward half cycle, north beam-column joint cracked, and in the backward half cycle, south beam column joint has cracked.
- Brick infill started to crack diagonally in the third cycle. Base separation was formed at the north column in the forward half cycle and at the south column in the backward half cycle.
- Another bending crack was formed at the outer surface of the north column 100 mm above the base, in the fourth forward half cycle. This crack appeared like a bending crack and close to the lap-splice end where stress concentration was expected (Figure 5.52). In the fourth backward half cycle, top south corner of the infill started crushing. Crushing was seen at the opposite corner in the fifth forward half cycle. A sudden jump was seen in the load-shear displacement graph related with infill crushing. In the backward loading of the fifth cycle, multiple bending cracks were seen at the south column. In the fifth forward half cycle, the maximum lateral load of the test was recorded as 65.5 kN. Joint cracks progressed. After this cycle, the experiment was continued on a displacement controlled basis. The next cycle was carried out until 10-mm top deformation and the following cycles were continued with 5-mm increments. In the next cycles, significant loss of lateral strength and stiffness was observed from the load-displacement graph.
- In the sixth, seventh and eighth cycles, many new column cracks were formed and the existing ones grew larger. In the eighth cycle, plaster started to fall down and the dial gauges on the infill were detached.
- In the later cycles, severe damage of frame members was observed. Both columns developed many cracks and their deformation was noticeable (Figure 5.53). Joint cracks extended to the outer surface with large widths. Infill crushed completely at the corners. Due to excessive damage, the experiment was ended at the end of the fifteenth forward half cycle. The final view of the frame from the front and back can be seen in Figure 5.54.

Figure 5.52 – Cracking at the Column Base and Lap-Splice Level in the Fourth Cycle, Specimen LR

Figure 5.53 – Deformation in the Frame during the Test, Specimen LR

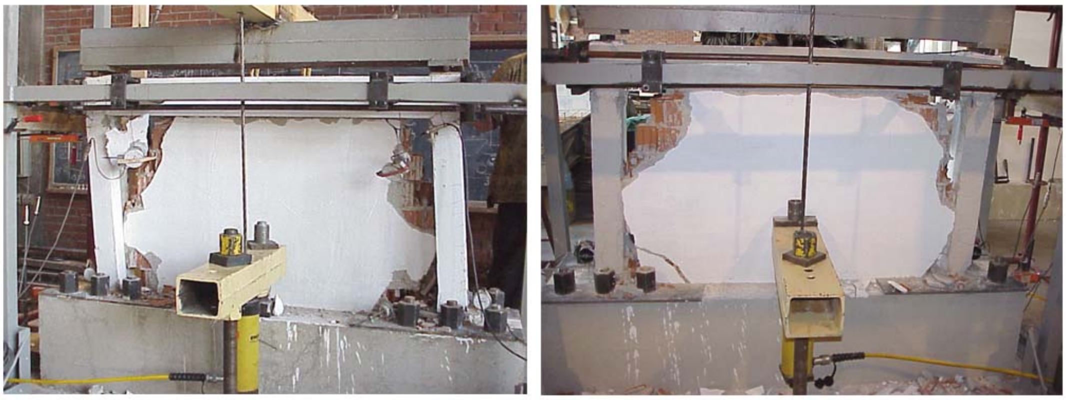

Figure 5.54 – General View of Specimen LR after the Test

5.8 SPECIMEN LIC4

This specimen was a lap-spliced specimen identical with the reference specimen LR, except that it had been strengthened with Type C precast panels bonded on the masonry infill. Dowels were used along four sides. The reinforcement bars had the same lap-spliced connection which was 20ϕ (=160 mm). Each column of this frame was applied 30 kN constant axial load ($N/N_o = 0.13$) throughout the experiment like all lap-spliced specimens.

Load-displacement graph (Figure 5.55) shows a desirable behavior having stable loops with very slowly declining peaks. Highest load reached in the experiment was 148.9 kN at 10.3 mm top displacement. This capacity is much higher than the reference specimen with lap-spliced connection, being 65.5 kN.

Load-column deformation at the base graphs in Figure 5.56 and Figure 5.57 show considerable deformation in both directions. According to Figure 5.56, north column base experiences more deformation in forward loading. Since the capacity of the infill does not disappear after cracking, excessive deformation at the column base should be related with cracking due to tensile forces from overturning. Slipping of bars at the lap-splice region seems to be the most important cause of excessive cracking in forward loading direction. North column also made significant deformation during backward half cycles, especially after diagonal cracks form on the infill. South column base, on the contrary, showed less deformation during backward loading and very significant deformation during forward loading. The inconsistency of column deformation at the base diagrams arise from asymmetrical infill cracking. This asymmetry is also observed in load-shear deformation graph (Figure 5.58). Large deformations in this graph reflect very wide openings observed at major diagonal cracks on the infill.

The most important proof of bar slip is the pronounced shear pinching in load-column deformation at the base graphs (Figure 5.56 and Figure 5.57) and load-shear displacement graph (Figure 5.58). The curves in Figure 5.56 and Figure 5.57 show a very steep drop in the positive displacement direction after loading is stopped. This means that when unloaded, the column base does not have rotational stiffness to return to original position, since the bar has slipped. The curves continue horizontally while reverse loading as the bars slip back to their place. The pinched shape in load-shear displacement graph has also similar meaning. Cracks do not close when load is removed, since the column bases have lost rotational stiffness due to slipping.

Experimental observations for this specimen are given below:

- In the second cycle, separation started at the column-infill connection from the bottom. Separation was observed at the north side in the forward half cycle and at the south side in the backward half cycle.
- Hairline column base cracks were observed on the outer faces of the columns; north column in the forward half cycle and south column in the backward half cycle.

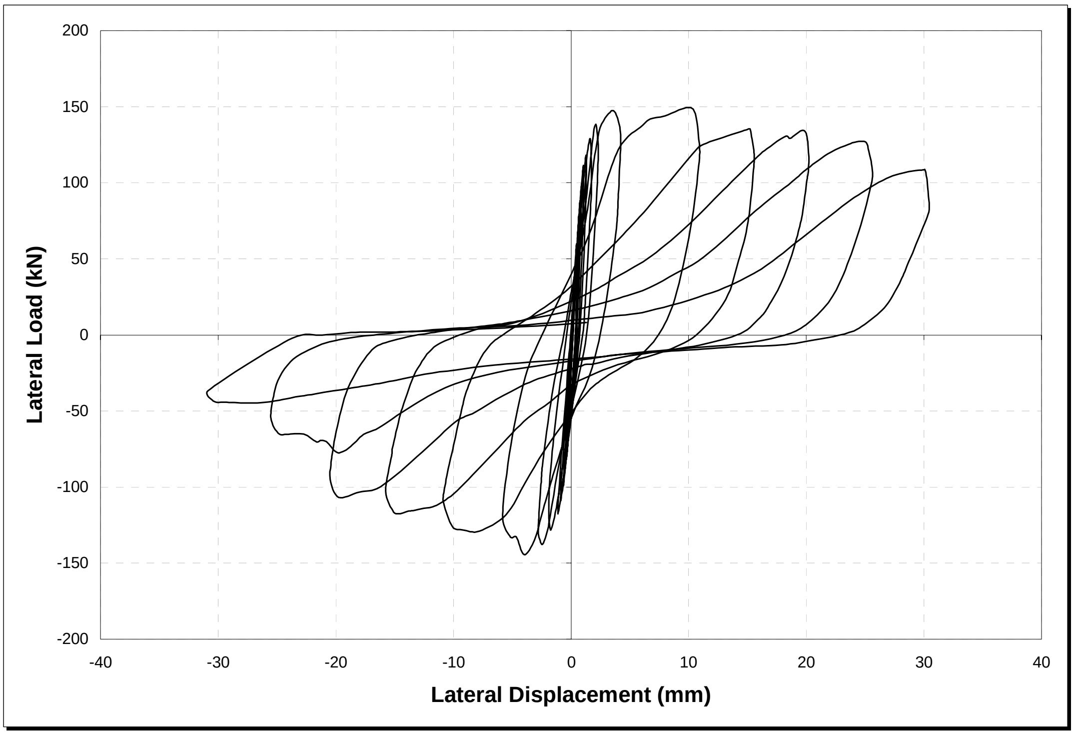

Figure 5.55 – Lateral Load - Top Displacement Curve, Specimen LIC4

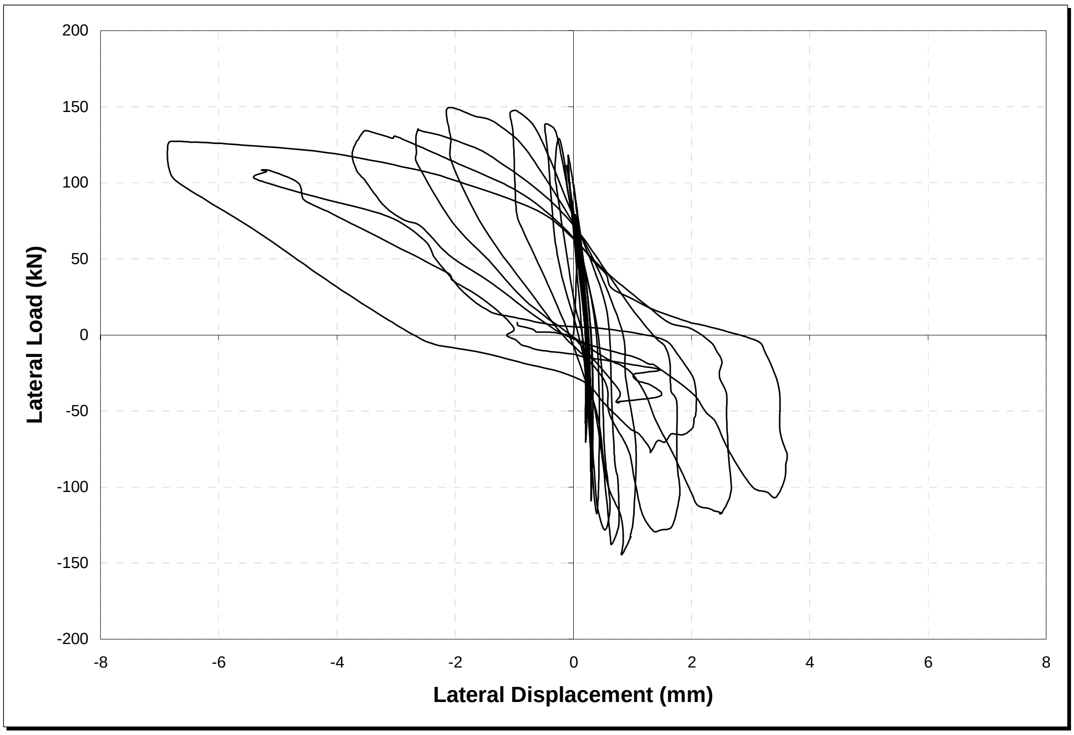

Figure 5.56 – Lateral Load-North Column Deformation at the Base, Specimen LIC4

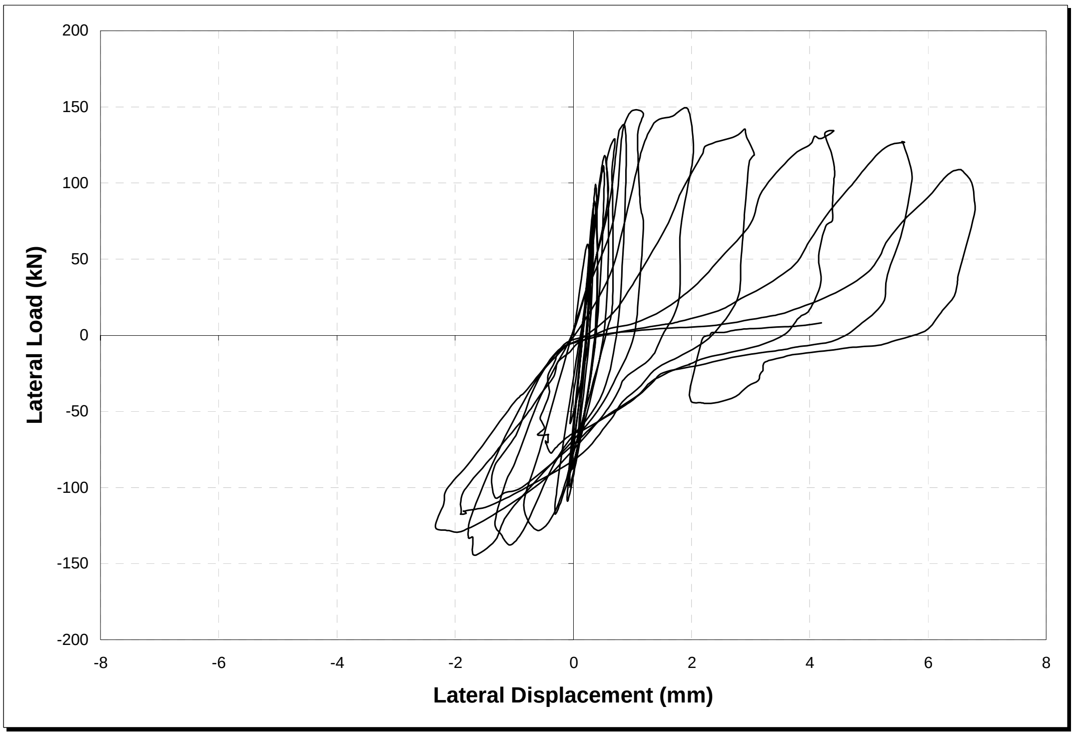

Figure 5.57 – Lateral Load-South Column Deformation at the Base, Specimen LIC4

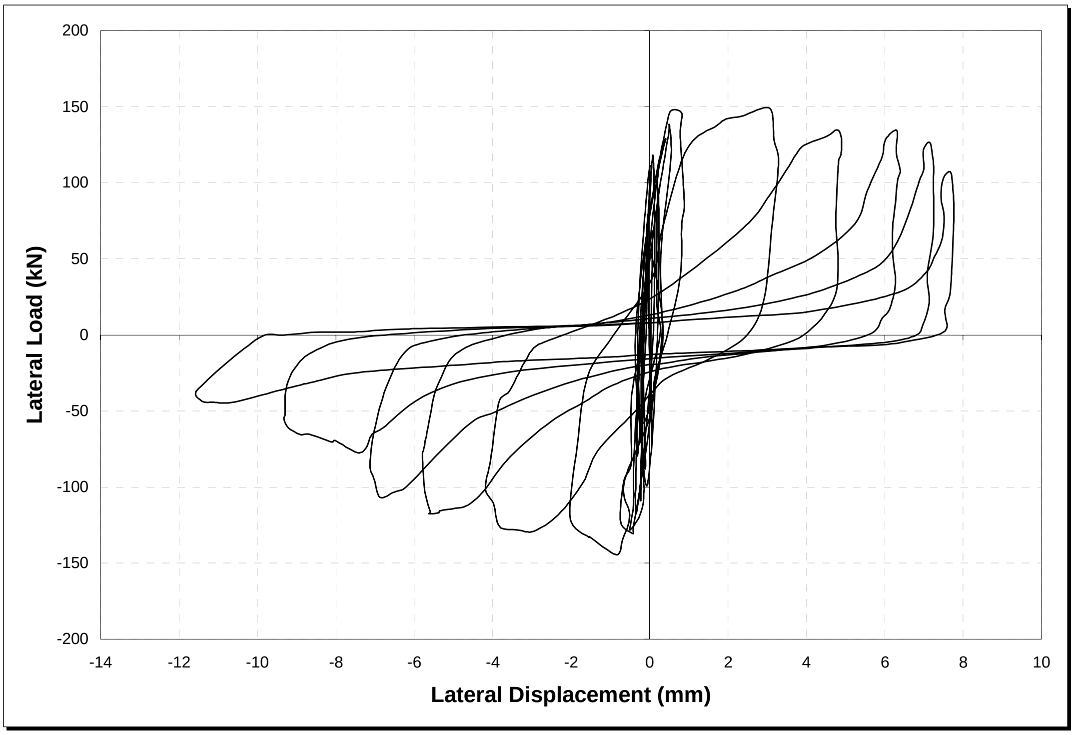

Figure 5.58 – Lateral Load-Shear Displacement Curve, Specimen LIC4

- Infill base started separate in the fifth half cycle. In the forward half cycle, separation started from the bottom north corner and extended towards the center about 400 mm. In the backward half cycle, a symmetrical separation started to develop from the south corner and reached to approximately same length.
- North column cracked at the mid-height in the seventh forward half cycle and this crack progressed further in the eighth forward half cycle. First joint crack was observed at the north beam-column joint in the seventh forward half cycle and this crack extended diagonally (Figure 5.59). Separation was observed at the base of the south column in the eighth backward half cycle.
- Separation of the infill along the column edges widened in the ninth cycle. The south beam-column joint cracked in the ninth backward half cycle.
- Panel cracking started in the tenth forward and backward half cycles, close to north and south sides, respectively. The cracking pattern is shown in Figure 5.60. Load-displacement curve started turning to horizontal direction towards

the peak. The curve in the load-shear displacement graph also had a bend due to stiffness degradation by opening of diagonal cracks.

- Maximum lateral load of this experiment (148.9 kN) was observed in the eleventh forward half cycle. Loading was continued until 10 mm top displacement. From this cycle on, testing was performed as displacement controlled with 5-mm increments of top level displacement for each successive cycle. Loops of load-displacement graph became rounder at each successive cycle, but maximum loads of the loops did not decrease significantly.
- From the twelfth cycle on, major diagonal cracks on the infill were formed depending on the loading direction, and opened up with increasing load levels. With unloading and reloading in the opposite direction, the crack narrowed down and diminished, while the diagonal crack for the opposite direction was becoming larger. In Figure 5.61, the views on the left and right are during loading in the forward and backward directions, respectively. Large displacements were observed in load-shear deformation graph due to continuous widening of these diagonal cracks under increasing load. The frame was also suffering further damage with increasing drift levels. The damage in the frame was mainly concentrated at the beam-column joint regions, where many significant diagonal cracks and crushing were observed.
- Column base deformations increased to more than 4 mm, and indication of bar slip at the lap-splice region was observed for the tension sides (Figure 5.62). Large tensile deformations at column end dial gauges also support the evidence of bar slipping. The experiment was ended after the fifteenth cycle, in which ±30 mm top displacement was given to the specimen. The final views of the specimen from the front and back are given in Figure 5.63.

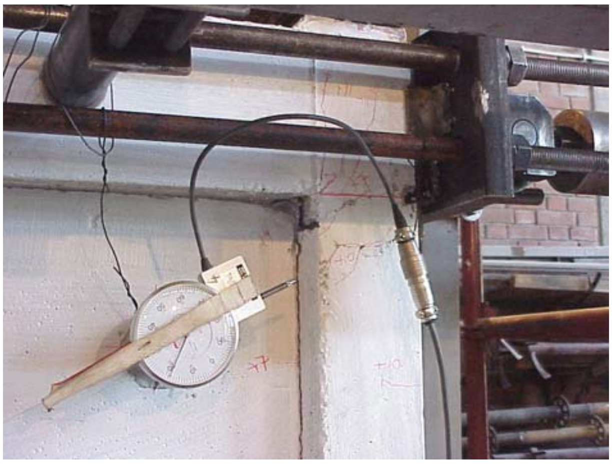

Figure 5.59 – Damage in the Column and Joint Region in the Seventh Cycle, Specimen LIC4

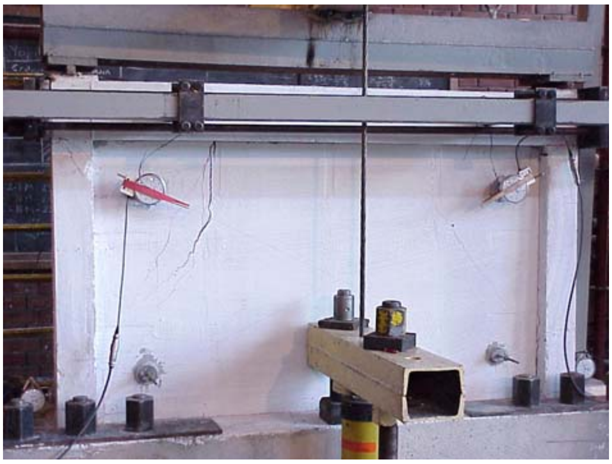

Figure 5.60 – Cracks on the Infill in the Tenth Cycle, Specimen LIC4

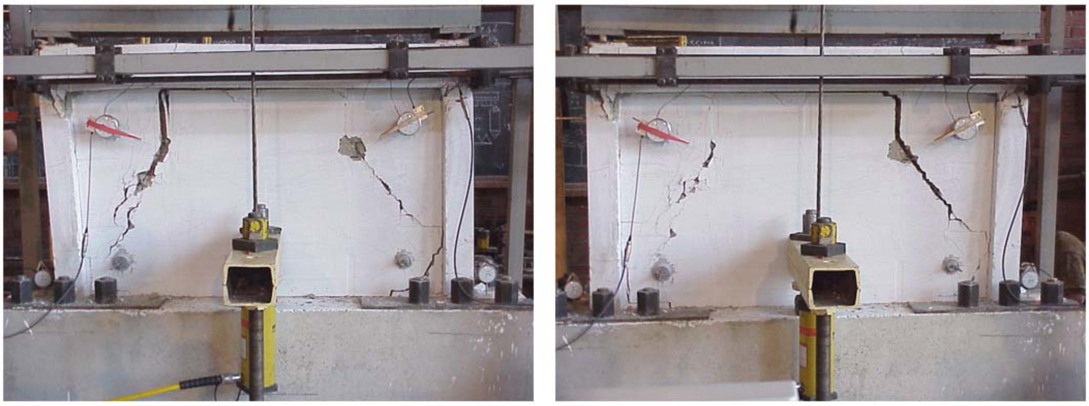

Figure 5.61 – Widening of Cracks According to Loading Direction, Specimen LIC4

Figure 5.62 – Column Base Crack (left) and Joint Cracks (right), Specimen LIC4

Figure 5.63 – General View of Specimen LIC4 after the Test

5.9 SPECIMEN LID4

LID4 was a frame with lap-spliced connection (20ϕ = 160 mm) in its column longitudinal reinforcement. This frame was strengthened with Type D precast panels and dowels were employed along four sides. In the test, each column of this frame was applied 30 kN constant axial load ($N/N_o = 0.13$).

This specimen also showed a good lateral strength increase with respect to the reference specimen, as can be seen from the lateral load-lateral displacement graph in Figure 5.64. The behavior of the specimen seems to be very desirable according to the graph with considerable capacity increase with respect to the reference specimen. Highest load was 199.6 kN for this specimen.

Inspection of load-column deformation at the base graphs shown in Figure 5.66 and Figure 5.67 reveals that column bases suffer large deformations while being at the tension side according to lateral loading direction. Similar to the lap-spliced LIC4 specimen, large deformations in this direction can be accepted as proof of bar slip at lap-splice regions. Pinching is very significant in load-column deformation at the base and load-shear displacement graphs, and as explained for the previous specimen (LIC4), this is a very open indication for bar slip.

Lateral load-shear displacement graph in Figure 5.65 reflects a very good behavior for the infill. According to this graph, the panel cracks were well distributed for both directions, which reflect the actual behavior during the test.

Following are the important experimental observations for specimen LID4:

- In the first forward half cycle, separation cracks started to develop at both sides of the infill, separating the column from the foundation level to the column mid-height.

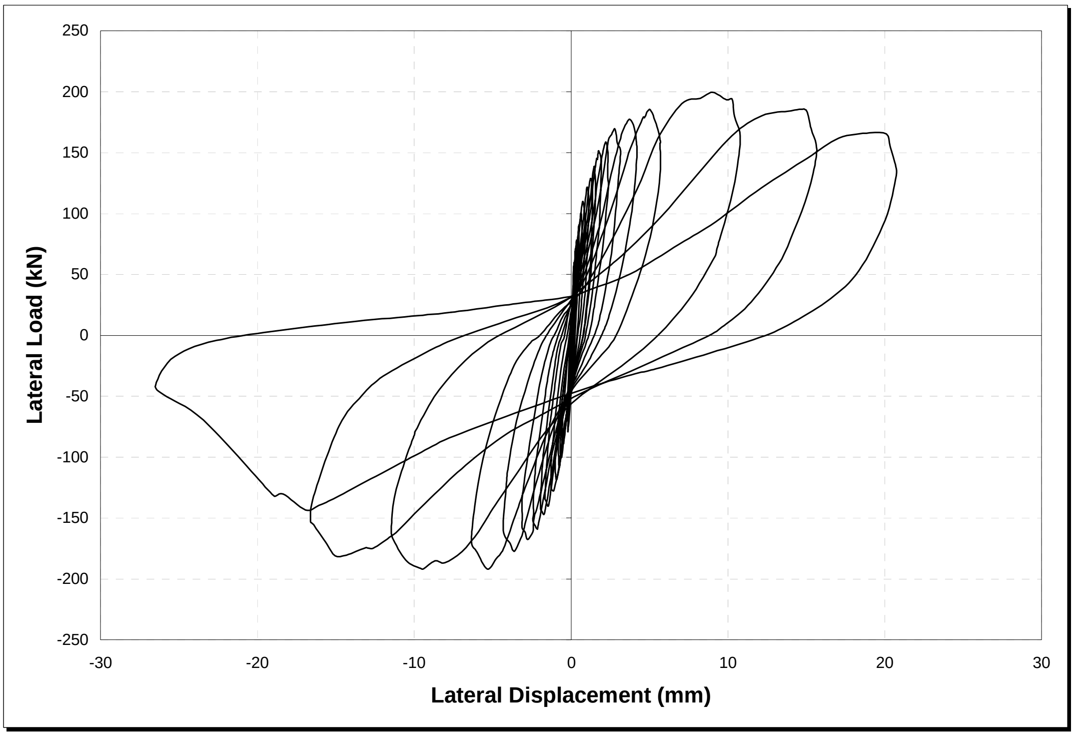

Figure 5.64 – Lateral Load - Top Displacement Curve, Specimen LID4

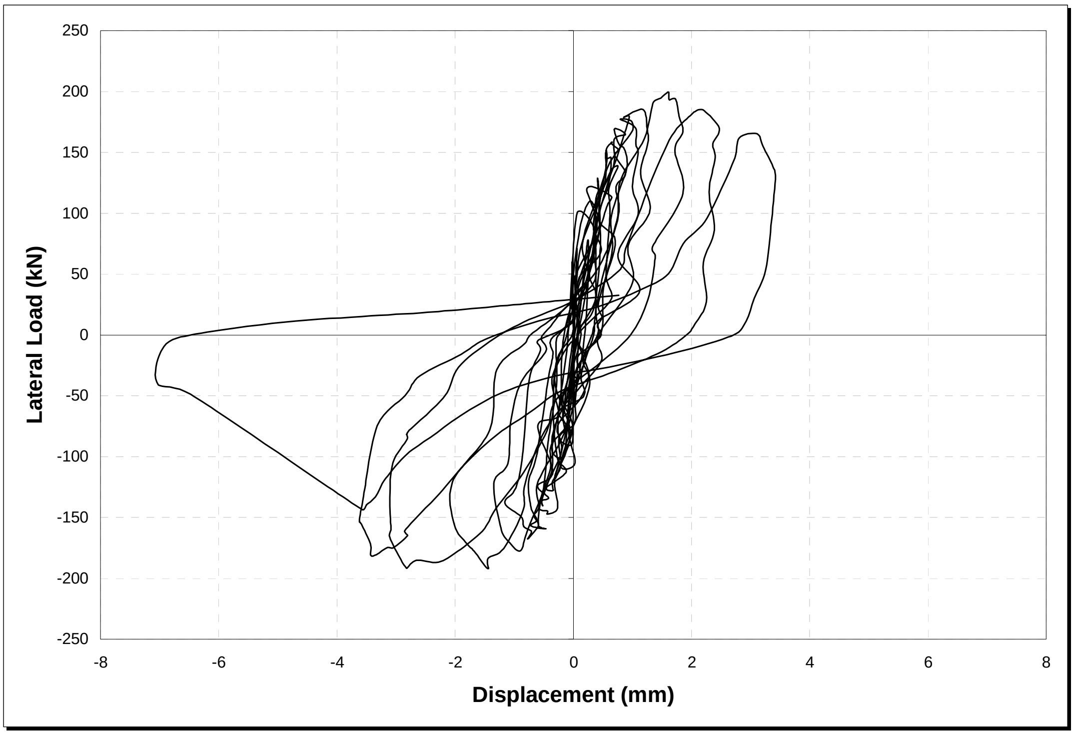

Figure 5.65 – Lateral Load - Shear Displacement Curve, Specimen LID4

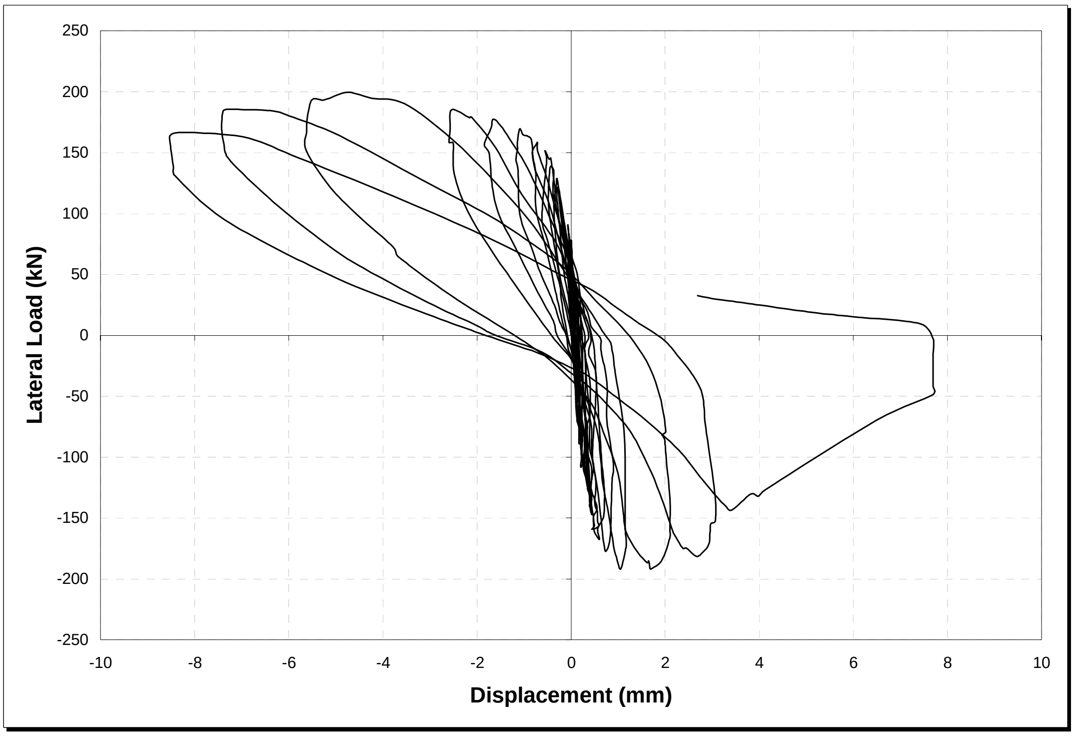

Figure 5.66 – Lateral Load - North Column Deformation at the Base, Specimen LID4

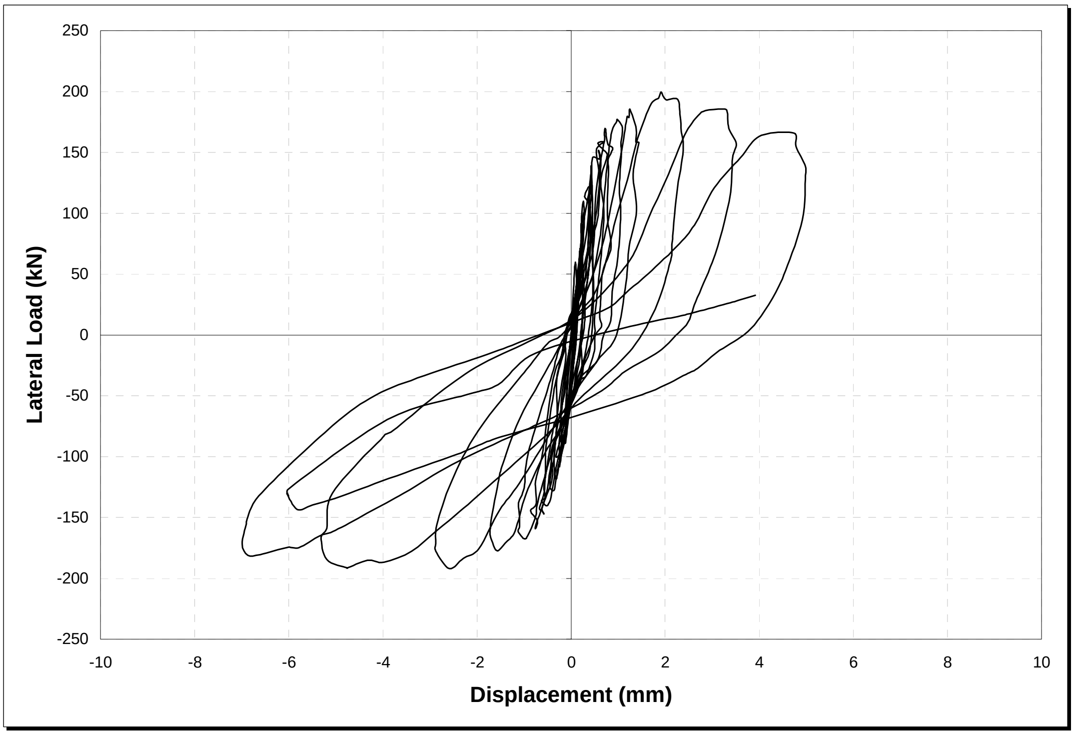

Figure 5.67 – Lateral Load - South Column Deformation at the Base, Specimen LID4

- First column base crack was observed in the third forward half cycle at the north column. The base of the south column cracked in the backward loading of the third cycle.
- The infill started to separate from the base from the north end in the fifth forward cycle. Also, separation started on the plaster at the back side of the frame in this half cycle.
- The front face of the south column cracked in the sixth backward half cycle. In the seventh forward half cycle, a crack was observed on the outer surface of the north column. This crack increased in the eighth cycle. Another crack was formed at the south column in the ninth negative half cycle.
- The first diagonal panel crack was formed in the tenth backward half cycle for which the maximum lateral load was 150 kN. This was a hairline crack and occurred closer to the bottom south corner of the infill. Also, in this cycle, a crack at the south beam-column joint was observed as the first joint crack. The opposite joint cracked in the eleventh forward half cycle.

- In the cycles twelve to fourteen, many thin cracks appeared over the infill and their length and distribution increased with consequent cycles. Cracks developing in the opposite loading directions started intersecting each other and forming X marks on the infill.
- Base crack of the north column grew significantly in the thirteenth forward half cycle, showing evidence for slip at the lap-splice. The crack width was approximated as 1.5 mm. Base crack of the south column also increased in the negative thirteenth half cycle and was accepted as indication for bar slip at the lap splice. The north column deformation at the base became as much as 2.5 mm in the fourteenth forward half cycle. Large increase in crack widths is also obvious in load-column deformation at the base graphs, especially for the north column.
- The maximum load of the experiment was recorded in the fifteenth forward half cycle as 199.6 kN. From this point, the load started to decrease and deformations started increasing more rapidly. The fifteenth cycle was limited by 10-mm top deformation and the following cycles by 5-mm increments.
- Some cracks on the infill joined to form major diagonal cracks starting from the fifteenth cycle. Column bases and beam-column joints suffered heavy cracking in the sixteenth cycle. Column base cover concrete has crushed and reinforcement became visible.
- During loading in the seventeenth backward half cycle, the specimen failed suddenly at -18.9 mm displacement.

Figure 5.68 – Infill Cracking Pattern, Specimen LID4

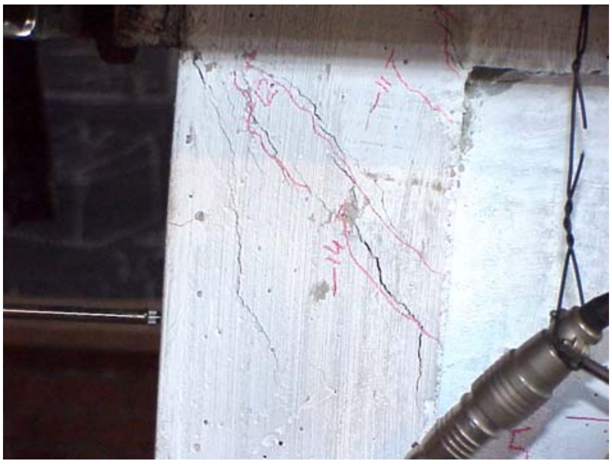

Figure 5.69 – Damage in the South Beam-Column Joint, Specimen LID4

Figure 5.70 – Development of Infill Cracks, Specimen LID4

Figure 5.71 – Cracking at the Column Base and Lap-Splice Region, Specimen LID4

Figure 5.72 – Damage in the Lap-Splice Region of the Column, Specimen LID4

Figure 5.73 – General View of Specimen LID4 after the Test

CHAPTER 6

EVALUATION OF TEST RESULTS

6.1 GENERAL

In this chapter, test results are evaluated in terms of strength, stiffness, energy dissipation and interstory drift characteristics and compared with the test results of the reference specimen.

6.2 RESPONSE ENVELOPES

Response envelope curves are produced by connecting the peak points of the hysteretic load-top displacement curves of the specimens. They are used for representing strength and stiffness characteristics of the specimens. Response envelopes are useful for comparison of strength and stiffness of different specimens.

In Figure 6.1, response envelopes of the specimens with continuous reinforcement are plotted together. In this figure, the strength increase of the four strengthened specimens with respect to the reference specimen can be observed. Response envelopes for specimens CIA4 and CIB4 follow a very similar trend. They both exhibit more than twice of the lateral strength of the reference specimen. Specimen CIC4 also shows a very similar behavior having the response envelope almost coinciding with that of CIA4 and CIB4. The only difference is the lower ductility level, and this can be attributed to the simpler connection details between the panels and the frame members and among the panels. It appears that this specimen also exhibits frame behavior after diagonal cracking and crushing of its infill.

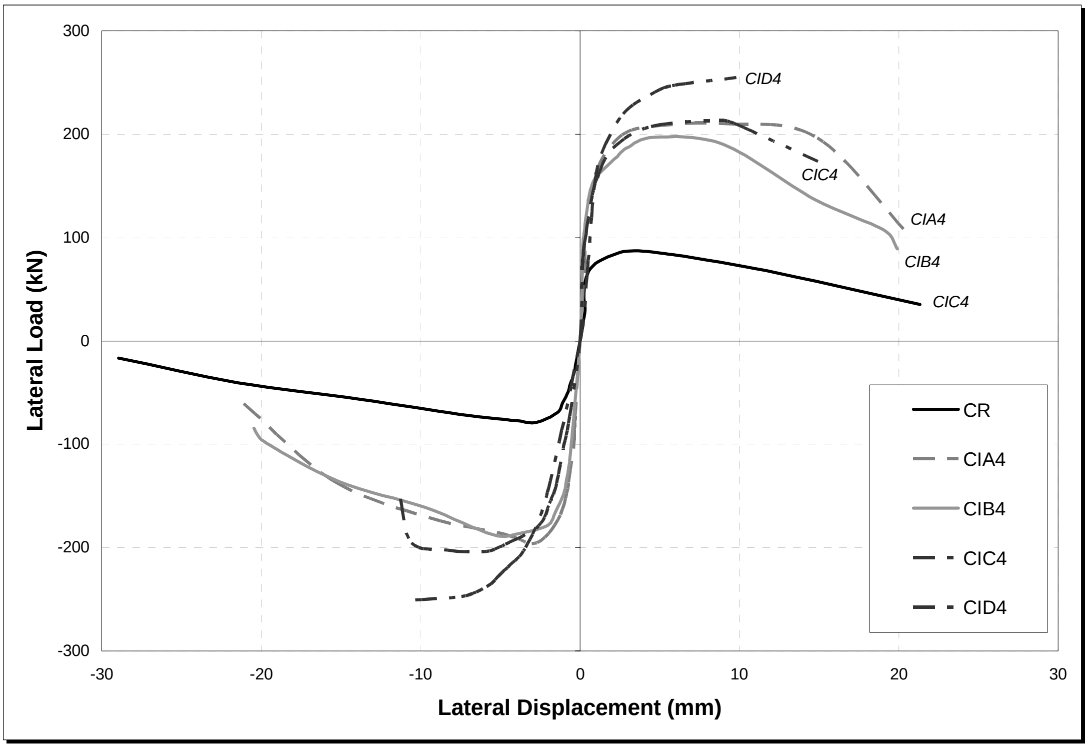

Figure 6.1 – Response Envelopes of Specimens with Continuous Reinforcement

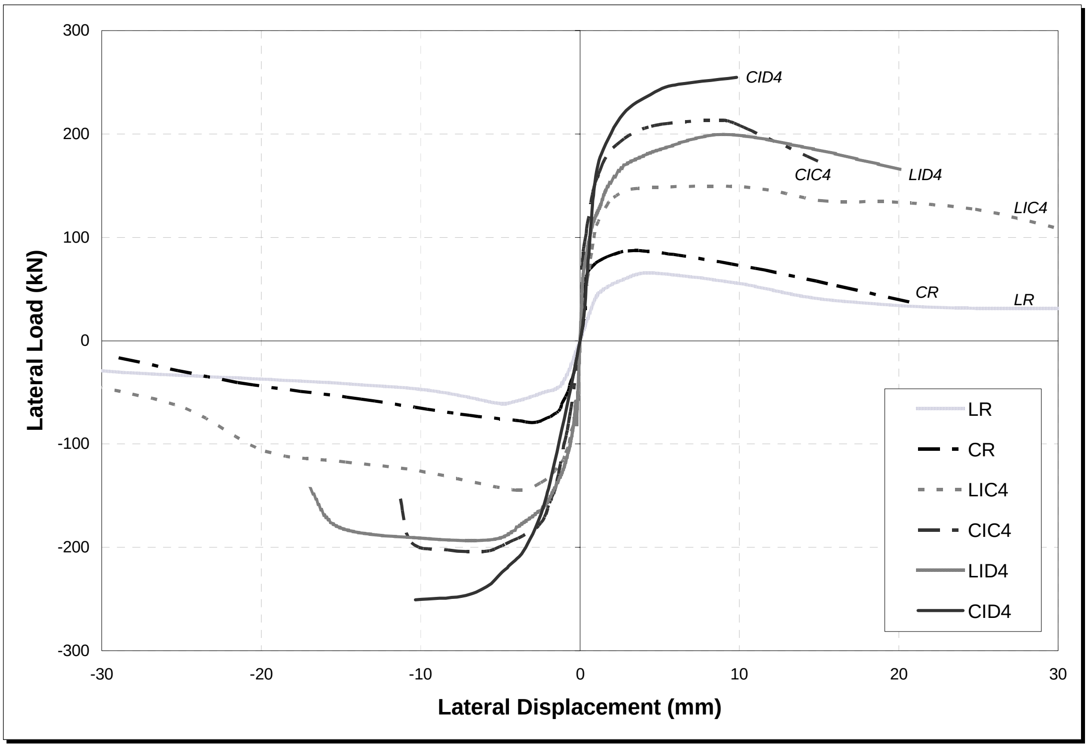

Figure 6.2 – Comparison for Response Envelopes of Lap-Spliced Specimens

However, the response envelope of the other strengthened specimen CID4 has significant difference. CID4 has distinctively higher lateral load capacity than all other specimens. On the other hand, the response envelope shows much less ductility, not reaching half of the maximum lateral displacements of other specimens. The infill panels of specimen CID4 had dowel connections to all frame members, and due to the strip shape of the panels, it had a greater number of dowels at the foundation and beam.

According to the test results, intense dowels and panel shapes provided CID4 with an infill of relatively high load capacity. The capacity of this specimen was even higher than that of specimen CIB4 which had dowels along the four sides of the frame weld-connected to the bars at the panel corners. This result suggests that, the anchorage type in CID4 is more effective than CIB4, since the two specimens have the same panel concrete strength and close frame concrete strength. CID4 and CIB4 have the same number of dowels, but the dowels of CID4 have larger diameter and are longer, extending 150 mm between the panels. Although CIB4 had welding, the dowels were much shorter and they were welded to panel bars with only 4-mm diameter. Having longer and thicker dowel bars bonded to panels as effectively as welding by means of the epoxy mortar, better behavior was observed in the testing of specimen CID4. Experimental observations showed that specimens CID4 and LID4 had a better frame-infill connection, remaining intact

In Figure 6.2, response envelopes of lap-spliced specimens are provided together with the specimens with continuous reinforcement having the same panel types but different axial load level. The strengthened lap-spliced specimens show similar strength increase as the specimens with continuous reinforcement with respect to the reference specimen. When compared with specimens with continuous reinforcement, corresponding lap-spliced specimens had relatively lower strength. Lower lateral load capacity is due to lower frame capacity owing to bar slip and additional deformations at the lap-splice regions and lower axial load level. Behavior of lap-spliced specimens was closer to frame behavior. Lower axial load level applied to the lap-spliced specimens led to widening of diagonal cracks on the infill.

As the result of this, larger diagonal cracks decreased capacity of the infill and increased deformations.

6.3 STRENGTH

Providing sufficient lateral strength is one of the most important aims for seismic strengthening. Therefore, the ultimate strength of the rehabilitated specimens and strength increase relative to the unstrengthened specimens is critical. In Table 6.1, the maximum values of lateral load are listed for each test specimen, for loading in the forward and backward directions. It was observed that the maximum loads of the specimens were obtained during loading in forward direction but not much different from the capacity in the opposite direction. Lap-spliced specimens had carried considerably less lateral load than the corresponding specimens with continuous reinforcement. Some effect of lower axial load is also expected on lateral load capacity. Among the specimens with continuous reinforcement, CID4 has the largest load capacity. CIC4 and CID4 specimens showed higher strength than CIA4 and CIB4 although there was no shear key and welding between the panels. However, dowels from four sides of the infill extended between panels in CIC4 and CID4 specimens, and they seem to provide better connection than welding.

In Table 6.2, the strength increase relative to the corresponding reference specimen is given separately for specimens with continuous reinforcement and specimens with lap-spliced reinforcement. The superior capacity of specimens strengthened with type D panels (CIC4 and LIC4) over specimens strengthened with type C panels (CIC4 and LIC4) is very significant. The most influential factor is the number of dowel bars. At the foundation level and beam level, 5 dowels were used for type C dowels, whereas 13 dowels were employed between panels of type D, due to different shape of the panels. Also, the strip shape of type D panels can be more effective for load transfer between the panels.

Table 6.1 – Maximum Recorded Lateral Load for Each Specimen

Specimen	Lap-Splice	Frame f_{cm} (MPa)	Panel f_{cm} (MPa)	Axial Load per Column (kN)	Max. Forward Load (kN)	Disp. at max. load (mm)	Max. Backward Load (kN)	Disp. at max. load (mm)
CR	-	15.6	-	60	87	3.0	79	2.8
CIA4	-	18.7	34.6	60	210	9.2	196	3.0
CIB4	-	12.2	46.5	60	197	4.6	187	5.5
CIC4	-	14.2	38.2	60	214	8.7	204	6.0
CID4	-	11.1	45.1	60	255	9.8	251	10.3
LR	20ϕ	9.7	-	30	66	4.4	61	5.1
LIC4	20ϕ	15.7	38.2	30	149	10.3	145	4.0
LID4	20ϕ	10.1	45.1	30	200	9.0	192	5.3

Table 6.2 – Strength Increase for Specimens with Continuous and Lap-Spliced Reinforcement

Continuous Reinforcement		Lap-Spliced Reinforcement	
Specimen	Strength Increase	Specimen	Strength Increase
CIA4	2.42	LIC4	2.27
CIB4	2.27	LID4	3.05
CIC4	2.47		
CID4	2.94		

6.4 STIFFNESS

Stiffness of a structure can be defined as its resistance against the imposed displacements. The higher the stiffness, the less deformation the structure will experience. Considering earthquake effects, stiffness of a structure is an important parameter for controlling structural damage. One of the major deficiencies that lead to failure of structures is the lack of sufficient lateral stiffness. This problem is observed as the main reason of collapse for a high proportion of failures after major earthquakes in Turkey. Load effects on vertical load carrying elements of a structure are amplified by second-order effects created by excessive deformations and may lead to collapse. For seismic safety, enough lateral stiffness should be provided in order to limit the interstory drift that a structure would make as a result of ground motion. Even if not resulting in structural failure, lack of lateral stiffness leads to extensive damage to non-structural elements producing a huge economic loss which may be sometimes as high as the rebuilding cost of the structure. Therefore, effective seismic strengthening must definitely involve increasing the lateral stiffness of the structure for seismic safety and reducing non-structural damage. A major aim of this study is increasing the lateral stiffness and the experimental results were also evaluated in terms of stiffness properties.

Stiffness of the test specimens were calculated from the load-deformation curves for each cycle. Stiffness of a cycle was obtained from the slope of the tangent line drawn to the load-deformation curve. Slope of the first cycle was designated as initial slope and although it is not related with the actual stiffness, it was used for comparing the behavior of the test specimens. Initial slope values of test specimens are tabulated in Table 6.3. The table shows that initial slopes of the specimens with continuous reinforcement increased about three times after strengthening.

It was noted that CIA4 and CIB4 specimens, which had welded connections between its panels, showed the highest initial slope. Therefore, shear keys prevent relative displacement between the panels and make the infill stiffer. Specimens CIC4 and CID4 had a little less initial slope since they do not have shear keys between precast panels, but they are not too different. Presence of lap-splice and lower axial load seems to decrease initial slope from the comparison of CR and LR specimens. LIC4 had provided good increase in initial slope with respect to the lap-spliced reference LR, but had less initial slope than CIC4, the corresponding specimen with continuous reinforcement. The specimen LID4 showed an initial slope almost the same as specimen CID4 and a great increase with respect to the reference specimen.

Table 6.3 – Initial Slope of Test Specimens

Continuous Reinforcement			Lap-Spliced Reinforcement		
Specimen	Initial Slope (kN/mm)	Increase	Specimen	Initial Slope (kN/mm)	Increase
CR	96	–	LR	60	–
CIA4	312	3.26	LIC4	159	2.66
CIB4	308	3.22	LID4	280	4.69
CIC4	294	3.07			
CID4	276	2.88			

By plotting the stiffness in each cycle, stiffness degradation curve of a specimen is obtained. In Figure 6.3 and Figure 6.4, stiffness degradation curves of specimens with continuous reinforcement and all specimens are given respectively with the same scale.

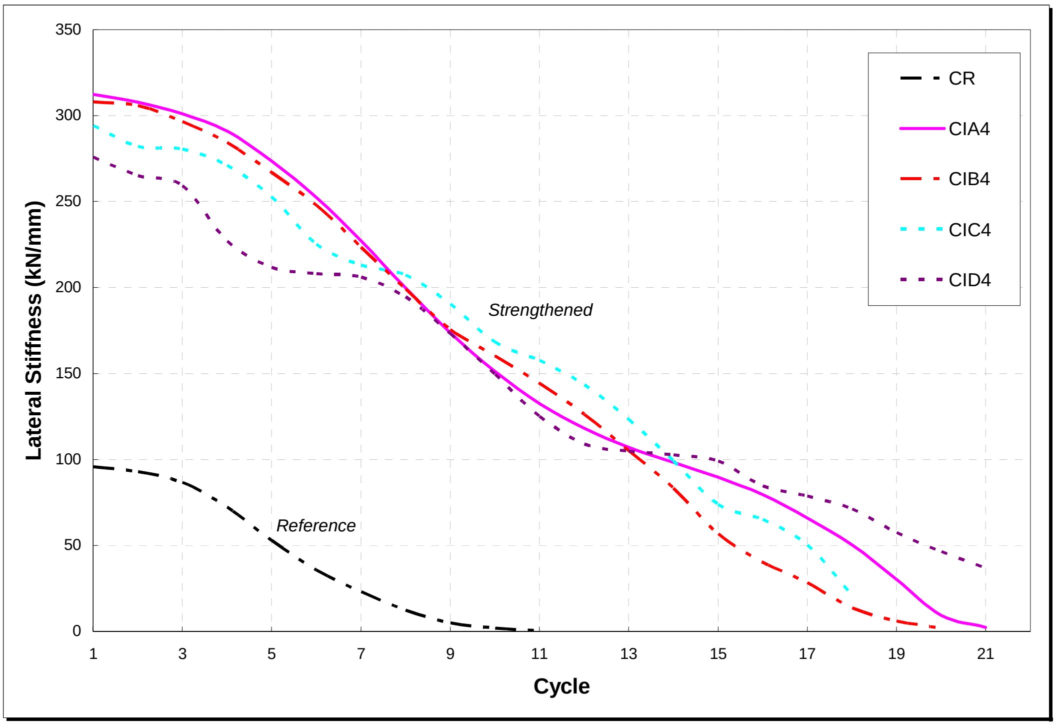

Figure 6.3 – Stiffness Degradation Curves for Specimens with Continuous Reinforcement

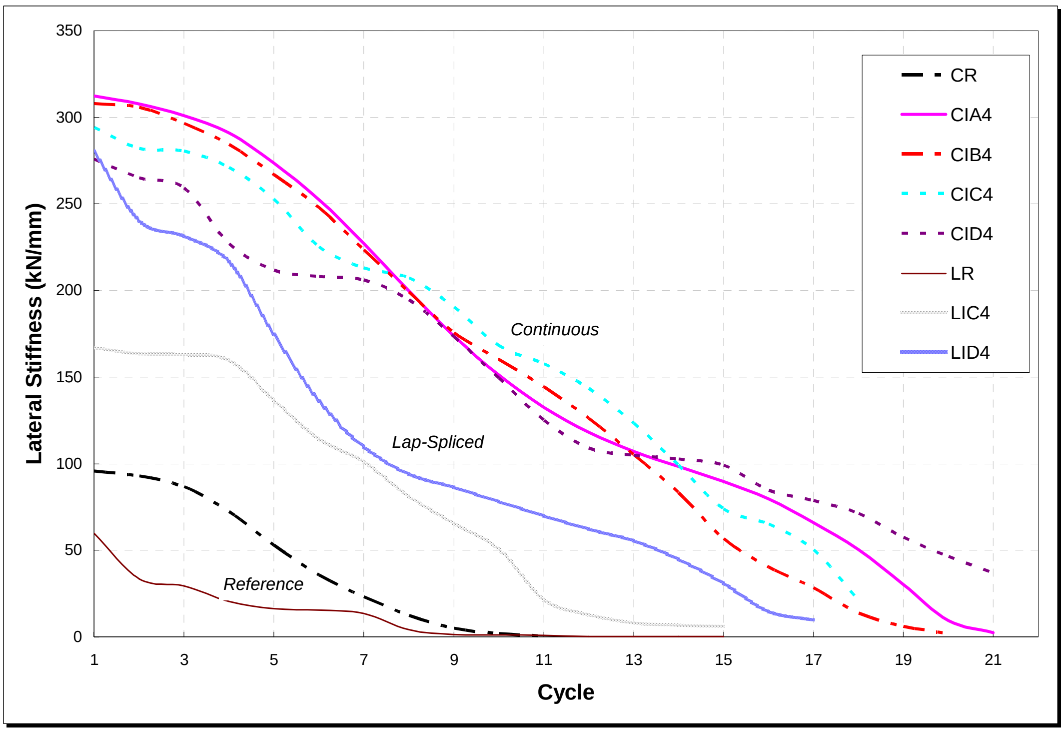

Figure 6.4 – Stiffness Degradation Curves for All Specimens

In Figure 6.3, stiffness degradation curves of strengthened specimens are almost the same. This figure also shows the great increase in stiffness with respect to the unstrengthened specimen. Degradation curves show a gradual decrease in stiffness at each cycle. Stiffness degradation curves of all specimens were plotted together in Figure 6.4. A comparison can be easily made according to this figure. It is observed that curves belonging to lap-spliced specimens are below the curves of specimens with continuous reinforcement. Lap-splice and lower axial load decreased the lateral stiffness. This chart shows great increase of lateral stiffness provided by strengthening with precast concrete panels bonded on brick masonry infill.

6.5 ENERGY DISSIPATION

When a structure undergoes deformation, it absorbs a certain amount of energy through the elastic range. This energy can be calculated from the area under the load-deformation curve. However, structures going beyond the elastic range and experiencing permanent deformations lose some of their internal energy to the environment. This energy is dissipated by producing heat, yielding and damage to the structural members. The amount of dissipated energy can be calculated from the area enclosed within each loop of a loading-unloading cycle in a load-deformation curve. Energy dissipation is also an indicator of ductility of a structure.

The capacity of a structure to resist the seismic action by large hysteretic lateral forces without collapse depends on its capacity to dissipate energy. Therefore, one of the major aims of seismic strengthening is to provide ductility to the structure, in order to increase its energy dissipation capacity.

For each test specimen, dissipated energy was calculated from load-deformation curves and plotted against each cycle. In Figure 6.5, cumulative dissipated energy curves of specimens with continuous reinforcement are given. Figure 6.6 shows cumulative energy curves of lap-spliced specimens. Total amount of dissipated energy of each specimen is tabulated in Table 6.4.

Table 6.4 – Total Energy Dissipation of Each Test Specimen

Continuous Reinforcement		Lap-Spliced Reinforcement	
Specimen	Total Dissipated Energy (Joule)	Specimen	Total Dissipated Energy (Joule)
CR	5700	LR	8600
CIA4	15500	LIC4	14300
CIB4	15100	LID4	14400
CIC4	9200		
CID4	8400		

For all panel types, strengthening increased the total dissipated energy considerably. The increase is about 1.5 to 2.5 times with respect to the reference. The highest energy was dissipated by specimens strengthened with type A and type B panels. The effective energy dissipation of these specimens is due to the presence of welding between the panels. Specimens with continuous reinforcement strengthened with type C and type D panels have dissipated much less energy compared to CIA4 and CIB4 specimens, since they did not have welding or shear keys. The lowest energy dissipation was obtained from CID4, which is even less than that of lap-spliced reference specimen. Low energy dissipation of this specimen was because of its brittle behavior and insufficiency to develop frame behavior after crushing of the infill.

Figure 6.5 and Figure 6.6 show cumulative energy dissipation curves. All curves follow a relatively linear trend showing linear action until the slope suddenly changes. Start of increased dissipation rate marks the point where plastification starts. Higher curves mean higher total energy dissipation.

Cumulative energy dissipation curves of specimens with continuous reinforcement can be seen in Figure 6.5. The curve for the reference specimen shows much less energy dissipation and early plastification. Curves of strengthened specimens are similar to each other and go much higher. Especially CIA4 and CIB4 specimens are very similar but CIB4 has earlier plastification. Both specimens indicate relatively high energy dissipation. CIC4 follows the same trend with CIA4, but it is shorter. CID4 has a very different curve which is relatively shorter and without significant bending point. This curve also indicates the brittle behavior of specimen CID4.

Figure 6.6 contains energy dissipation curves for lap-spliced specimens and equivalent specimens with continuous reinforcement for comparison. Energy dissipation of lap-spliced specimens is greater than specimens with continuous reinforcement. Also, plastic action starts earlier in lap-spliced specimens. Lap-spliced specimens have lower capacity which makes plastification start earlier, and they are more ductile due to the lap-splice and lower axial load level. Curves go higher due to higher ductility. Their rate of energy dissipation is approximately the same as energy dissipation rate of specimen CIC4.

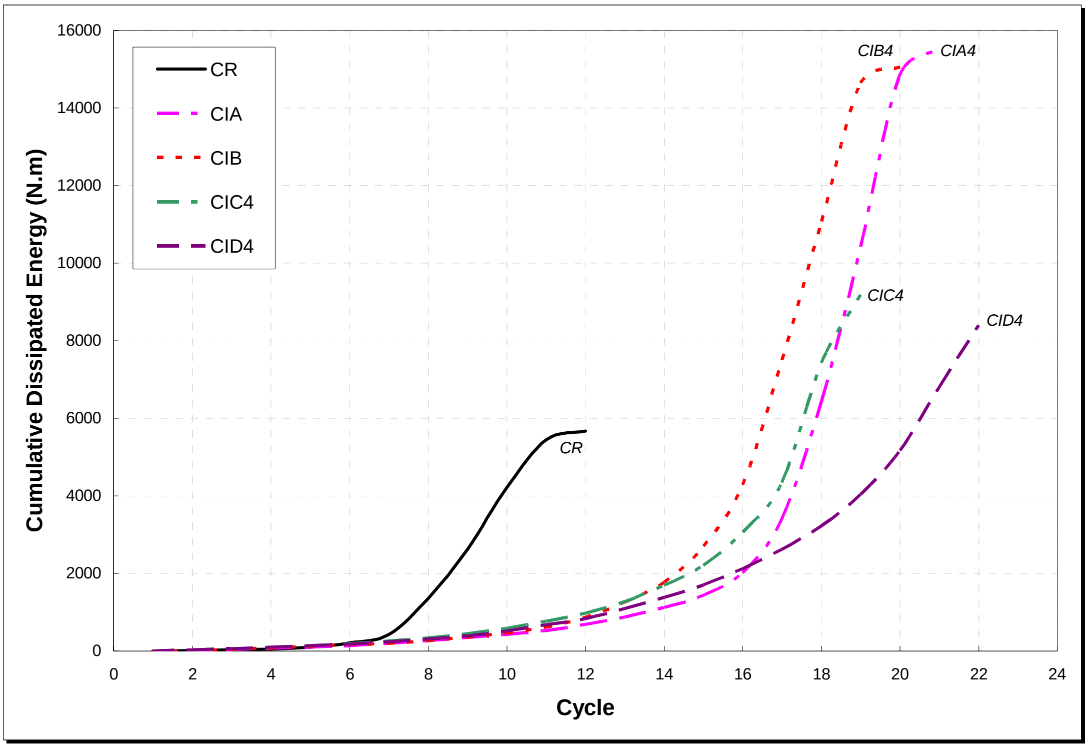

Figure 6.5 – Cumulative Energy Dissipation for Specimens with Continuous Column Steel

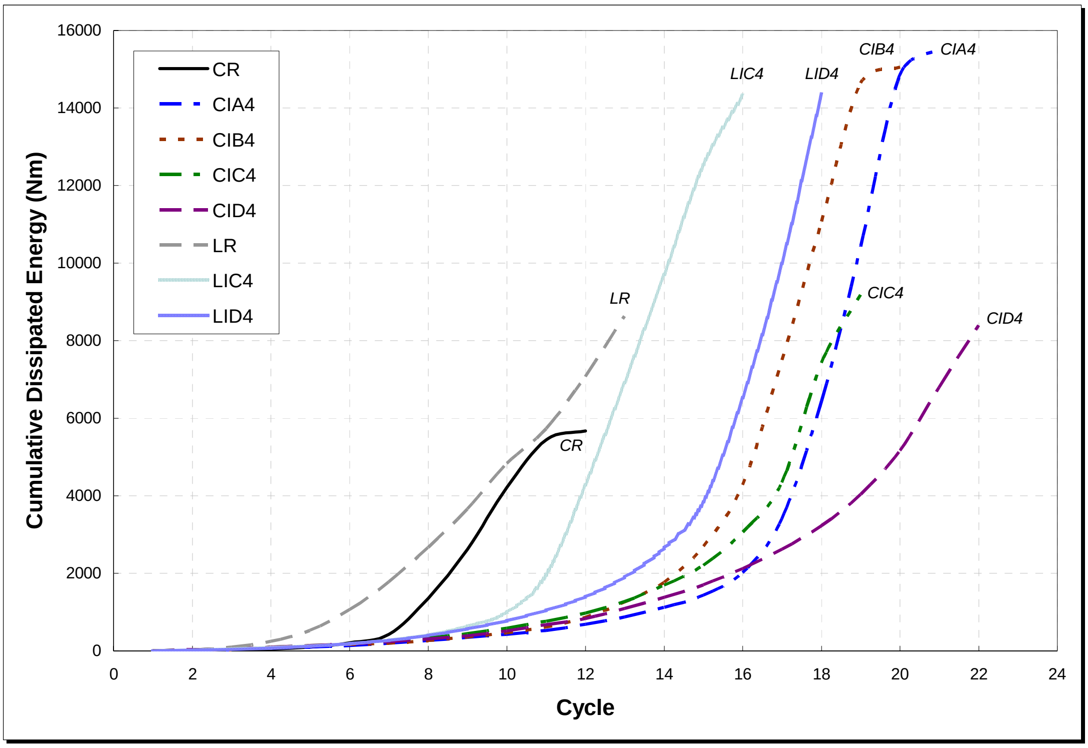

Figure 6.6 – Comparison of Cumulative Energy Dissipation Curves for All Specimens

6.6 DISPLACEMENT HISTORY

Displacement history of each specimen is given in Figure 6.7. These charts provide a basis for comparison of displacement behavior. These charts can also give an idea for the stiffness of each specimen. Higher deformation as observed for the reference specimens indicates less stiffness.

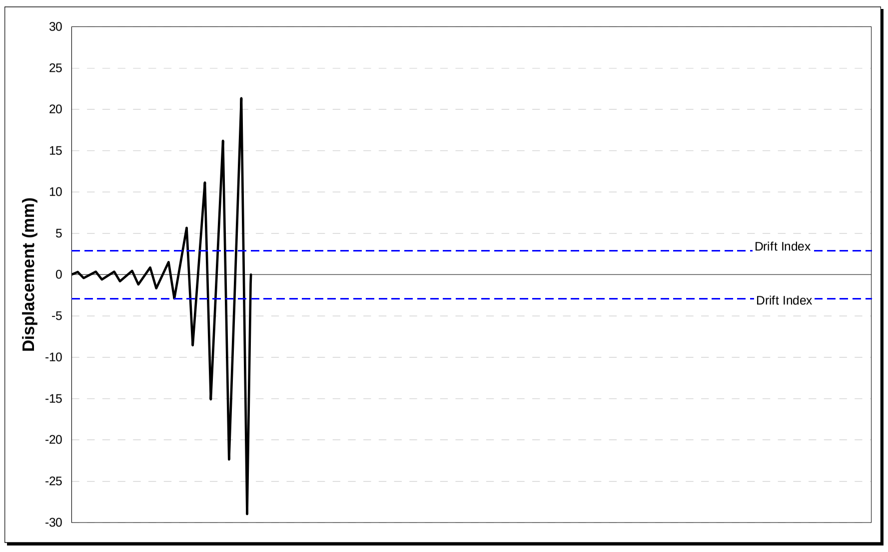

a. CR

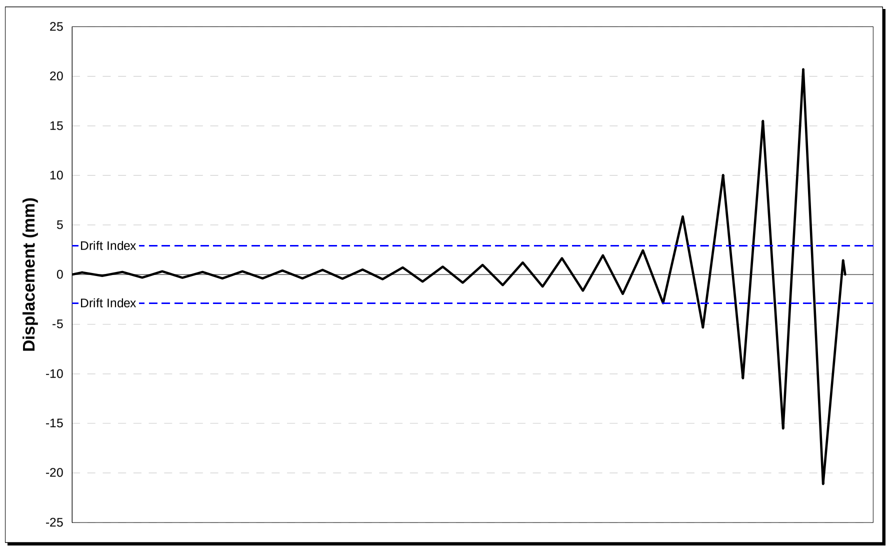

b. CIA4

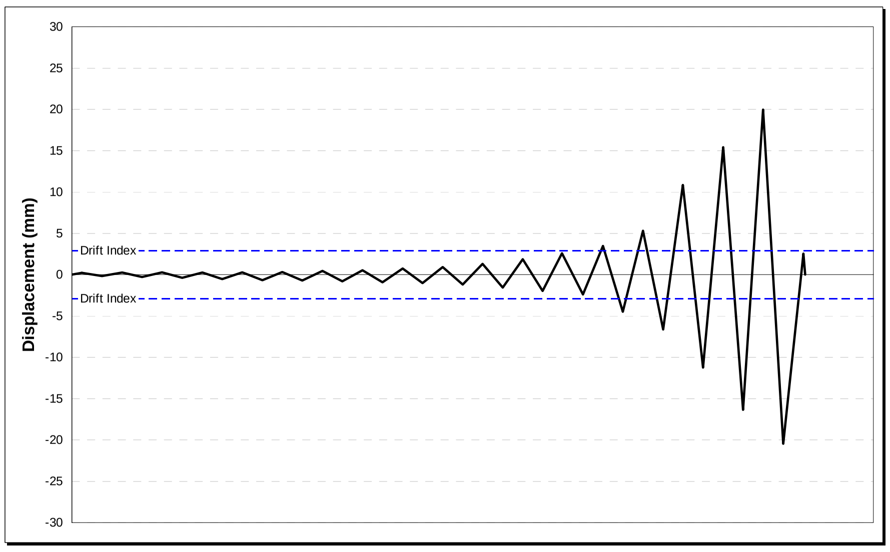

c. CIB4

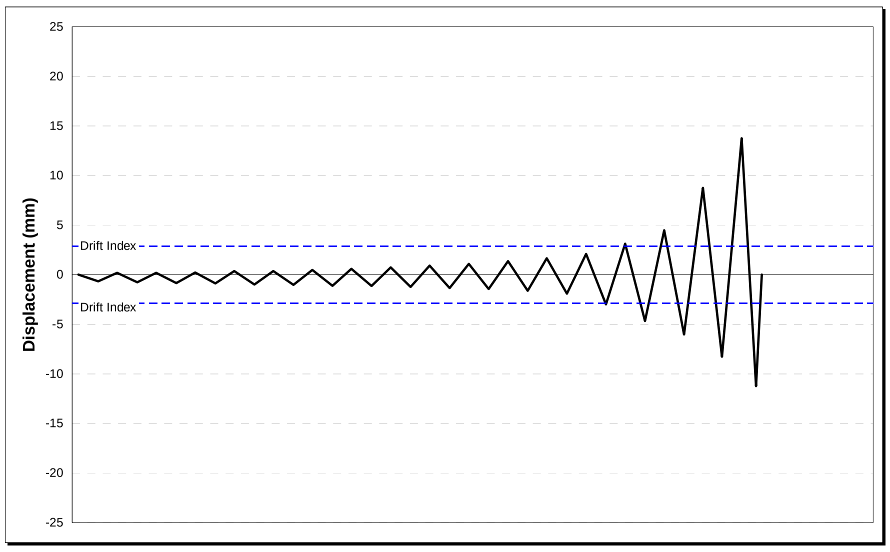

d. CIC4

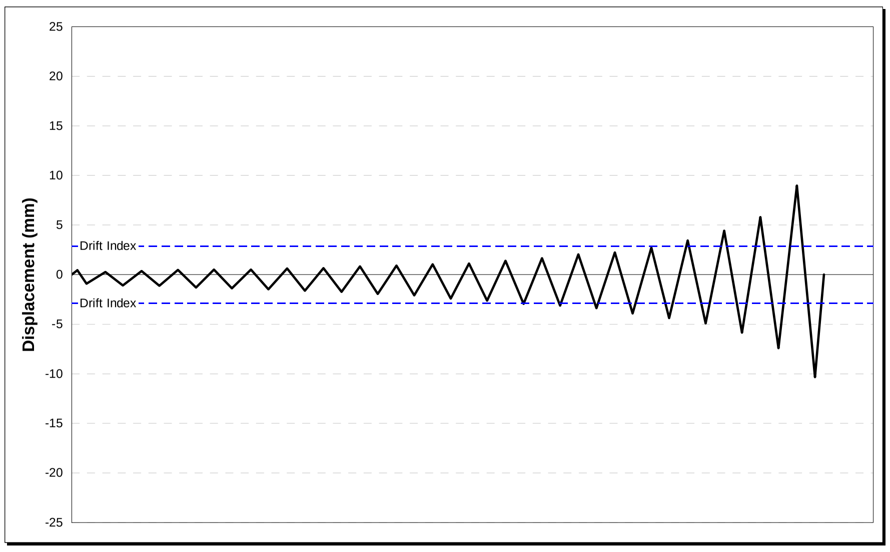

e. CID4

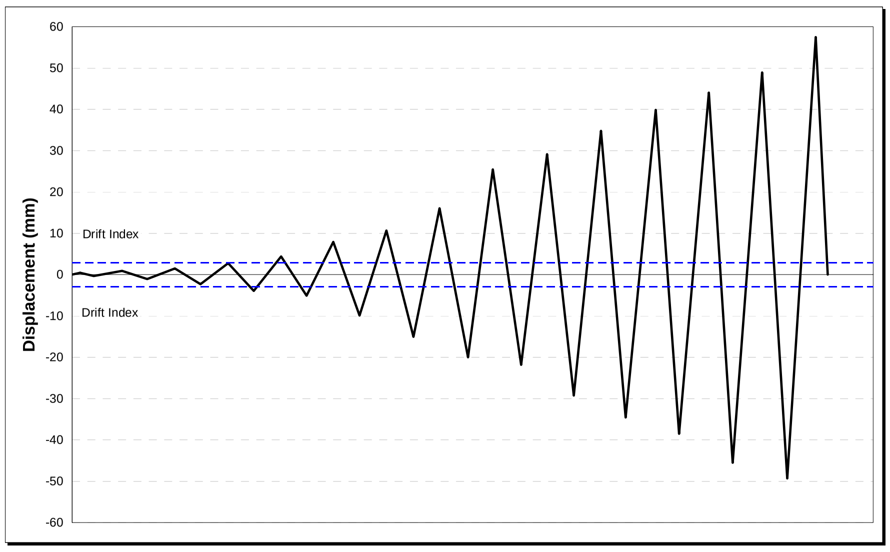

f. LR

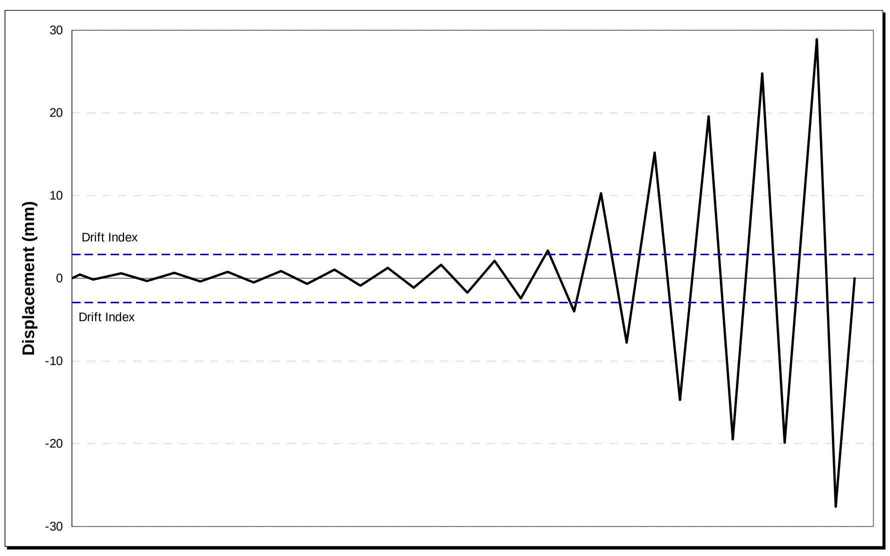

g. LIC4

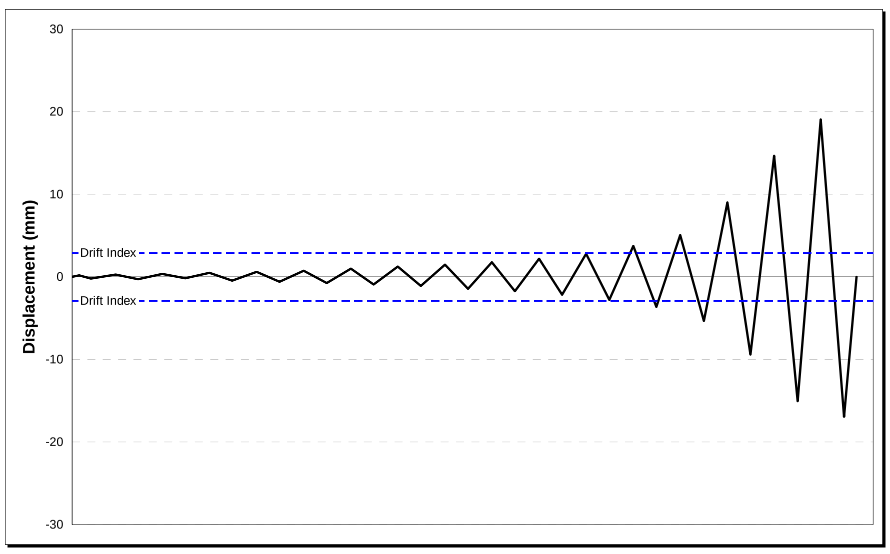

g. LID4

Figure 6.7 – Displacement Histories

6.7 SUMMARY

Evaluation of test results show that strengthening by bonding precast concrete panels on brick masonry infills of reinforced concrete frames is an effective technique for increasing lateral strength. Summary of test results are given in Table 6.5. Highest lateral load was observed for specimen CID4. However, this specimen showed a brittle behavior and energy dissipation was relatively low. Higher strength of CIC4 and CID4 over CIA4 and CIB4 show that dowels have a major effect on lateral strength. CIC4 and CID4 had dowels extending 150 mm between the panels from all sides of the frame. Dowels were welded to the corners of the panels in CIA4 and CIB4. Lap-splice effect together with lower axial load had a negative influence on lateral strength of strengthened specimens. Good capacity increase was observed also for lap-spliced specimens. Generally, strengthening with type D panels seems to provide the most increase of lateral load capacity. At maximum load, strengthened specimens were at higher displacement than unstrengthened specimens. Strengthening also improved initial lateral stiffness. Specimens with type A and type B showed greatest initial stiffness due to better connection between each panel element.

Table 6.5 – Summary of the Test Results

Specimen	Frame f_{cm} (MPa)	Panel f_{cm} (MPa)	Lap-Splice	Axial Load (Percent of axial load capacity)	Max. Lateral Load (kN)	Disp. at Max. Load (mm)	Initial Slope (kN/mm)
CR	15.6	-	-	25%	86.6	3.01	96
CIA4	18.7	34.6	-	25%	209.9	9.22	312
CIB4	12.2	46.5	-	25%	197.0	4.63	308
CIC4	14.2	38.2	-	25%	213.5	8.74	294
CID4	11.1	45.1	-	25%	254.7	9.84	276
LR	9.7	-	20ϕ	13%	65.5	4.38	60
LIC4	15.7	38.2	20ϕ	13%	148.9	10.29	159
LID4	10.1	45.1	20ϕ	13%	199.6	9.01	280

6.8 COMPARISON WITH TWO-STORY TEST SPECIMENS

6.8.1 General

The previous test series were performed on one-bay two storey reinforced concrete frames. Parallel tests of reference and strengthened specimens were conducted for two frame types. Tests on two-story frames were performed by Duvarci [3] and Baran [4]. In this section, the test results of some specimens in this series will be compared with the test results of equivalent two-story specimens and similarities and differences will be analyzed. It will be sought if the one-story test frame is a satisfactory representation of the first story of the two-story frame. Figure 6.8 shows the assumption that the one-story frame behaves the same way with the individual stories of the two-story frame.

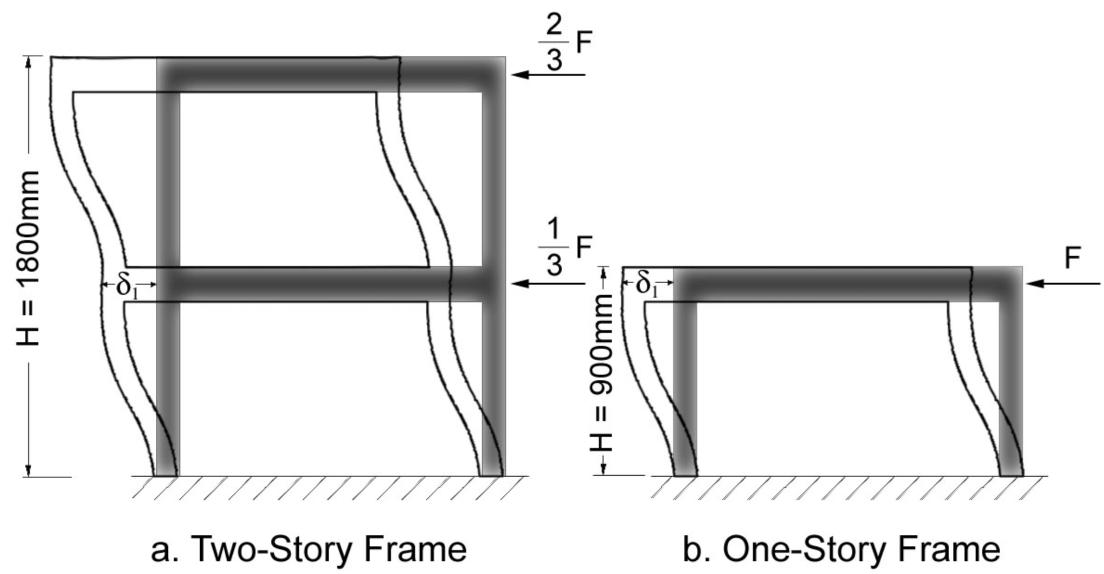

Figure 6.8 – Elastic Frame Deformations Assuming Infinitely Rigid Beams for Comparison of Two-story and One-story Test Frames

6.8.2 Specimens CR

CR denotes unstrengthened specimens for one and two story specimens. These reference frames had continuous reinforcement and only masonry infill. Two-story CR specimen was tested by Duvarci [3]. The two test frames had similar concrete strength. From Table 6.6, it can be seen that the one-story frame has a greater lateral load capacity. But when loading in the negative direction is considered, one-story and two-story frames have lateral load capacities of 79.1 kN and 78.8 kN, respectively. The closeness of the capacity can be observed in the comparison of load-displacement curves (Figure 6.9) and response envelopes (Figure 6.10).

In the test, diagonal cracking started earlier on the first story infill of the two-story frame than that of the one-story frame. For both frame types, infill started crushing from the corners and the lateral load started to be carried by the frame members. Transformation of behavior into frame action occurred about the eighth cycle for both frames. The behavior was very similar considering the first stories and the failure of the frames occurred by crushing at column bases.

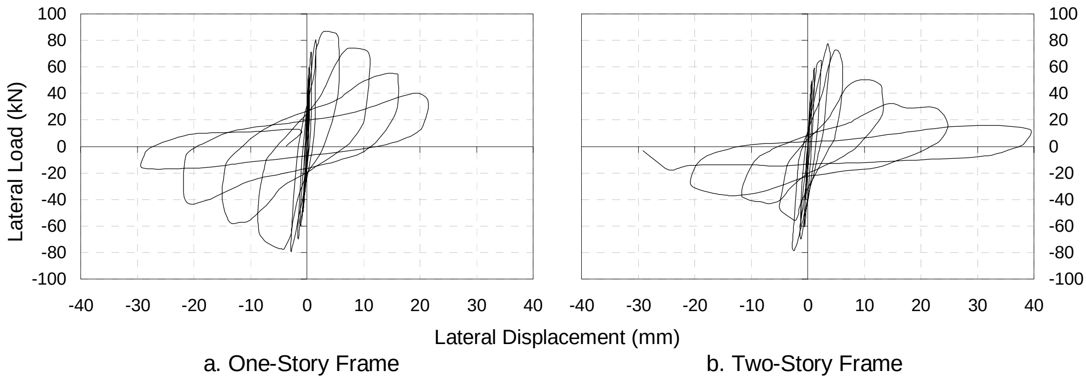

Figure 6.9 – Lateral Load vs. First Story Displacement of CR Specimens

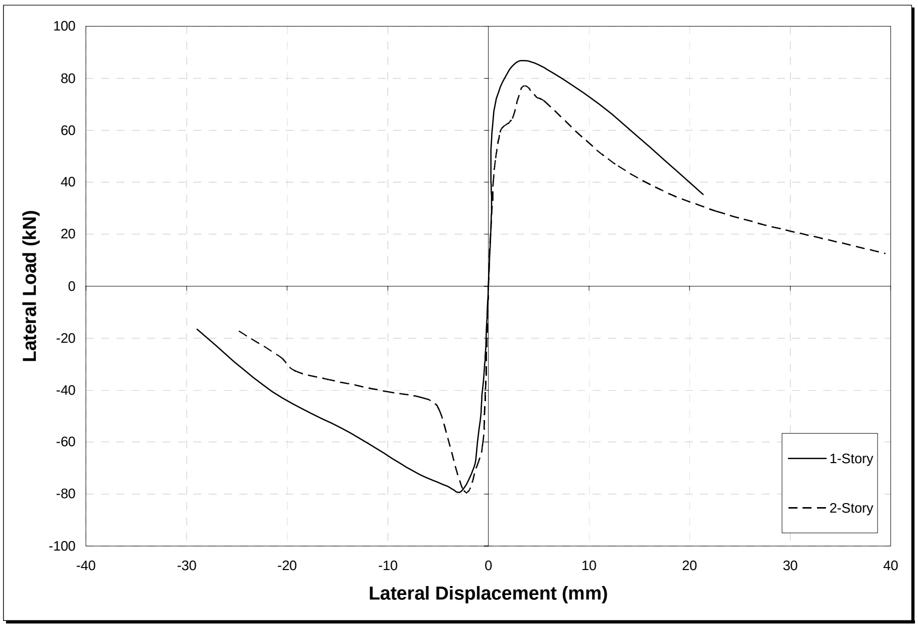

Figure 6.10 – Comparison of Response Envelopes of CR Specimens

Table 6.6 – Test Results of CR Specimens

	One-Story	Two-Story	$\frac{\text{One Story}}{\text{Two Story}}$
f_{ck} (MPa)	15.6	16.6	-
Max. Lateral Load (kN)	86.6	78.8	1.10
First Story Displacement at Max. Load (mm)	3.01	2.44	1.23
Initial Stiffness (kN/mm)	95.8	64.7	1.48

6.8.3 Specimens CIA4

CIA4 specimens were frames strengthened by Type A precast panels bonded on the interior surface of the masonry infill. Duvarci [3] has tested the two-story CIA4 specimen. The lateral load capacities are especially close for negative direction, which are 196.0 kN and 192.5 kN, respectively for one-story and two-story frames. One story frame has more ductility as can be observed from the comparison of envelope curves in Figure 6.12. The difference in ductility is significant in the forward direction, but it does not seem to be much different in the backward direction.

Separating of the infill from the column appeared in the one-story frame earlier than the two-story frame. Columns cracked from bending for both frames, but earlier in the two-story frame. Panel cracking started in the twelfth cycle at the two-story frame, but in the sixteenth cycle at the one-story frame. Large diagonal cracks developed on the infills in the following cycles. Beam-column joint crushing was more significant at the one story frame. For both frames, the test was terminated with crushing at column bases. Test results for both frame types are summarized in Table 6.7.

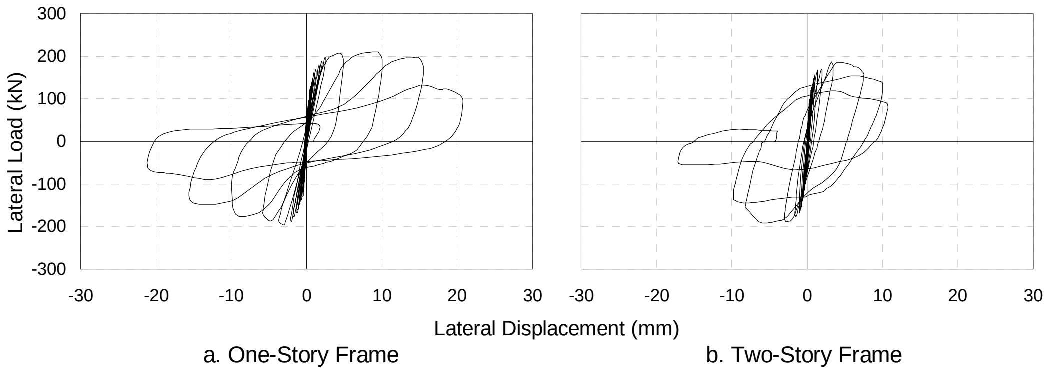

Figure 6.11 – Lateral Load vs. First Story Displacement of CIA4 Specimens

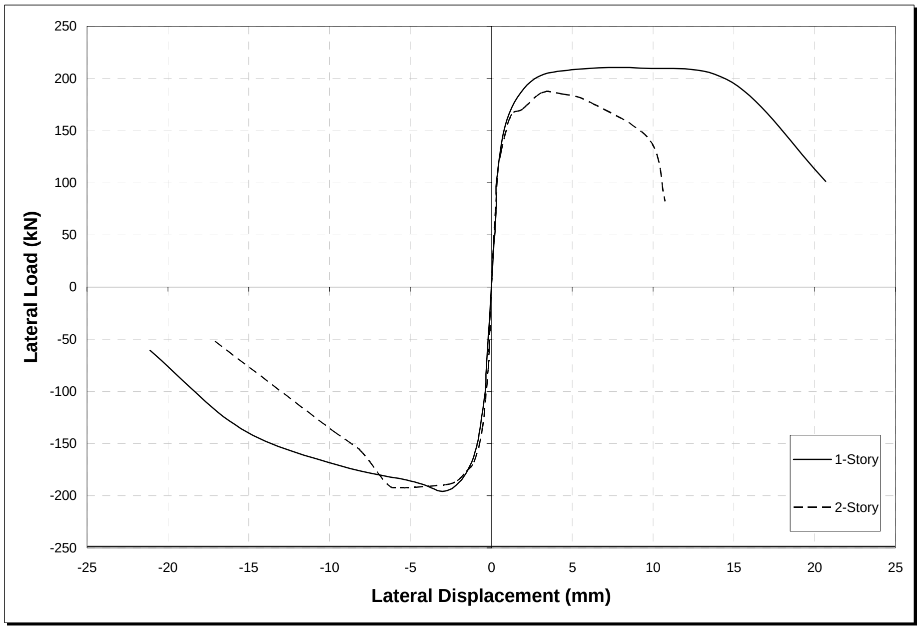

Figure 6.12 – Comparison of Response Envelopes of CIA4 Specimens

Table 6.7 – Test Results of CIA4 Specimens

	One-Story	Two-Story	$\frac{\text{One Story}}{\text{Two Story}}$
f_{ck} (MPa)	18.7	18.2	-
Max. Lateral Load (kN)	209.9	192.5	1.09
First Story Displacement at Max. Load (mm)	9.22	5.66	1.63
Initial Stiffness (kN/mm)	312.4	275.9	1.13

6.8.4 Specimens CIB4

One or two story frames strengthened with Type B panels were denoted as CIB4. Duvarci [3] has tested two-story CIB4 specimen. The two types of frames showed significantly similar behavior for both loading directions in the perspective of lateral load capacity and response envelopes (Figure 6.14). The response envelopes seem to be almost coinciding with each other. There is some difference between the curve shapes in the load-deformation plots of two frame types.

For both frames, cracking started at column bases at the same load level. Then, infill separation cracks were formed, a little later at the two-story frame. Beam-column joint cracks appeared earlier and were more significant at the one-story frame. At the two-story frame, column flexural cracks were observed before joint cracking. Panel cracking started at later cycles, and the infill was separated from the frame. The two tests ended similarly by excessive damage in the column bases, but the one-story frame had much greater damage at the joint region.

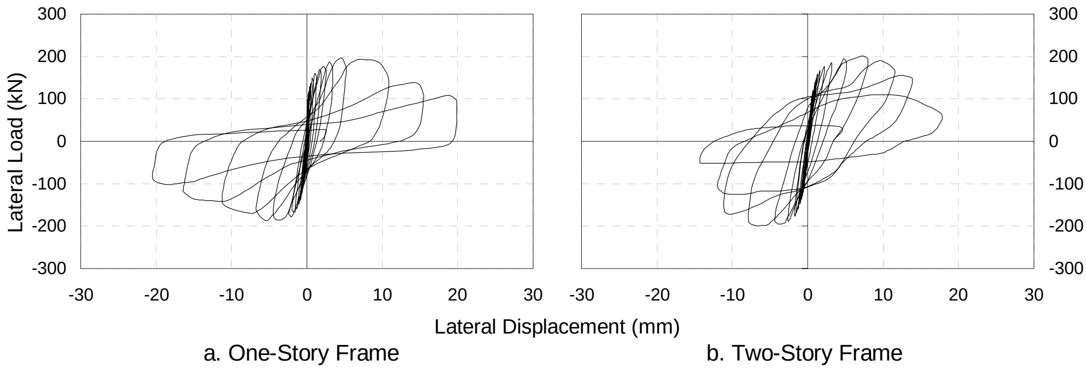

Figure 6.13 – Lateral Load vs. First Story Displacement of CIB4 Specimens

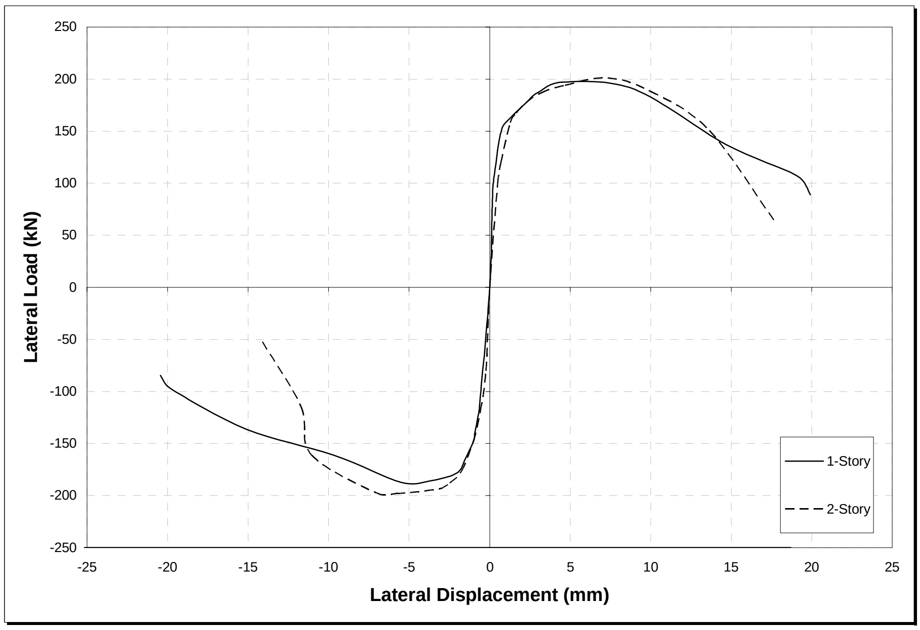

Figure 6.14 – Comparison of Response Envelopes of CIB4 Specimens

Table 6.8 – Test Results of CIB4 Specimens

	One-Story	Two-Story	$\frac{\text{One Story}}{\text{Two Story}}$
f_{ck} (MPa)	12.2	13.0	-
Max. Lateral Load (kN)	197.0	201.3	0.98
First Story Displacement at Max. Load (mm)	4.63	7.33	0.63
Initial Stiffness (kN/mm)	308.0	197.6	1.56

6.8.5 Specimens CIC4

CIC4 specimens were Type C panel strengthened frames with anchorage to all frame members. Two-story CIC4 specimen was tested by Baran [4]. Two frame types showed similar response as can be observed from Table 6.9 and the response envelopes (Figure 6.16). One-story specimen has higher ductility than the two-story specimen, especially in the positive direction. In the negative direction, maximum lateral displacement of two specimen types seems to be similar.

Separation of the infill from the columns and cracking at the column bases started in early cycles of both tests. Also, diagonal cracking on the panels started at the same load level for both cases. However, beam-column joints cracked at the one-story frame before panel cracking, but at the two-story frame, beam-column joint cracks occurred after panels started cracking. In the last cycles of both tests, column bases started to crush and the cover concrete dispersed. The two-story frame failed from the column base crushing. On the other hand, the one-story frame, also having significant damage at the column bases, failed by crushing at the beam-column joint suddenly.

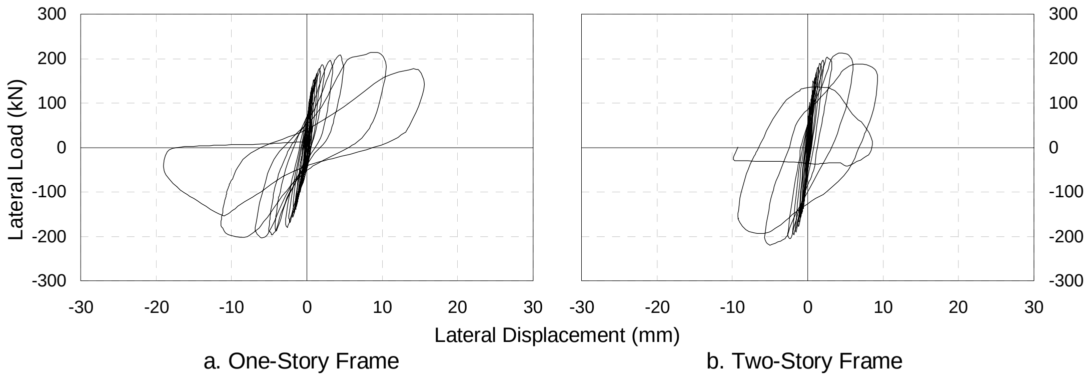

Figure 6.15 – Lateral Load vs. First Story Displacement of CIC4 Specimens

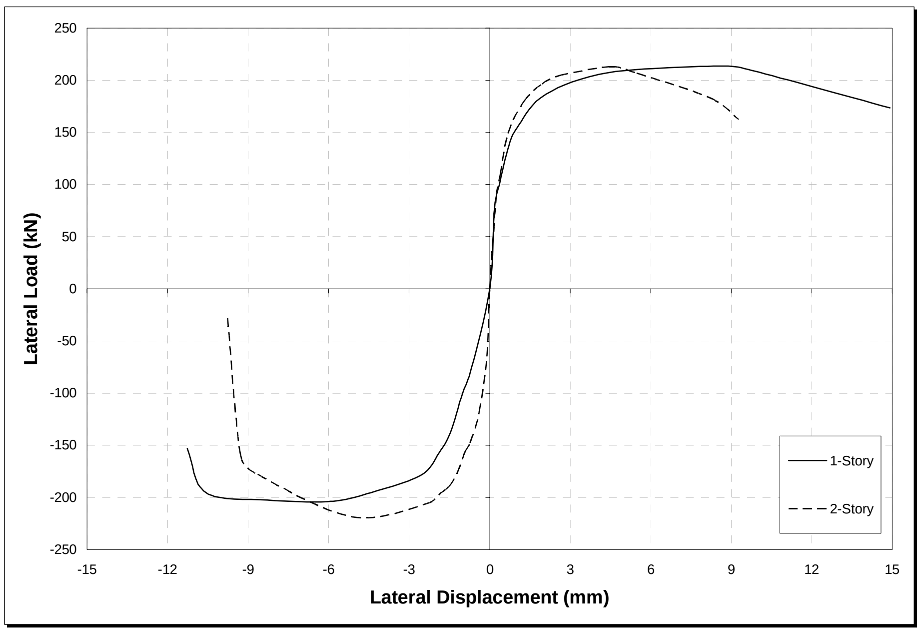

Figure 6.16 – Comparison of Response Envelopes of CIC4 Specimens

Table 6.9 – Test Results of CIC4 Specimens

	One-Story	Two-Story	$\frac{\text{One Story}}{\text{Two Story}}$
f_{ck} (MPa)	14.2	19.4	-
Max. Lateral Load (kN)	213.5	218.5	0.98
First Story Displacement at Max. Load (mm)	8.74	5.13	1.70
Initial Stiffness (kN/mm)	294.0	196.1	1.50

6.8.6 Summary of Comparisons

At the tests for two-story frames, the behavior of the one-story frame is very similar to the first story of the two-story frame, while the upper story of the two-story frame remains with minor damage. Cracking at the frame members and the infill starts and progresses similarly in all cases. After some cracks occur on frame members, diagonal cracks start on the infill. Then, heavy damage concentrates at the column bases and beam-column joints, and following the failure or damage of the infill, the frame members fail at these regions. The main difference of observed damage between the one-story and the two-story frames is that the first story beam-column joint region of the one-story frame receives much more significant damage than the same place of the two-story frame.

One-story and two-story frames of same application showed very similar behavior. Lateral load capacities of two frame types are very close. One of the main differences is the application level of loading. In two-story frames, the lateral load was applied at a greater height and therefore moment arm is greater. Greater moment arm of lateral load results in more overturning effect. So, more tensile stress occurs at the tension side column of two-story frames. Compressive and shear stresses are more dominant in one-story frames. This is the most possible reason for higher initial stiffness of one-story frames. Ductility of the two frame types are not largely different, but generally one-story frames showed higher ductility. Higher ductility can be a result of more efficient behavior of the infill, which can be positively influenced by the confining effect of compressive forces.

When the lateral load-lateral displacement graphs for one and two story frames are compared, it is observed that there is a significant difference at the shape of the loops. Load-displacement curves for one-story frames have a much more pinched shape than the curves for two-story frames. This difference is small for the reference specimens. Pinching is the result of higher shear stresses causing larger crack widths, because when the loading is reversed, no stiffness can be observed while the cracks are closing. Therefore, the main reason for more pinching in one-story frames is the higher level of shear action.

CHAPTER 7

CONCLUSIONS

7.1 SUMMARY

Currently, many buildings in Turkey do not have sufficient capacity to stand against a major earthquake, which is expected to occur anytime. Major earthquakes in the previous years have caused enormous damage to the economy of the country as well as human lives. In order to prevent such a loss due to a future earthquake, seismic strengthening measures should be applied to as many vulnerable buildings as possible. Commonly used strengthening techniques require great and lengthy construction work which also necessitates evacuation of buildings.

In order to introduce a new strengthening method which is rapid, practical, economical and occupant-friendly, a series of experimental and analytical studies are being conducted in METU Structural Mechanics Laboratory. This study is a part of this comprehensive research program sponsored by NATO and TUBITAK.

In this study, eight single-story single-bay reinforced concrete frame specimens of one-third scale were used in order to test the efficiency of strengthening with precast concrete panels. The specimens were subjected to cyclic lateral loading after being strengthened with precast concrete panels epoxy-bonded on masonry infills. Effects of different panel shapes and connection techniques were investigated.

Test results were evaluated considering strength, stiffness and energy dissipation characteristics. Also, results of one-story test frames were compared with two-story test frames used within this research program.

7.2 CONCLUSIONS

In the light of the results and analyses from eight tests in this experimental study, the following conclusions were obtained:

- Strengthening with precast concrete panels was found to be a very effective and convenient method for strengthening seismically vulnerable reinforced concrete structures.
- Average strength increase was 2.5 times with respect to the reference specimen after strengthening with precast panels. Initial lateral stiffness increased about 3.3 times.
- Test results show that, Type-C (nearly square) and Type-D (full height strip) panels can be used instead of Type-A and Type-B panels which have shear keys and require laborious application. Welded connections and shear keys were found to be unnecessary, only epoxy was shown to be satisfactory for all panel connections.
- Strengthened infill failed by excessive diagonal cracking on the panels, and the frame failed by crushing or failure at the column bases or at the beam-column joints. After the failure of the infill, the behavior of the system became similar to a frame behavior. Stronger infills provided higher lateral load capacity, but hampered frame action, thus, limiting the ductility.
- The method proved to be effective also for specimens with lap-spliced reinforcement, although bar slip problems were observed. Lower axial load and presence of lap-spliced reinforcement created a negative effect on the lateral strength. Lower axial load was also expected to decrease the flexural capacity of the columns.
- Utilization of one-story, one-bay reinforced concrete test frames were proved to be successful and almost equivalent to two-story, one-bay test frames, as they have provided similar results. Some difference in behavior was observed between the two frame types, as shear forces were more dominant for one-story specimens. However, from the point of view of strength and ductility, they gave almost the same results. It was therefore concluded that one-story test

frames can be used taking advantages of simplicity in specimen construction and testing procedure.

- Strengthening with precast concrete panels epoxy-bonded on brick masonry infills can be an effective strengthening method which is suitable for the existing seismically vulnerable reinforced concrete buildings in Turkey, and faster, easier and more economical than strengthening with cast-in-place shear walls. This method also does not interfere with the function of the building and therefore it is occupant-friendly.

7.3 RECOMMENDATIONS

- Analytical studies should be made in order to derive design recommendations for this strengthening technique.
- Additional experiments with test frames of different aspect ratio and scale would be useful for determining the behavior of precast panels further.

REFERENCES

1. Sugano, S., "Aseismic Strengthening of Existing Reinforced Concrete Buildings", Proceedings of the First Seminar on Repair and Retrofit of Structures, US/Japan Cooperative Earthquake Engineering Research Program, May, 1980, pp.13-40.

2. Sugano, S., "State-of-the-Art in Techniques for Rehabilitation of Buildings", Proceedings of the 11th WCEE, Paper No. 2175, 1996.

3. Duvarci, M., "Seismic Strengthening of Reinforced Concrete Frames with Precast Concrete Panels", MSc thesis, Middle East Technical University, Ankara, 2003.

4. Baran, M., "Precast Concrete Panel Reinforced Infill Walls for Seismic Strengthening of Reinforced Concrete Framed Structures", PhD thesis in progress, Middle East Technical University, Ankara.

5. Baran, M., Duvarci, M., Tankut, T., Ersoy, U., Ozcebe, G., "Occupant Friendly Seismic Retrofit (OFR) of RC Framed Buildings", Proceedings of NATO Advanced Research Workshop, Seismic Assessment and Rehabilitation of Existing Buildings, Izmir, 2003.

6. Wyllie, L.A.Jr., "Strengthening Strategies for Improved Seismic Performance", Proceedings of the 11th WCEE, Paper No. 1424, 1996.

7. Ersoy, U., "Seismic Rehabilitation – Applications, Research and Current Needs", Proceedings of the 11th WCEE, Paper No. 2099, 1996.

8. Ersoy, U., Tankut, T., "Current Research at METU on Repair and Strengthening of Reinforced Concrete Structures" Department of Civil Eng., Middle East Technical University, Ankara, Turkey.

9. Hanson, Robert D., “Strengthening of Reinforced Concrete Members in Buildings”, ACI Seminar Course Manual on Seismic Design for Existing Structures, Detroit, Michigan, 1986.

10. Sugano, S., “Guideline for Seismic Retrofitting Design of Existing Reinforced Concrete Buildings”, Proceedings of the 2nd Seminar on Repair and Retrofit of Structures, US/Japan Cooperative Earthquake Research Program, Dept. of Civil Engineering, University of Michigan, May 1981, pp.189-237.

11. Sugano, S., “An Overview of the State of the Art in Seismic Strengthening of Existing Reinforced Concrete Buildings in Japan”, Proceedings of the 3rd Seminar on Repair and Retrofit of Structures, US/Japan Cooperative Earthquake Research Program, Dept. of Civil Engineering, University of Michigan, May 1982, pp.328-349.

12. Turkish Seismic Code, Ministry of Public Work and Settlement, Government of Republic of Turkey, Ankara, 1997.

13. Erdik, M., “Report on 1999 Kocaeli and Düzce Earthquakes”, Bogazici University, Dept. of Earthquake Engineering, Istanbul, Turkey, 2000.

14. Ersoy, U., Uzsoy, S., “The Behavior and Strength of Infilled Specimens”, Report No. MAG-205, TUBITAK, Ankara, Turkey, 1971, In Turkish.

15. Higashi, Y., Kokusho, S., ”The Strengthening Method of Existing Reinforced Concrete Buildings”, US-Japan Cooperative Research Program in Earthquake Engineering, Honolulu, 1975.

16. Kahn, L.F., Hanson, R.D., ”Infilled Walls for Earthquake Strengthening”, Proc. of the ASCE, Vol.105, No. ST2, February, 1979, pp.283-296.

17. Yuzugullu, O., “Repair of Reinforced Concrete Specimens with Reinforced Concrete Precast Panels”, Report No. MAG-494, TUBITAK, Ankara, Turkey, 1979, In Turkish.

18. Higashi, Y., Endo, T., Okubo, M., Shimizu, Y., “Experimental Study on Strengthening Reinforced Concrete Structure by Adding Shear Wall”, Proc. of the 7th WCEE, Istanbul, 1980,Vol.7, pp.173-180.

19. Higashi, Y., Endo, T., Shimizu, Y., ”Experimental Studies on Retrofitting of Reinforced Concrete Structural Members”, Proc. of 3rd Seminar on Repair and Retrofit of Structures, US/Japan Cooperative Earthquake Research Program, Dept. of Civil Engineering, University of Michigan, May 1982, pp.126-155.

20. Kaldjian, M.J., “Efficiency of Bolt Connected Reinforced Concrete Shear Panels to Repair and Strengthen the Structures”, Presented in Jordan 1984.

21. Higashi, Y., Endo, T., Shimizu, Y.,” Experimental Studies on Retrofitting of Reinforced Concrete Building Specimens” Proc. of the 8th WCEE, San Francisco 1984, Vol.1, pp.477-484.

22. Phan, T.L., Cheok, S.G., Todd, R.D., “Strengthening Methodology for Lightly Reinforced Concrete Specimens, Recommended Guidelines for Strengthening with Infill Walls”, Building and Fire Research Laboratory National Institute of Standards and Technology, Gaithersburg, MD, July 1995.

23. Frosch, R., “Seismic Rehabilitation Using Precast Infill Walls” PhD. Thesis, University of Texas at Austin, Department of Civil Eng., Texas, 1996.

24. Frosch, R., Li, W., Jirsa, J., Kreger, M., “Seismic Strengthening of Nonductile RC Specimens Using Precast Infill Panels”, 11th World Conference on Earthquake Engineering, Acapulco, Mexico, 1996.

25. Li, W., “Experimental Evaluation and Computer Simulation of Post Tensioned Precast Infill Wall System”, PhD. Thesis, University of Texas at Austin, Department of Civil Eng., Texas, 1997.

26. Matsumoto, Toshio, “Structural performance of SRC multi-story shear walls with infilled precast concrete panels” Japan Concrete Institute, Tokyo, 1998.

27. Frosch, R.J., "Shear Transfer Between Concrete Elements Using a Steel Pipe", ACI Structural Journal, Vol. 96, No. 6, November-December 1999, pp. 1003-1008.

28. Frosch, R.J., "Panel Connections for Precast Concrete Infill Walls," ACI Structural Journal, Vol. 96, No. 4, July-August 1999, pp. 467-472.

29. Mertol, H., C., “Carbon Fiber Reinforced Masonry Infilled Reinforced Concrete Specimen Behavior” MS. Thesis, Department of Civil Engineering, Middle East Technical University, Ankara, Turkey, June 2002.

30. Keskin, R., S., “ Behavior of Brick Infilled Reinforced Concrete Specimens Strengthened by CFRP Reinforcement”, MS. Thesis, Department of Civil Engineering, Middle East Technical University, Ankara, Turkey, July 2002.

31. Erduran, E., ” MS. Thesis, Department of Civil Engineering, Middle East Technical University, Ankara, Turkey, July 2002.

32. Sonuvar, M., O., “Hysteretic Response of Reinforced Concrete Specimens Repaired by Means of Reinforced Concrete Infills” PhD Thesis Department of Civil Engineering, Middle East Technical University, Ankara, Turkey, June 2001.

33. Canbay, E., “Contribution of Reinforced Concrete Infills to the Seismic Behavior of Structural Systems”, PhD Thesis, Department of Civil Engineering, Middle East Technical University, Ankara, Turkey, December 2001.

34. Altın, S., “Strengthening of Reinforced Concrete Specimens with Reinforced Concrete Infills” PhD. Thesis, Dept. of Civil Eng., Middle East Technical University, Ankara, Turkey, February 1990.

35. Smith, B.S., “Model Test Results of Vertical and Horizontal Loading of Infilled Specimens”, ACI Journal, August 1968, pp. 618-624.

36. "Efficiency of Bolt Connected Reinforced Concrete Shear Panels to Strengthen Building Structures," (with O. Yuzugullu), Proceedings of the First Conference on Concrete Technology for Developing Countries, Yarmouk University, Amman, October 1983.

37. Axley, J.W., Bertero, V.V., "Infill Panels: Their Influence on Seismic Response of Building", Report No. EERC 79-28, Earthquake Engineering Research Center, University of California, Berkeley, California, USA, 1976.

38. Govindan, P., Lakshmipathy, M., Santhakumar, A.R., "Ductility of Infilled Frames", ACI Journal, July-August 1986, pp.83-50.

39. Klingner, R.E., Bertero, V.V., "Earthquake Resistance of Infilled Frames", Journal of the Structural Division, pp.973-989, June 1978.

40. Liauw, T.C., "Tests on Multistory Infilled Frames Subject to Dynamic Lateral Loading", ACI Journal, pp.551-563, April 1979.

41. Marjani, F., Ersoy, U., "Behavior of Brick Infilled Reinforced Concrete Frames Under Reversed Cyclic Loading", International Symposium on Structural and Earthquake Engineering, October 2002, Middle East Technical University, Ankara, Turkey

APPENDIX

EVALUATION OF SHEAR DEFORMATION

Shear deformations on the panels were measured by means of diagonally placed dial gauges. For each time step, readings taken from these transducers were recorded. Since two displacement readings were taken along the diagonals, it is possible to determine the deformed shape of the wall panel. Approximate deformed shape of the panel is presented in A.1

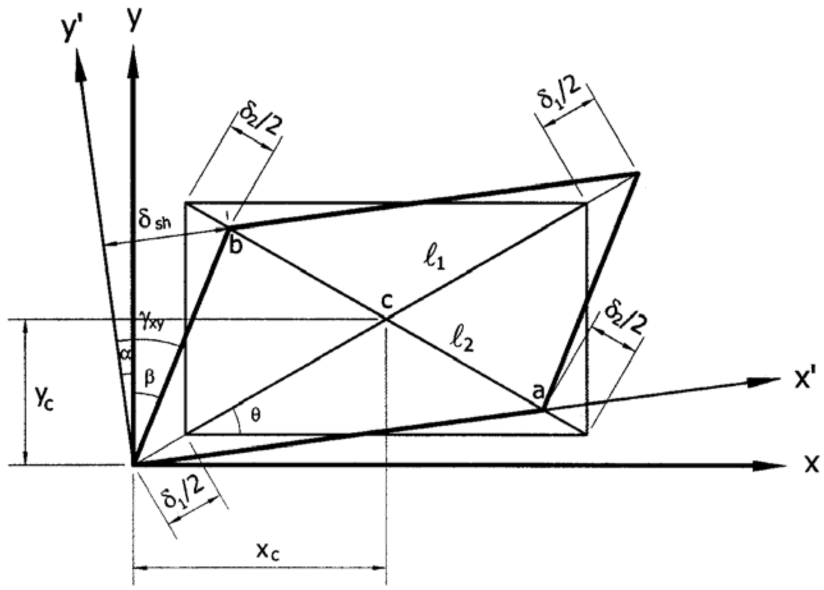

Figure A.1 – Rectangular shape distortion

According to the geometry shown above, shear deformations can be computed approximately as follows.

$$\theta = \arctan\left(h/w \right)$$

h height of the rectangle

w width of the rectangle

$$\ell'_1 = \ell_1 + \delta_1 = \ell_1(1+\varepsilon_1)$$

$$\ell'_2 = \ell_2 + \delta_2 = \ell_2(1+\varepsilon_2)$$

ℓ_1 length of diagonal 1

ℓ_2 length of diagonal 2

ℓ'_1 length of diagonal 1 after deformation

ℓ'_2 length of diagonal 2 after deformation

ε_1 strain in diagonal 1 direction

ε_2 strain in diagonal 2 direction

δ_1 total elongation in diagonal 1 direction

δ_2 total elongation in diagonal 2 direction

$$x_c = \frac{\ell'_1}{2}\cos(\theta)$$

$$y_c = \frac{\ell'_1}{2}\sin(\theta)$$

$$x_a = x_c + \frac{\ell'_2}{2}\cos(\theta) = \left(\frac{\ell'_1 + \ell'_2}{2}\right)\cos(\theta)$$

$$y_a = y_c - \frac{\ell'_2}{2}\sin(\theta) = \left(\frac{\ell'_1 - \ell'_2}{2}\right)\sin(\theta)$$

$$x_b = x_c - \frac{\ell'_2}{2}\cos(\theta) = \left(\frac{\ell'_1 - \ell'_2}{2}\right)\cos(\theta)$$

$$y_b = y_c + \frac{\ell'_2}{2}\sin(\theta) = \left(\frac{\ell'_1 + \ell'_2}{2}\right)\sin(\theta)$$

Shear deformation γ_{xy} is defined as the sum of the angles α and β shown in Figure A.1. Angles α and β can be obtained easily from the following equations.

$$\alpha = \arctan\left(\frac{y_a}{x_a}\right) = \arctan\left(\frac{\left(\frac{\ell'_1 - \ell'_2}{2}\right)\sin(\theta)}{\left(\frac{\ell'_1 + \ell'_2}{2}\right)\cos(\theta)}\right) = \arctan\left(\frac{\ell'_1 - \ell'_2}{\ell'_1 + \ell'_2}\tan(\theta)\right)$$

$$= \arctan\left(\frac{\ell'_1 - \ell'_2}{\ell'_1 + \ell'_2}\left(h/w\right)\right) = \arctan\left(\frac{\varepsilon_1 - \varepsilon_2}{2 + \varepsilon_1 + \varepsilon_2}\left(h/w\right)\right)$$

$$\beta = \arctan\left(\frac{x_b}{y_b}\right) = \arctan\left(\frac{\left(\frac{\ell'_1 - \ell'_2}{2}\right)\cos(\theta)}{\left(\frac{\ell'_1 + \ell'_2}{2}\right)\sin(\theta)}\right) = \arctan\left(\frac{\ell'_1 - \ell'_2}{\ell'_1 + \ell'_2}\cot(\theta)\right)$$

$$= \arctan\left(\frac{\ell'_1 - \ell'_2}{\ell'_1 + \ell'_2}\left(w/h\right)\right) = \arctan\left(\frac{\varepsilon_1 - \varepsilon_2}{2 + \varepsilon_1 + \varepsilon_2}\left(w/h\right)\right)$$

$$\gamma_{xy} = \alpha + \beta$$

δ_{sh} shown in Figure A.1 could easily be obtained from geometry. The shear-displacement values could than be computed using the following equation.

$$\delta_{sh} = \gamma_{xy} \cdot h$$

Shear-displacement value (δ_{sh}) measured for each panel was the interstory shear-displacement for that story. Total shear-displacement curve can be calculated by summing the shear-displacements of each panel.

It must be realized that the sensitivity and placement of the instrumentation was not sufficient to obtain accurate values of the shear distortions at infill panel. It is difficult to get accurate measurements of shear deformations due to uncertainties introduced by panel cracking.